

# MOMENT CONNECTIONS FOR WIDE-FLANGE BEAMS TO RHS COLUMNS

by

Rebecca K. Clahane

Submitted in partial fulfilment of the requirements  
for the degree of Master of Applied Science

at

Dalhousie University  
Halifax, Nova Scotia  
August 2023

Dalhousie University is located in Mi'kmaq'i,  
the ancestral and unceded territory of the Mi'kmaq.  
We are all Treaty people.

# TABLE OF CONTENTS

List of Tables .....	v
List of Figures .....	vi
Abstract .....	viii
List of Abbreviations and Symbols Used .....	ix
Acknowledgements .....	xiii
Chapter 1: Introduction .....	1
1.1. Problem Description .....	1
1.2. Research Motivation .....	2
1.3. Project Objectives .....	3
1.4. Thesis Overview .....	4
Chapter 2: Background and Literature Review .....	5
2.1. Rectangular Hollow Structural Sections .....	5
2.2. Applications of Type LD MRFs in Canada .....	6
2.3. North American Design Requirements .....	7
2.3.1. CSA S16:19, Clause 27.4 Type LD MRFs ( $R_d = 2.0$ , $R_o = 1.3$ ) .....	7
2.3.2. CSA S16:19, Annex J (AISC 341-22, Section K2) .....	8
2.3.3. AISC 360, Commentary B3 .....	9
2.3.4. AISC 341-22, Clause E1. Ordinary Moment Frames (OMF) .....	10
2.3.5. Comparison of Design Requirements .....	11
2.4. Types of Moment Connections .....	11
2.4.1. CISC Prequalified Connections .....	11
2.4.2. AISC Prequalified Connections .....	13
2.4.3. Non-Qualified Connections .....	14
2.4.4. Summary of Connection Types .....	17
2.5. Research Overview .....	19
Chapter 3: Moment Connection Design .....	20
3.1. Connection Design Philosophies .....	20
3.1.1. T-Stiffener Connection .....	21
3.1.2. Doubler Plate Connection .....	23
3.2. Connection Design Summaries .....	26

	3.2.1. T-Stiffener Connection .....	26
	3.2.2. Doubler Plate Connection .....	27
Chapter 4:	Experimental Program .....	28
4.1.	Testing Overview .....	28
4.2.	Test Specimens .....	29
4.3.	Geometric Properties .....	30
4.4.	Mechanical Properties.....	31
	4.4.1. Base Metal Tensile Coupon Tests .....	32
	4.4.2. Base Metal Tensile Coupon Results .....	33
	4.4.3. All Weld Metal Tensile Coupon Tests.....	36
	4.4.4. All Weld Metal Tensile Coupon Results .....	37
4.5.	Test Setup and Instrumentation.....	38
	4.5.1. Test Setup and Arrangement.....	38
	4.5.2. Instrumentation .....	40
	4.5.3. Surface Treatments .....	44
Chapter 5:	Experimental Results .....	45
5.1.	Quasi-Static Test Results .....	45
	5.1.1. Visual Observations.....	45
	5.1.2. Instrumentation Observations .....	46
	5.1.3. Strain Observations.....	48
	5.1.4. Connection Stiffness .....	50
	5.1.5. Interstorey Drift .....	51
5.2.	Cyclic Test Results .....	51
	5.2.1. Visual Observations.....	52
	5.2.2. Strain Observations.....	53
	5.2.3. Hysteretic Observations.....	56
Chapter 6:	Conclusions and Recommendations .....	59
6.1.	Summary .....	59
6.2.	Conclusion .....	59
6.3.	Recommendations and Future Work.....	60
References.....		61
Appendix A:	Design Calculations .....	63
A.1.	Beam and Column Member Parameters.....	63
A.2.	AISC Design Loads.....	63
A.3.	Clip Angle Design.....	63
A.4.	T-Stiffener Connection Design .....	64

A.5. Doubler Plate Connection .....	67
Appendix B: Fabrication Design Considerations .....	75
B.1. Initial Comments .....	75
B.2. Final Comments .....	76
Appendix C: Initial Design Drawings .....	78
Appendix D: Specimen and Metal Coupon Fabrication Drawings .....	80
Appendix E: Test Setup and Instrumentation.....	83
Appendix F: Geometric Properties .....	86
Appendix G: Material Property Test Results.....	89
Appendix H: Experimental Test Data.....	97
H.1. Static Test Results for Connection Assembly T1.....	98
H.2. Static Test Results for Connection Assembly DP3 .....	101
H.3. Cyclic Results for Connection Assembly T2 .....	104
H.4. Cyclic Results for Connection Assembly T3 .....	108
H.5. Cyclic Results for Connection Assembly DP1.....	112
H.6. Cyclic Results for Connection Assembly DP2.....	116
Appendix I: Documentation from Marid Industries Limited.....	119
I.1. Site Measurements and Checklists .....	120
I.2. Mill Test Reports .....	123
Appendix J: Procedure for Soldering Strain Gauge Wire Ends .....	131
Appendix K: Procedure for Installing Strain Gauges to Steel.....	132
Appendix L: Limewash Formula .....	135



# LIST OF TABLES

Table 2-1. Comparison of HSS to W-section to maintain weak-axis bending strength (CISC 2016) .....	5
Table 2-2. Beam-to-column configurations and ductility classes for available moment connections.....	18
Table 3-1. Summary of Doubler Plate connection failure moments.....	27
Table 4-1. Cyclic testing string pot target deflection used to control cyclic testing. ....	29
Table 4-2. Average base metal property summary .....	35
Table 5-1. T-Stiffener and Doubler Plate connection stiffness values.....	50
Table A-1. Properties of weld treated as a line (Blodgett 1967).....	71
Table F-1. Dimensions of HSS and W-section members .....	86
Table F-2. Dimensions of doubler and flange plates .....	87
Table F-3. Dimensions of T-stiffeners.....	87
Table F-4. Dimensions of clip angle.....	88

# LIST OF FIGURES

Fig. 1.1. Simplified 3D finite-element model view of case study building, MRFs highlighted in orange were the focus of this research (sensitive information has been removed to ensure compliance with confidentiality agreement) .....	2
Fig. 1.2. Case study idealized MRF dimensions and members. ....	3
Fig. 2.1. Moment vs. rotation relationship for different classes of beams (CISC 2021) .....	7
Fig. 2.2. Target loading sequence for beam-to-column moment connections according to AISC 341-22 Clause K.2.4b .....	9
Fig. 2.3. Classification of moment-rotation response connections (AISC 2022c).....	10
Fig. 2.4. CISC pre-qualified connections.....	12
Fig. 2.5. AISC pre-qualified connections (AISC 2022b).....	13
Fig. 2.6. Non-qualified connections.....	15
Fig. 3.1. T-Stiffener (a) and Doubler Plate (b) reinforced moment connections .....	20
Fig. 3.2. T-Stiffener cross-sectional area and dimensions .....	21
Fig. 3.3. T-Stiffener connection shear distributions at failure .....	22
Fig. 3.4. Assumed shear distribution around doubler plate.....	24
Fig. 3.5. T-Stiffener (a) and Doubler Plate (b) reinforced moment connection design details.....	26
Fig. 4.1. Fabrication process for the T-Stiffener (a-c) and Doubler Plate (d-f) moment connections .....	30
Fig. 4.2. TC post-fracture for base metals and all weld metal .....	31
Fig. 4.3. All weld metal TC instrumented and in the 2 MN MTS universal testing machine.....	31
Fig. 4.4. Sheet-type TC from HSS and W-section material.....	32
Fig. 4.6. Sheet-type TC from plate material .....	33
Fig. 4.7. Stress vs. strain curves for base metals.....	34
Fig. 4.8. Weld metal coupon details.....	36
Fig. 4.9. All weld metal groove assembly plates fabricated before weld metal added.....	37
Fig. 4.10. Stress vs. strain curves for all weld metal coupons .....	37
Fig. 4.11. Testing arrangement schematic with dimensions .....	38
Fig. 4.12. Testing arrangement photographs.....	39
Fig. 4.15. Photographs of surface treatments applied to connection assembly pre-testing.....	44
Fig. 5.1. Photographs of T-Stiffener (a) and Doubler Plate (b) moment connections (taken after testing) .....	45
Fig. 5.3. Load vs. linear potentiometer connection deflections (LP1 & LP2) for quasi-static tests .....	46
Fig. 5.4. Load vs. linear potentiometer column deflections (LP3 & LP4) for quasi-static tests.....	47

Fig. 5.5. Load vs. string pot deflections for quasi-static tests .....	47
Fig. 5.6. Moment vs. connection, column, and beam rotations for quasi-static tests .....	48
Fig. 5.7. Strain distributions for the T-Stiffener and the Doubler Plate connections .....	49
Fig. 5.8. Stiffener yielding after failure (Shanmugan et al. 1991) .....	49
Fig. 5.9. Connection moment vs. rotation plot for quasi-static tests.....	50
Fig. 5.10. Connection moment vs. interstorey drift plot for quasi-static tests .....	51
Fig. 5.11. Initial yielding occurring within the first 50 mm from the ends of the connections.....	52
Fig. 5.12. High stress yielding in connection welds after interstorey drift of 0.03 rads .....	52
Fig. 5.13. Plastic hinges of the connection assemblies post-cyclic cyclic testing.....	52
Fig. 5.14. T-Stiffener connection strain distributions .....	54
Fig. 5.15. Doubler plate connection strain distributions .....	55
Fig. 5.16. T-Stiffener normalized moment-interstorey drift hysteretic curves (T2 & T3 assemblies) .....	57
Fig. 5.17. Doubler Plate normalized moment-interstorey drift hysteretic curves (DP1 & DP2 assemblies) .....	57
Fig. 5.18. Actuator beam connection .....	58
Fig. B.1. Recommended construction weld types.....	76
Fig. F.1. Dimensions of HSS and W-section members.....	86
Fig. F.2. Dimensions of doubler and flange plates .....	86
Fig. F.3. Dimensions of T-stiffeners .....	87
Fig. F.4. Dimensions of clip angle .....	87
Fig. G.1. Tensile coupons (post-testing).....	89
Fig. H.1. T-Stiffener static test rotations.....	98
Fig. H.2. T-Stiffener mock cyclic response .....	98
Fig. H.3. T-Stiffener static test strain response.....	99
Fig. H.4. T-Stiffener post-testing photos .....	100
Fig. H.5. Doubler Plate static test rotations .....	101
Fig. H.6. Doubler Plate mock cyclic response .....	101
Fig. H.7. Doubler Plate static test strain response .....	102
Fig. H.8. Doubler Plate post-testing photos .....	103
Fig. H.9. T2 hysteretic curves.....	105
Fig. H.10. T2 testing photos.....	107
Fig. H.11. T3 hysteretic curves.....	109
Fig. H.12. T3 testing photos.....	111
Fig. H.13. DP1 hysteretic curves .....	113
Fig. H.14. DP1 testing photos.....	115
Fig. H.15. DP2 hysteretic curves .....	117
Fig. H.16. DP2 post-testing photos.....	118

# ABSTRACT

Since the 1994 Northridge and 1995 Kobe earthquakes, physical testing and analytical studies have been conducted to develop ductile and moderately ductile connections for moment-resisting frames. In contrast, advancements for limited-ductility moment-resisting frame connections have lagged, causing design requirements to be based more on judgment than research. In Canada, for example, CSA S16:19 Clause 27.4.4.1 presents three methods that can be used to satisfy the design requirements for Type LD MRF connections. Two of the three methods inadvertently prohibit the use of Rectangular Hollow Section (RHS) columns, leaving the last method of demonstrating a connection performance through at least two physical qualifying cyclic tests (as described in CSA S16:19 Annex J) the only option to use RHS columns in Type LD MRFs. This thesis investigates if connections designed following AISC 341-22 prescriptive design approach for ordinary moment frames can satisfy the performance requirements of CSA S16:19 Clause 27.4.4.1c).

# LIST OF ABBREVIATIONS AND SYMBOLS USED

AISC	=	American Institute of Steel Construction
CISC	=	Canadian Institute of Steel Construction
CJP	=	Complete Joint Penetration
CSA	=	Canadian Standard Association
DP	=	Doubler Plate
FE	=	Finite Element
FR	=	Fully Restrained
HSS	=	Hollow Structural Section
IMF	=	Intermediate Moment Frame
LD	=	Limited Ductility
LLRS	=	Lateral Load Resisting System
LP	=	Linear Potentiometers
MD	=	Moderately Ductile
MRF	=	Moment Resisting Frame
OMF	=	Ordinary Moment Frame
PJP	=	Partial Joint Penetration
PR	=	Partially Restrained
RHS	=	Rectangular Hollow Section
SG	=	Strain Gauge
SMF	=	Special Moment Frame
$A$	=	original cross-sectional area of coupon reduced area
$A_{ne}$	=	net effective area for shear lag according to CSA S16:19 Clause 12.3.3.3
$A_w$	=	effective throat area of weld ( $t_w \times l_w$ )
$E$	=	elastic modulus of steel, 200 GPa nominal
$F_{y0}$	=	specified minimum tensile strength of RHS
$F_k$	=	unit buckling stress of the RHS wall as described in CSA S16:19

$F_u$	=	specified minimum tensile strength
$F_{ut}$	=	specified minimum tensile strength of the T-stiffener
$F_y$	=	specified minimum yield stress
$F_{yb}$	=	specified minimum yield stress of beam
$F_{yf}$	=	specified minimum yield stress of flange plate
$F_{yp}$	=	specified minimum yield stress of doubler plate
$F_{yt}$	=	specified minimum yield stress of T-stiffener
$I_b$	=	moment of inertia of the beam
$I_E$	=	earthquake importance factor
$I_x$	=	moment of inertia about the x-axis
$I_y$	=	moment of inertia about the y-axis
$K_s$	=	connections secant stiffness
$L$	=	beam length, distance from the string pot to the center of the column, moment arm to the applied load
$L_{cf}$	=	clear length of the beam
$L_f$	=	gauge length after failure
$L_0$	=	initial gauge length
$\Delta L$	=	elongation reading from the extensometer
$M$	=	Moment at the column face
$M_{max}$	=	moment corresponding to the actuator stroke limit
$M_{pb}$	=	the beam nominal plastic moment resistance
$M_{r1}^*$	=	factored moment resistance
$M_S$	=	connection moment at service load
$M_u$	=	design moment
$P$	=	load from the MTS machine or actuator
$R_0$	=	over strength-related force modification factor accounting for the dependable portion of reserve strength in a structure designed according to provisions defined in NBCC (2020) Article 4.1.8.9
$R_d$	=	ductility-related force modification factor reflecting the capacity of a structure to dissipate energy through reversed cyclic in elastic behaviour as given in NBCC (2020) Article 4.1.8.9
$R_y$	=	ratio of expected yield stress to the specified minimum yield stress ( $F_y$ )
$S(T)$	=	design spectral response acceleration expressed as a ratio to gravitational acceleration

$T$	=	acceleration period, seconds
$T_u$	=	design tension force = $C_u = M_u/d_i$
$V_u$	=	design shear
$X_u$	=	ultimate strength of the weld, nominally 490 MPa for the study
$Z_b$	=	section modulus of beam
$Z_t$	=	section modulus of T-stiffeners
$b_0$	=	width of column
$b_a$	=	width of angle
$b_b$	=	width of beam
$b_e$	=	effective width
$b_f$	=	width of flange plate
$b'_f$	=	tapered width of flange plate
$b_p$	=	width of doubler plate
$b_t$	=	width of T-stiffener
$d_a$	=	depth of angle
$d_f$	=	depth of flange plate
$d_i$	=	center-to-center distance between T-stiffener webs
$d_p$	=	depth of doubler plate
$d_t$	=	depth of T-stiffener
$h_0$	=	depth of column
$h_b$	=	depth of beam
$l_a$	=	length of angle
$l_s$	=	T-stiffener minimum design length
$l_t$	=	length of T-stiffener
$s$	=	fillet weld leg size = $w_t - 2$ mm (according to CISC's Handbook)
$t_0$	=	HSS wall thickness
$t_a$	=	thickness of angle flange
$t_b$	=	thickness of beam flange
$t_f$	=	thickness of flange plate
$t_p$	=	thickness of doubler plate
$t_t$	=	thickness of T-stiffener flange

$w_b$	=	thickness of beam web
$w_t$	=	thickness of T-stiffener web
$\alpha_s$	=	LRFD-ASD force level adjustment factor = 1.0 for LRFD
$\Delta$	=	deflection readings from string pot
$\varepsilon$	=	strain
$\varepsilon_f$	=	ultimate strain
$\varepsilon_y$	=	yield strain
$\theta$	=	connection rotation
$\theta_S$	=	connection rotation at service load
$\theta_w$	=	angle (in degrees) between the weld axis and the applied force (= 0° for a longitudinal weld)
$\sigma$	=	engineering stress
$\phi_w$	=	weld metal resistance factor (= 0.67)



# ACKNOWLEDGEMENTS

First and foremost, I am incredibly grateful to my supervisor, Dr. Kyle Tousignant. His unwavering support and guidance have significantly impacted my research and professional career. His undergraduate courses first sparked my interest in steel design, which ultimately led me to complete my master's degree. I cannot thank him enough for his inspiration and mentorship.

I would also like to express my appreciation to the structural department at CBCL Limited. They supported me throughout my academic journey and quickly collaborated with me on a Mitacs internship. With their help, we were able to identify and address a recurring issue through the successful completion of this project. Support for this research was also provided by Mitacs through the Mitacs Accelerate Program, CISC (research grant), NSERC (funding), and Atlas Tube Inc. (HSS material donations).

Special thanks to Tim Houstma, Tom Parsons, and the team at Marid Industries Ltd. for their fabrication and recommendations throughout the project.

I must also acknowledge the invaluable assistance provided by the Dalhousie lab technicians: Jordan Maerz, Jesse Keane, and Dean Grijm. They provided guidance during the development of the test setup, machining of parts and tensile coupons, and instrumental and prototype testing.

I am also grateful for my research group, which provided a collaborative and supportive environment. We were able to bounce ideas off each other and navigate the challenges of post-COVID-19 graduate school together. The journey was more enjoyable with each member's contribution.

Finally, I thank my family and friends for their unwavering support and belief in me. They have been my constant source of inspiration and encouragement, even when I doubted myself. I owe it to them for who I am today.

# Chapter 1: INTRODUCTION

## 1.1. PROBLEM DESCRIPTION

The seismic design approach for steel buildings was radically changed after the devastating results of the 1994 Northridge earthquake and the 1995 Kobe earthquake. While the Northridge earthquake, with an estimated \$20 billion in damage (Ghosh 1995), had no steel building collapses, more than 150 buildings with steel moment resisting frames (MRFs) required remediation of the welded beam-to-column connections (Tremblay et al. 1995). The Kobe earthquake, on the other hand, had an estimated \$100 billion in property damage and countless deaths and injuries due to the collapse of steel buildings (Ghosh 1995). Investigations by structural engineers following both events concluded that the beam-to-column connections at the time were insufficient.

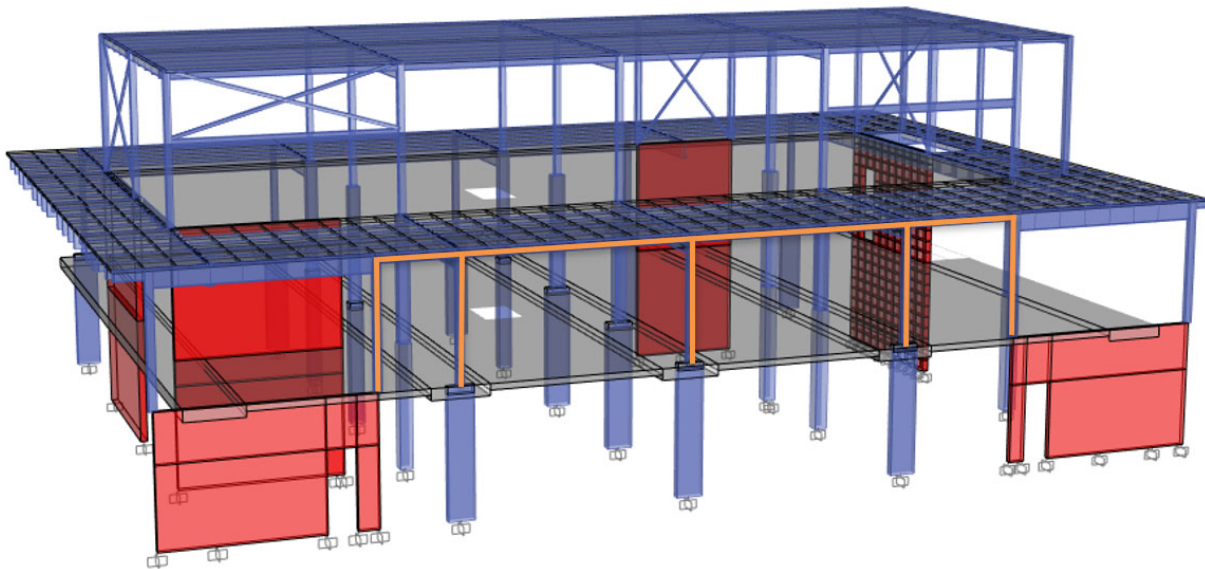
In the years since, physical testing and analytical studies have been conducted to determine better moment connections for ductile (D) and moderately ductile (MD) MRFs in Canada (CISC 2021). However, research on moment connections for limited ductility (LD) MRFs, with high strength and low ductility, has lagged.

Type LD MRFs can, in general, make use of traditional connection detailing, making them less-expensive and easier-to-fabricate than Type D and MD MRFs; however, in Canada, CSA S16:19 Clause 27.4.4.1 parts a) and b) provides limited options for Type LD MRF connections (Section 2.3.1), which also inadvertently preclude the use of Rectangular Hollow Section (RHS) columns in Type LD MRFs.

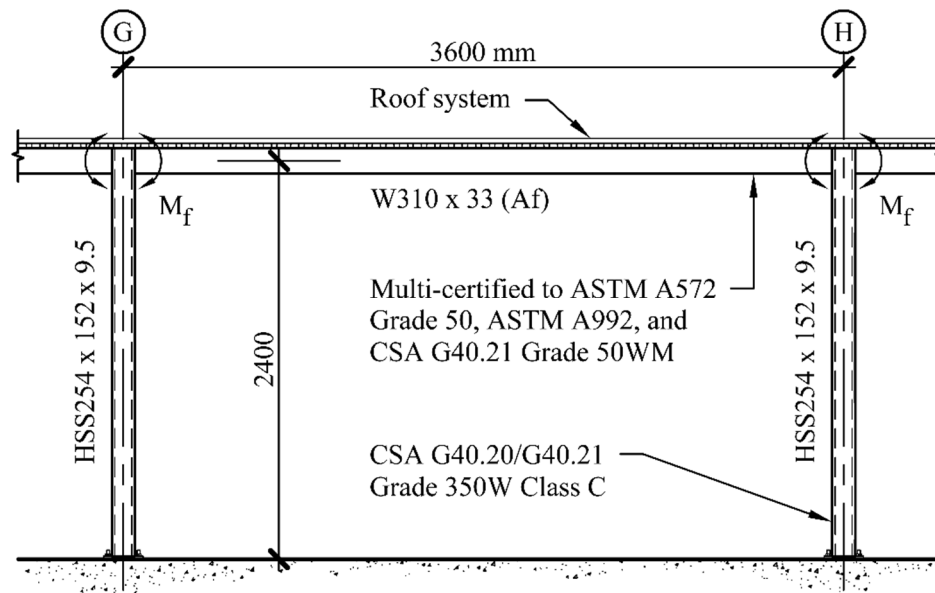
Experience has shown that RHS columns can improve Type LD MRF efficiency, due to their high strength-to-weight ratio, advantageous bending and compression strength, and high torsional resistance relative to wide-flange columns. However, since MRF connections are designed to be rigid, RHS columns with unstiffened connections are not typically considered viable.

## 1.2. RESEARCH MOTIVATION

CBCL Limited has encountered recurrent situations when designing buildings with Type LD MRFs when using RHS columns is optimal (architecturally and structurally). In view of the above-mentioned restrictions, I-shaped columns have been used instead (i.e., to meet the requirements of CSA S16:19 Clause 27.4.4). This project investigates the use of RHS columns in a post-disaster building with Type LD MRFs designed in accordance with the National Building Code of Canada and CSA S16:19 for a location in Moncton, New Brunswick. The MRFs focused on by this project are part of a second-storey exterior wall framing assembly (highlighted in orange in Fig. 1.1) in which the columns were subjected to axial loads and bi-axial bending due principally to snow (including snow drift), wind, and earthquake loading. It was therefore desired (but hitherto not permitted) to use RHS columns, which were deemed – by the designers – to be optimal under the above loading conditions. The connection assemblies produced for this research have a column height of 2.7 m and a beam length of 1.8 m to represent the ideal inflection points (points of contraflexure) of an idealized MRF with 2.4 m high by 3.6 m long bays, shown in Fig. 1.2. The columns in the MRFs were comprised of Class 1 HSS254 × 152 × 9.5 members made to CSA G40.20/G.40.21 Grade 350W Class C (CSA 2018), and the beams were Class 2 W310 × 33 members were multi-certified to ASTM S572 Grade 50 (ASTM 2021a), ASTM A992 (ASTM 2022) and CSA G40.20/G.40.21 Grade 50WM (CSA 2018). For this idealized MRF, two connection types (T-Stiffener and Doubler Plate connections) were selected after reviewing existing moment connection types (Section 2.4) to be designed and tested according to CSA S16:19 Clause 27.4.4.1c).



**Fig. 1.1.** Simplified 3D finite-element model view of case study building, MRFs highlighted in orange were the focus of this research (sensitive information has been removed to ensure compliance with confidentiality agreement)



**Fig. 1.2.** Case study idealized MRF dimensions and members.

### 1.3. PROJECT OBJECTIVES

As discussed in the Abstract, this thesis aims to investigate (through the above-described case study) if connections designed following AISC 341-22 prescriptive design approach for ordinary moment frames (OMFs) can satisfy the performance requirements of CSA S16:19 Clause 27.4.4.1c).

To enable this, the following sub-objectives/activities were performed:

- Activity 1:** Design and detail two practical and economical W-section-to-RHS column moment connection prototypes that satisfy the criteria for Type LD MFRs in Canada (CSA S16:19) and OMF in the United States (AISC 341-22).
- Activity 2:** Fabricate and test connections, in accordance with CSA S16:19 Annex J1.2, large-scale connection sub-assemblages.
- Activity 3:** Demonstrate connections acceptable performance (in accordance with CSA S16:19 Clause 27.4.4.1 part c).
- Activity 4:** Compare the design criteria for Type LD MRF (or OMF) beam-to-column connections.

## 1.4. THESIS OVERVIEW

The following information is provided herein:

- Chapter 2:** This chapter presents an overview of RHS members, applications of Type LD MRFs in Canada, the North American design requirements for low seismic moment connections, and existing moment connections (Type LD and OMF) for RHS or built-up box columns designed for use in North America.
- Chapter 3:** This chapter reviews existing design philosophies for the T-Stiffener and Doubler Plate connections as well as modifications made to the connection designs used in this study based on consultations with a local fabricator, Marid Industries Ltd.
- Chapter 4:** This chapter presents an overview of the experimental program, geometric and mechanical properties of the base metal materials as well as the welding material. Additionally, the arrangement and instrumentation for the connection assembly testing under static and cyclic loading is outlined in this chapter.
- Chapter 5:** This chapter presents experimental results for static and cyclic tests performed as part of this research, and a comparison of the CSA S16:19 and AISC 341-22 low seismic moment connection design requirements.
- Chapter 6:** This chapter presents a summary and conclusions of the foregoing research and provides recommendations for future work.

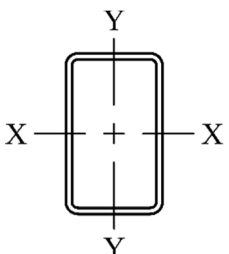
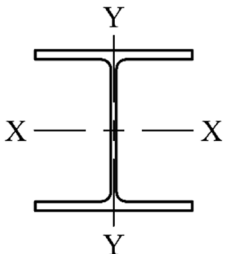
# Chapter 2: BACKGROUND AND LITERATURE REVIEW

## 2.1. RECTANGULAR HOLLOW STRUCTURAL SECTIONS

RHS members in North America are typically cold formed using a continuous forming process that molds plate steel into so-called circular mother tubes, and then into the final desired rectangular shape and dimension. This cold-forming process creates residual stresses in the member, which causes the corners of RHS to have higher yield stresses and lower ductility. Conversely, the RHS flats tend to have lower residual stresses and higher ductility.

RHS make ideal columns for seismic building applications due to their high bi-axial strength (relative to W-sections) and high torsional resistance (due to their closed shape). A stronger weak-axis resistance can often be required in seismic applications where lateral loading is expected to be applied in perpendicular directions, such as with certain combinations of wind, snow, and earthquake loading. RHS columns can achieve high bi-axial strength while keeping the floor area needed (i.e., footprint) small; in contrast, a W-section column would typically require a much larger footprint for the same design load(s). Table 2-1 compares the properties of a typical RHS column [i.e., the one(s) used in this study] to the lightest W-section required to maintain the same weak-axis bending strength. This W-section is 70% deeper, takes up 30% more floor area, and weighs 17kg/m more than the RHS member. RHS columns also tend to better suit architectural requirements (for preferred wall or column sizes) and have smooth surfaces/lines that make finishing the column more economical.

**Table 2-1.** Comparison of HSS to W-section to maintain weak-axis bending strength (CISC 2016)

HSS254 × 152 × 9.5 (CSA G40.20)		W250 × 73 (ASTM A992)	
	Depth = 254 mm		Depth = 253 mm
	Width = 152 mm		Width = 254 mm
	Area = 7150 mm <sup>2</sup>		Area = 9290 mm <sup>2</sup>
	Mass = 56.1 kg/m		Mass = 72.9 kg/m
	$I_x = 60.4 \times 10^6 \text{ mm}^4$		$I_x = 113 \times 10^6 \text{ mm}^4$
	$I_y = 27.2 \times 10^6 \text{ mm}^4$		$I_y = 38.3 \times 10^6 \text{ mm}^4$

## 2.2. APPLICATIONS OF TYPE LD MRFs IN CANADA

In steel building design, two lateral load resisting systems (LLRS) are typically used (though several others exist): braced frames and MRFs. Braced frames are generally regarded to be “stiff,” with pinned connections at the beam-to-column joints and bracing (e.g., diagonal or X-bracing members) used to transfer lateral loads downwards through the building structure. In comparison, MRFs are relatively “flexible,” with rigid beam-to-column connections that transfer lateral load and moments downwards through the connections. Both system types are outlined in CSA S16:19 Clause 27 for use in seismic applications. MRFs are typically found in exterior or interior walls where uninterrupted visual space is desired in statically and seismically designed buildings.

CSA S16:19 Clause 27 seismic design defines three types of moment-resisting frames: Type D MRFs, Type MD MRFs and Type LD MRFs. Type LD MRFs, with high strength and low ductility, are important to areas like the Maritimes, with low seismic activity. The National Building Code of Canada (NBCC 2020) defines two critical parameters in the analysis of earthquakes on a building, the over strength-related force modification factor ( $R_o$ ) and the ductility-related force modification factor ( $R_d$ ) (where  $R_o$  is a modification factor that accounts for the dependable portion of reserve strength in a structure design and  $R_d$  is a modification factor that reflects the capacity a structure has to dissipate energy through cyclic loading in elastic behaviour). Both modification factors are applied to the expected load and decrease the demand when ductile behaviour is expected. Type LD MRF modification factors ( $R_o = 2.0$  and  $R_d = 1.3$ ) are lower than those for Type D MRFs ( $R_o = 5.0$  and  $R_d = 1.5$ ) because there is less expected ductility and reserve strength (NBCC 2020). Because of the lower ductile demand required for Type LD MRF connections, conventional construction methods can often be applied (See Section 2.4), resulting in Type LD MRF connections being more economical despite having to be designed for higher loads. The National Building Code of Canada (NBCC 2020) states that there are two applications when buildings in Canada require Type LD MRFs or better, these are:

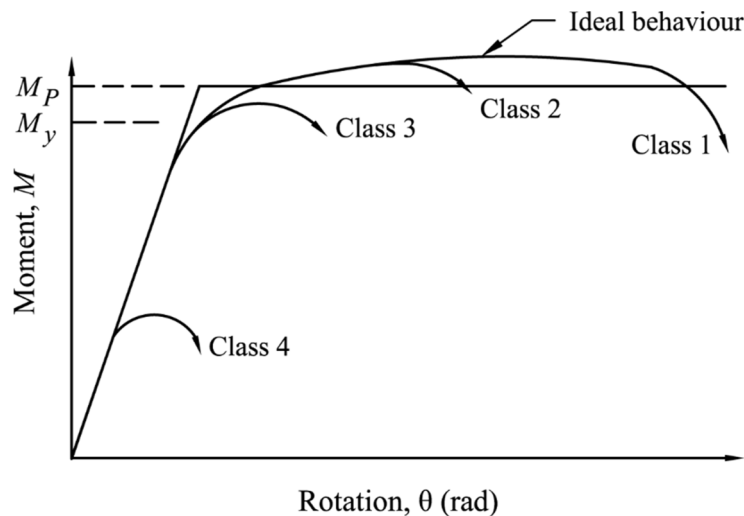
1. A high importance category building with a seismic category of SC4 ( $R_d = 2.0$ ). A high-importance building is one that provides a greater degree of safety to humans and would be used as a shelter and gathering location (i.e., schools and community centers). A seismic category of SC4, according to CSA S16:19, is when the short-term period is  $0.75 < I_E S(0.2)$  and the long term period is  $0.3 < I_E S(1.0)$  where  $I_E$  = the earthquake importance factor = 1.0 for high and 1.25 for post-disaster, and  $S(T)$  = the design spectral response acceleration, expressed as a ratio to gravitational acceleration for a period of T in seconds.
2. A post-disaster importance category building is when  $R_d \geq 2.0$ . A post-disaster building is essential to the provision of services in the event of a disaster (i.e., hospitals, communications, control centers, etc.).

## 2.3. NORTH AMERICAN DESIGN REQUIREMENTS

The design of MRF connections for low seismic regions in North America is defined by two codes. In Canada, CSA S16:19 Clause 27.4 “Type LD (limited-ductility) moment-resisting frames” outlines the design requirements. In the United States, AISC 341-22 Clause E1. “Ordinary Moment Frames (OMF)” defines the design requirements. Although the countries have similar areas of seismic applications and land geography, the requirements – in terms of their approach(es) to design Type LD MRF/OMF connections – vary significantly.

### 2.3.1. CSA S16:19, CLAUSE 27.4 TYPE LD MRFs ( $R_D = 2.0$ , $R_o = 1.3$ )

CSA S16:19 defines Type LD MRFs as those that can develop a limited amount of inelastic deformation through plastic hinging in the beams, columns, or joints (CSA 2019). The beams in the frame assemblies must be Class 1 or 2, and column members be Class 1 or Class 2 if the strong-column requirements (column strength is greater than that of the beam) of CSA S16:19 Clause 27.4.2.2 are met. Member classes are defined based on the member’s width-to-thickness ratios as defined in Clause 13.5 of CSA S16:19. Class 1 members are those that will reach the fully plastic moment,  $M_p$ , and retain it for a range of rotation before decreasing, and Class 2 members are those that will reach  $M_p$  but not necessarily retain it as the rotation increases (as shown in Fig. 2.1).



**Fig. 2.1.** Moment vs. rotation relationship for different classes of beams (CISC 2021)



Three methods of designing Type LD MRF beam-to-column connections are presented in CSA Clause 27.4.4.1:

- (i) designed and detail a connection according to Clause 27.4.4.2;
- (ii) use a connection designed and detailed according to CISC Moment Connections for Seismic Applications (CISC 2019); and lastly,
- (iii) demonstrate that the connection will meet the rotation requirements through at least two full-scale physical qualifying cyclic connection tests as described in CSA S16:19 Annex J.

For the first method, method (i), CSA S16:19 Clause 27.4.4.2 states the connections resistance shall be  $R_y M_{pb}$  (where  $R_y$  = ratio of expected yield stress to the specified minimum yield stress; and  $M_{pb}$  = the beam nominal plastic moment resistance), except when governing failure state is ductile then moment resistance is less than the effect of gravity loads combined with seismic load multiplied by two. However, this clause cannot be used for connections with RHS columns, as the clause states that “columns shall be I-shaped sections only” (CSA 2019).

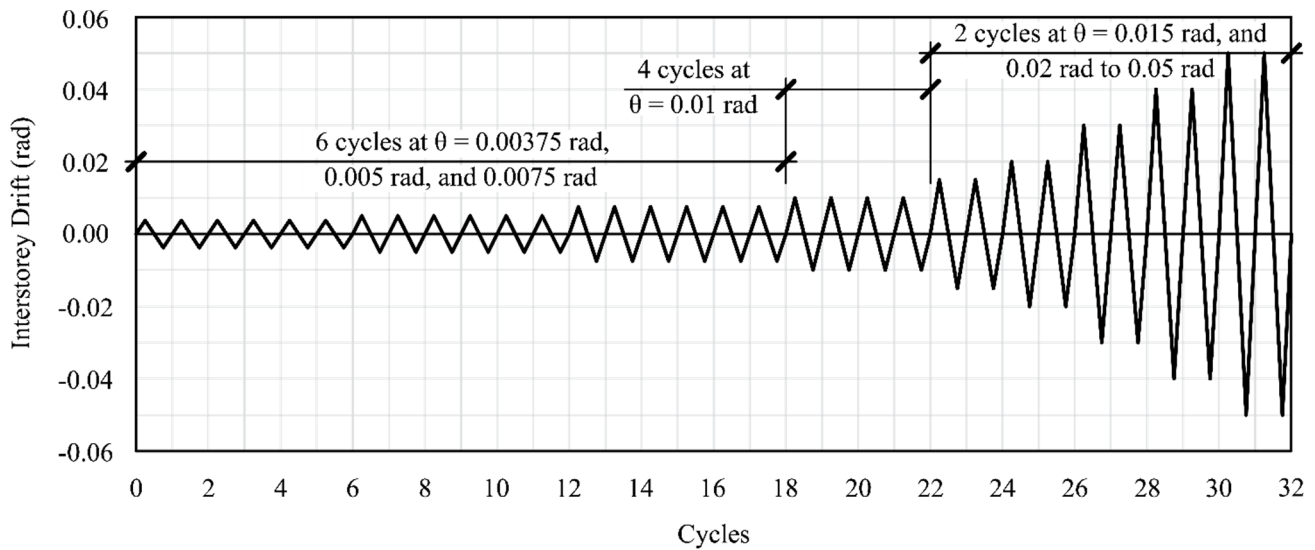
When using the second method, method (ii), the document CISC Moment Connections for Seismic Applications (see Section 2.4.1) provides options for beam-to-column connections using built-up box columns, but not RHS. With both these methods [(i) and (ii)] prohibiting the use of RHS columns, designers must design, fabricate, and test full-scale connections under cyclic loading to meet the requirements of (iii) if RHS columns are desired for a Type LD MRF in a project. The third method, method (iii), defines the rotation requirement of a beam-to-column connection to qualify for use in a Type LD MRF as maintaining 80% of  $M_{pb}$  at an interstorey drift of 0.02 radians during the physical qualifying cyclic connection tests (Section 2.3.2). This makes the use of RHS columns in these MRFs all but unfeasible (due to the additional cost and time of testing and analysis required, as described in the following section).

### 2.3.2. CSA S16:19, ANNEX J (AISC 341-22, SECTION K2)

Annex J of CSA S16:19 [i.e., for method (iii), above] defines the qualification testing provisions for seismic moment connections. Clause J.1.3 states that the assemblies tested must represent the actual size, arrangement (bracing), detailing, and fabrication as intended to be used in the building design for pre-qualification. Further, the testing shall comply with Section K2 of AISC 341-22 (AISC 2022a) with a modification to meet the interstorey drift limits outlined in CSA S16:19 Clause 27.

AISC 341-22 (AISC 2022a) Section K2 requires loading of the connection assemblies to be interstorey drift controlled, reaching a specified rotation for a defined number of cycles, shown in Fig. 2.2.

As noted in Section 2.3.1. for Type LD MRFs in Canada, the beam-to-column connections are expected to maintain 80%  $M_{pb}$  at an interstorey drift of 0.02 radians (cycle 24-26).

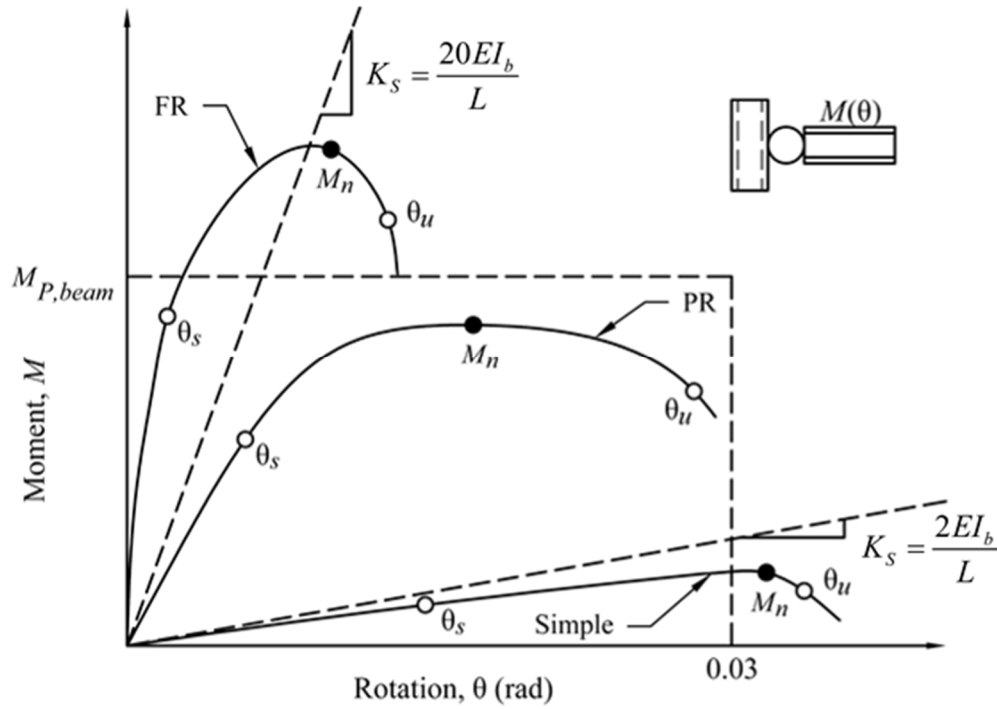


**Fig. 2.2.** Target loading sequence for beam-to-column moment connections according to AISC 341-22 Clause K.2.4b

### 2.3.3. AISC 360, COMMENTARY B3

In most structural analyses, connection elements are either modelled as pinned or fixed. Pinned connections represent simple connections that allow rotation but not translation. Fixed connections represent fully restrained (FR) connections that do not allow rotation or translation. When connections are simple or FR, the structural analysis may be completed first, then connection elements designed. This allows for a straightforward design procedure. According to AISC 360-22 Commentary B3 (AISC 2022c), a connection is acceptable to be classed as simple if its stiffness is relatively low, i.e.,  $K_s L / EI_b < 2$  (where  $K_s$  = connection secant stiffness at service load,  $L$  = length of the beam,  $E$  = elastic modulus of steel, and  $I_b$  = moment of inertia of the beam). A connection can be classified as FR when its stiffness is relatively high, i.e.,  $K_s L / EI_b \geq 20$ .

If a connection has a stiffness in-between the stiffness limits for simple and FR, as shown in Fig. 2.3, then the connection is considered partially restrained (PR). PR connections require the stiffness, strength, and ductility of the connection to be considered in the structural analysis. PR connection strength is dependent on element deformation, and therefore a structural analysis/design using PR connections tends to be iterative. Typical PR connection characteristics can be obtained from databases, testing, or finite element studies – but these are seldom used in practice/design.



**Fig. 2.3.** Classification of moment-rotation response connections (AISC 2022c)

### 2.3.4. AISC 341-22, CLAUSE E1. ORDINARY MOMENT FRAMES (OMF)

AISC 341-22 defines OMFs (which are comparable to Type LD MRFs in Canada) as frames that are expected to provide minimal inelastic deformation capacity in their members and connections (AISC 2022a). Connections are permitted to be fully restrained (FR) or partially restrained (PR), and all CJP welds are considered demand critical.

Physical qualifying full-scale cyclic tests are not required for OMF connections (unlike for Type LD MRFs in CSA S16:19). Instead, AISC 341-22 (AISC 2022a) requires FR moment connections for OMFs to be designed using specified moment and shear resistances ( $M_u$  and  $V_u$ ) equal or greater than:

$$M_u = \frac{1.1R_y M_{pb}}{\alpha_s} \quad (2.1)$$

$$V_u = \frac{2(1.1R_y M_{pb})}{L_{cf}} \quad (2.2)$$

where  $R_y = 1.1$  per Table A3.1 of AISC 341-22;  $\alpha_s$  = LRFD-ASD force level adjustment factor = 1.0 for LRFD); and  $L_{cf}$  = clear length of the beam.

### 2.3.5. COMPARISON OF DESIGN REQUIREMENTS

As shown above, CSA S16:19 and AISC 341-22 prequalification requirements for Type LD MRF and OMF connections with RHS columns vary significantly. CSA S16:19 (CSA 2019) requires two full-scale physical tests, whereas AISC 341-22 (AISC 2022a) only requires minimum strength requirements (i.e.,  $M_u$  and  $V_u$ ) to be met. The latter approach is advantageous, as it avoids the additional cost and time required by the former approach for physical testing.

The primary objective of the research presented herein is to determine if moment connections designed using the AISC 341-22 (AISC 2022a) prescriptive design approach will meet or exceed the performance requirements of CSA S16:19 Clause 27.4.4.1c).

## 2.4. TYPES OF MOMENT CONNECTIONS

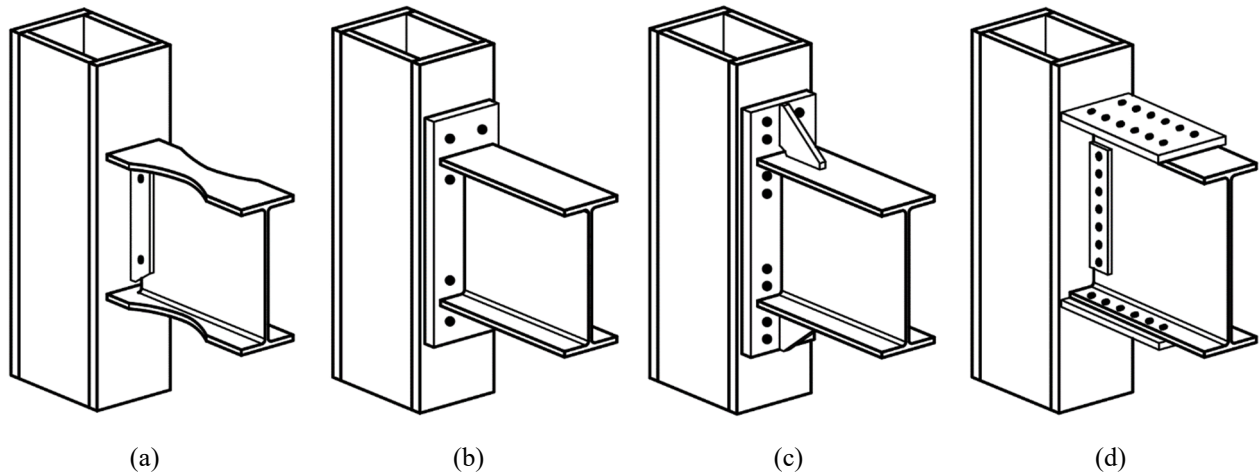
Prequalified connections allow designers to specify connections without the requirement of physical tests. The following sub-sections of this thesis present prequalified connections provided by CISC and AISC (in Sections 2.4.1 and 2.4.2) and additional connections that have been the subject(s) of testing (though not necessarily to the requirements of AISC 341-22 Section K2) in order to investigate/demonstrate the feasibility of using RHS columns in Type LD MRF (and other) seismic moment frames.

### 2.4.1. CISC PREQUALIFIED CONNECTIONS

It is important to note that the following connections, from CISC Moment Connections for Seismic Applications (CISC 2019), are not pre-qualified for RHS columns but built-up box columns. Nonetheless, they are deemed to demonstrate the feasibility of using RHS columns in Type LD MRFs. CISC (2019) provides limits of validation and design procedures for these connections.

#### 2.4.1.1. Reduced beam section connection

A reduced beam section connection (Fig. 2.4a) ensures strong-column requirements are met and controls the location of plastic hinging by reducing the beam's cross-sectional area. Welds connect the beam flanges to the face of the column, accompanied by a simple welded or bolted web beam-to-column connection. The reduced area controls the location of yielding and plastic hinging. According to CISC (2019), the beam depth, mass, and flange thickness have certain limitations. For Type D and MD MRFs, the clear span-to-depth should be seven or more, while for Type LD MRFs, it should be five (or more).



**Fig. 2.4.** CISC pre-qualified connections

#### 2.4.1.2. Bolted end-plate connection

Two types of bolted end-plate connections are pre-qualified by CISC (2019): unstiffened and stiffened. A bolted, unstiffened end-plate connection (Fig. 2.4b) uses the end-plate to thicken the column wall (CISC 2019). A bolted stiffened end-plate connection (Fig. 2.4c) uses the end-plate to thicken the column wall and stiffener plates connected to the beam flanges aligned with the beam web to allow more area to transfer the loading into the column (CISC 2019). In both connections, increasing column wall thickness and distribution of loading increases the column strength at the connection to achieve the weak beam-strong column system. The same limitations as above apply to the beam depth, mass, and flange thickness (CISC 2019).

#### 2.4.1.3. Bolted flange plate connection

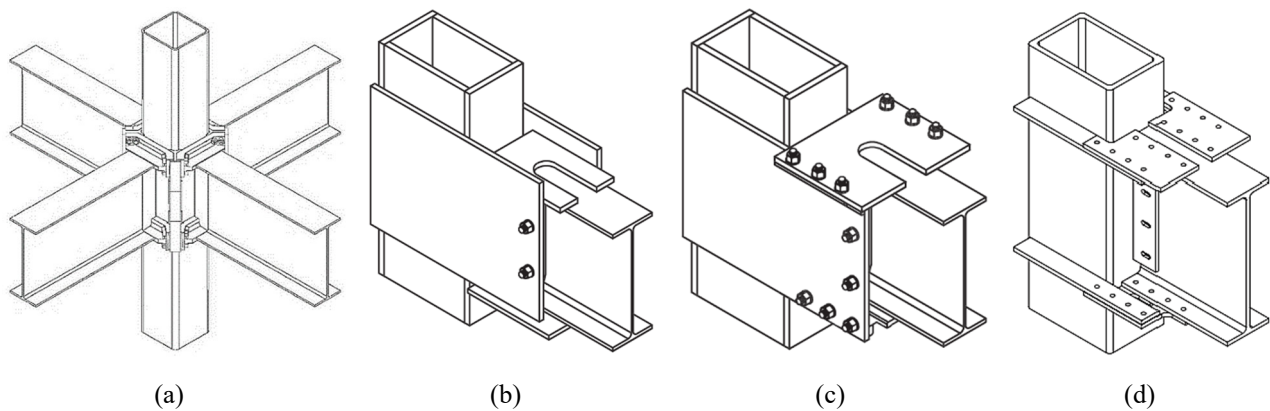
A bolted flange plate connection (Fig. 2.4d) utilizes flange plates to transfer moment into the column (as tension/compression line loading) and a shear tab/angle to transfer the beam shear into the column. Both the top and bottom flange plates must be identical for this connection type (CISC 2019). Flange plates are connected to the column using complete-joint-penetration (CJP) groove welds and high-strength bolts to attach to beam flanges (CISC 2019). The shear connection must be bolted with short-slotted holes (CISC 2019).

## 2.4.2. AISC PREQUALIFIED CONNECTIONS

The following connections have been prequalified for Type D (SMF) and Type MD (IMF) connections according to AISC 358-22 (AISC 2022b).

### 2.4.2.1. Conxtech® ConXL™ connection

Chapter 10 of AISC’s Prequalified Connections for Special and Intermediate Steel Moment Frames for Seismic Applications, AISC 358-22, outlines the design limitations and procedures for the patented ConXL fabrication and manufacturing process. The columns for these connections can be a square 400 mm (16 in) HSS or built-up box column. A sample geometry of a Conxtech® ConXL™ connection is shown in Fig. 2.5a. The entire collar flange assembly is required on all sides of the column, even if no beam is present. This means that all beam-to-column connections in the system are moment-resisting, creating redundancy within the structure and allowing reduced framing sizes to be used.



**Fig. 2.5.** AISC pre-qualified connections (AISC 2022b)

### 2.4.2.2. The Side Plate® connection

Chapter 11 of AISC’s Prequalified Connections for Special and Intermediate Steel Moment Frames for Seismic Applications, AISC 358-22, outlines the design limitations and procedure for The Side Plate® connections. This patented connection utilizes inter-connecting plates to connect beams to columns. The connection is designed to avoid contact between the column face and the beam end. Due to the use of box or RHS columns, the connection must be uniaxial (AISC 2022b). Flange cover plates connect the beam flanges to the column faces allowing the use of unmatched widths. Parallel full depth side plates that connect the beam and column. There are two categories of The Side Plate® connection, The first is the field-welded connection (Fig. 2.5b), and the second is the field-bolted connection (Fig. 2.5c) (AISC 2022b).

### 2.4.2.3. DuraFuse connection

Chapter 12 of AISC's Prequalified Connections for Special and Intermediate Steel Moment Frames for Seismic Applications, AISC 358-22, describes the design and applications of the DuraFuse Frames moment connection. These connections satisfy the requirements of IMF and SMF connections depending on the constraints applied. These connections work with wide-flange beams (or built-up I-shaped members) connected to any shape permitted in section 2.3 of AISC 358 (including HSS columns). Fig. 2.5d shows the connection when configured with an HSS column (or box), where the sides of the column function as the cover plates and four additional external continuity plates extending past the column's face are added. This connection's behaviour varies from the traditional moment connections because rather than having the beam form a plastic hinge, this connection incorporates a fuse plate that acts as the yielding element to make repairing the structure after a seismic event more feasible and economical (Richards 2022).

### 2.4.3. NON-QUALIFIED CONNECTIONS

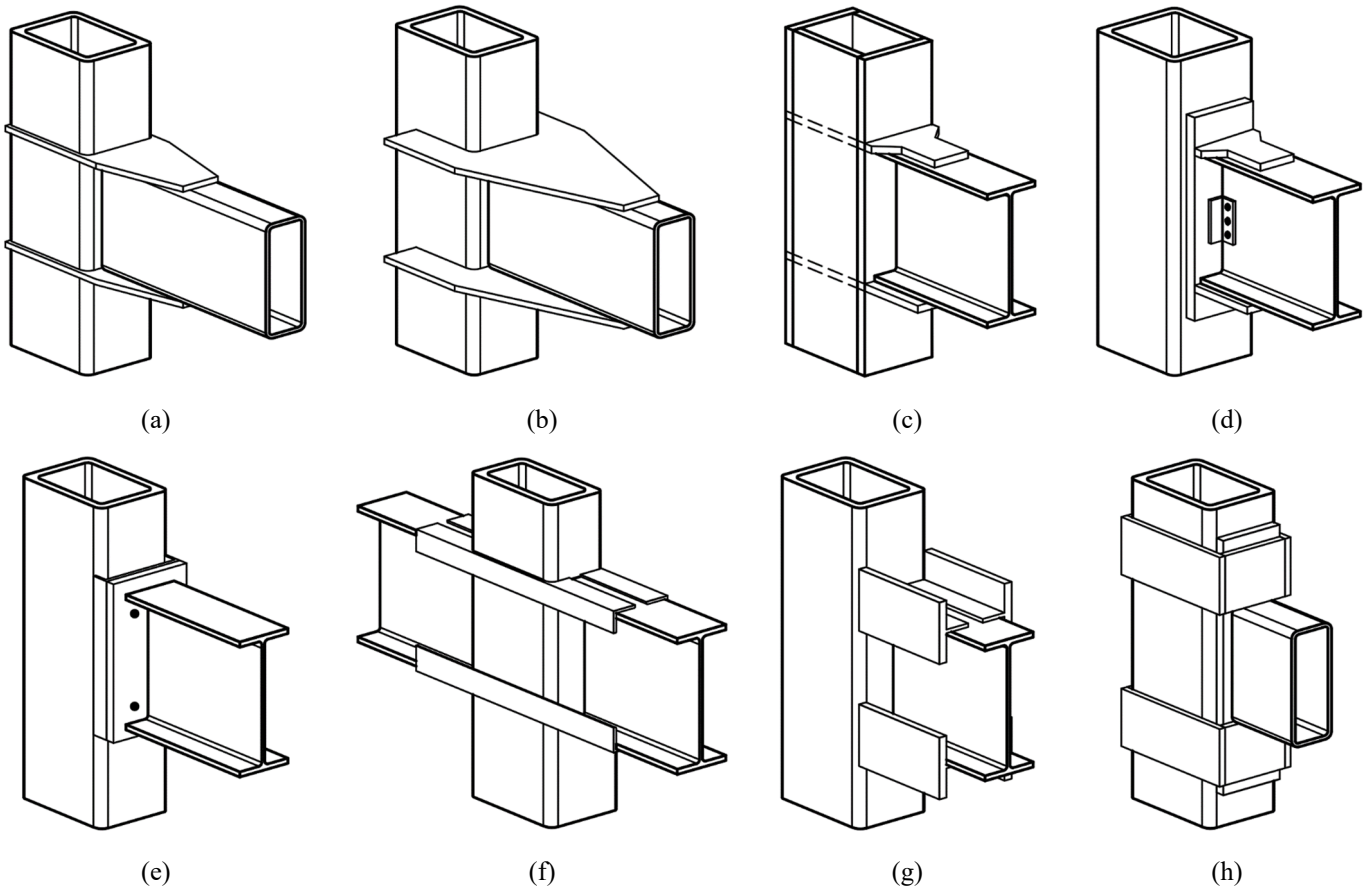
The following connections have been tested to determine how the connection maintains moment resistance under large inelastic deformations (0.02 rad - 0.04 rad). Many of the following connections need to be adapted by codes before they can be officially deemed as pre-qualified.

#### 2.4.3.1. Unreinforced weld connection

Two configurations of unreinforced welded connections were tested by Fadden et al. (2015) as a baseline connection, as these are common for static loading situations. The study used an HSS254 × 254 × 15.9 column paired with a matched (HSS304.8 × 203.2 × 90.5) and unmatched (HSS304.8 × 203.2 × 90.5) beam member. Both unmatched and matched connections maintained 80%  $M_{pb}$  until a rotation of 0.04 radians.

While this connection type meets the rotation requirements, a non-ductile failure mode (toe fracture of the CJP weld in the column base metal) governed in the tests conducted.

Reviewing the limited test data available, an un-reinforced connection would pre-qualify for an AISC 341-22 OMF connection but not a CSA S16:19 Type LD MRF connection. More tests on varying geometry and a parametric study would be required to understand this connection type better.



**Fig. 2.6.** Non-qualified connections

#### 2.4.3.2. Through flange plate connection

Fadden et al. (2015) also tested through flange plate connections, shown in Fig. 2.6a, and determined that the use of an RHS beam had an initial failure of plastic hinging of the beam, sometimes followed by local buckling at the plastic hinge region. Test data also confirmed that this connection type could maintain at least 80%  $M_{pb}$  at a rotation of 0.56 radians which would qualify this connection as suitable for a Type D MRF according to CSA S16:19.

#### 2.4.3.3. External diaphragm plate connection

Tests analyzed by Fadden et al. (2015) showed that external diaphragm plates (Fig. 2.6b) performed similarly to through flange plate connections with an RHS beam. At least 80%  $M_{pb}$  at a rotation of 0.53 radians was reported by Fadden et al. (2015), which theoretically qualifies this type of connection as suitable, according to CSA S16:19, for a Type D MRF. Fadden et al. (2015) noted that the external diaphragm plate connections were easier to fabricate than the similar through flange plate connections as no modification to the column is required.



#### 2.4.3.4. External flange plate connection

Gholami et al. (2013) tested connections similar to through flange plates, with the modification of installing continuity plates inside a box column instead of cutting and inserting the flange plates. These connections were tested using W-section beams shown in Fig. 2.6c. Plastic hinging and no damage to the column were observed during tests (Gholami et al. 2013). These connections meet the requirements for Type D or SMF connections.

Similar connections that used a doubler plate to reinforce the RHS column (Fig. 2.6d) instead of internal continuity plates were tested by Dawe & Grondin (1990). A range of rotations were measured for 80%  $M_{pb}$ , meaning this connection type could qualify for all types of ductile connections. More tests would be required to determine the limitations for each connection class. Dawe & Grondin (1990) also determined failure modes for this connection type and created design aids.

#### 2.4.3.5. Reverse-channel connection

Al Hendi & Celikag (2015) investigated the use of reversed channels (Fig. 2.6e) and double reverse angles, where the angles only exist behind the endplate at bolting locations. These connections achieved adequate rotation capacity but had a governing failure mode of bolt pull-out. Al Hendi & Celikag (2015) did not report what rotation 80%  $M_{pb}$  was maintained at and did not specify if beam plastic hinging occurred before bolt failure. Further investigation would be required to determine if this connection type would be economical and meet the qualification requirements of both AISC and CSA.

#### 2.4.3.6. Strap plate and angle connection

Strap plates and angles were analyzed by Picard & Giroux (1976). They tested three different geometries, the first used plates that created a continuous connection from the beam flanges to the column face; the second used angles coped to fit tight to the column surfaces (Fig. 2.6f) and the third used angles with cut-outs at areas of high-stress concentrations. The beam width must be matched to the column width for these connections.

Most of the tests completed by Picard & Giroux (1976) were stopped due to large deformations and not brittle failure meaning these connections are well suited for seismic applications. While the test sequence did not match that of CSA S16:19 and AISC 341-22, all tests maintained a minimum of 80%  $M_{pb}$  around 0.02 radians. More tests and analysis are required to understand better if these connections could be prequalified for use in a Type LD or more ductile MRF.

#### 2.4.3.7. T-Stiffener connection

Shanmugan et al. (1991) tested T-stiffeners in various configurations, including with and without internal continuity plates; one example configuration is shown in Fig. 2.6g. The limited tests performed show that these connections for box columns and w-shape beams perform well with initial loads and rotations. This performance is needed for Type LD MRF connections. More tests and sensitivity studies are required to determine if T-Stiffener connections may be possible for Type MD or Type D connections.

#### 2.4.3.8. Collar connection

Wei & McCormick (2017) tested collar connections that utilize shop welded collars to slip over the beam endplate in the field, allowing a smooth field erection, shown in Fig. 2.6h. Tests were conducted using RHS columns and beams. Results showed that these connections meet the requirements of Type D connections.

#### 2.4.3.9. Additional connections

Packer & Henderson (1997) provides additional connection types that research has not been conducted to better understand the behaviour under cyclic loading. One connection type is a continuous beam connection, which provides a direct moment transfer from the beam to the column (Packer & Henderson 1997). One disadvantage of this connection type is that the columns of a building are not continuous and must be terminated at each floor. Another is a Japanese-developed connection that thickens the wall of an HSS column by wrapping it with steel angles. Then beam end-plate is attached using steel studs or blind bolts. An additional reference for this connection is Tabuchi et al. (1994), but it is not publicly accessible.

### 2.4.4. SUMMARY OF CONNECTION TYPES

As discussed in the forgoing sections, many moment connections have been developed and tested for use in North America; however, not all connections are well-defined for use with RHS columns or in Type LD/OMF MRF assemblies. Table 2-2 summarizes the beam and column configurations that have been tested and the speculated MRF connection class from a review of the connections. Of the connections reviewed, 62.5% have been tested with RHS columns, with the remaining 37.5% were tested only using box columns (which are not considered a practical replacement column type). From this summary of available connections, it would appear that RHS columns are feasible to meet the connection performance requirements specified by CSA S16:19.

**Table 2-2.** Beam-to-column configurations and ductility classes for available moment connections

Connection	Column		Beam		Type D	Type MD	Type LD
	Box	RHS	W-section	RHS	(SMF)	(IMF)	(OMF)
Reduced beam section	X		X		X	X	X
Bolted unstiffened end-plate	X		X		X	X	X
Bolted stiffened end-plate	X		X		X	X	X
Bolted flange plate	X		X		X	X	X
Conxtech® ConXL™	X	X	X	X	X	X	X
The Side Plate®	X	X	X	X	X	X	X
DuraFuse Frames	X	X	X		X	X	X
Unreinforced weld		X		X			X
Through flange plate		X		X	X	X	X
Flange & continuity plates	X		X		X	X	X
Flange & doubler plates		X	X		X	X	X
External diaphragm plate		X		X	X	X	X
Reverse-channel		X	X				X
Strap plate and angle		X	X				X
T-Stiffener	X		X				X
Collar		X		X	X	X	X

## 2.5. RESEARCH OVERVIEW

To summarize what has been previously presented: RHS columns are well-suited for Type LD MRFs on the perimeter of a building in which the demands include bi-axial bending and/or high axial loads. Type LD MRFs or better are required for specific high importance and all post-disaster buildings in Canada. However, CSA S16:19 Clauses 27.4.4.1a) and 27.4.4.1b) provide only a few prequalified options for Type LD MRF beam-to-column connections, which inadvertently preclude the use of rectangular hollow section (RHS) columns as shown in Sections 2.3.1 and 2.4.1. In comparison, AISC 341-22 requires OMF beam-to-RHS column connections to be designed for a specified moment and shear resistances ( $M_u$  and  $V_u$ ). Considering the Canadian steel design code references the testing requirements defined in AISC 341 and has similar rotation requirements, these design procedures vastly differ from each other.

Thus, this research investigates if connections designed to AISC 341-22 design requirements for OMF connections meet the performance requirements of CSA S16:19 Clause 27.4.4.1c) for Type LD MRF beam-to-column connections. Although numerous connections are worth investigating from the literature review (Section 2.4), only two connection types were selected for this study. The connection types of a T-Stiffener connection without continuity plates (T-Stiffener connection) and an external diaphragm plate connection (Doubler Plate connection) were chosen (after consultation with local fabricators) as they are economical and easy to fabricate. The chosen connections were designed using existing non-seismic moment connection procedures (Ting et al. 1993, Packer & Henderson 1997) and connection design requirements defined in CSA S16:19 and AISC 360-22.

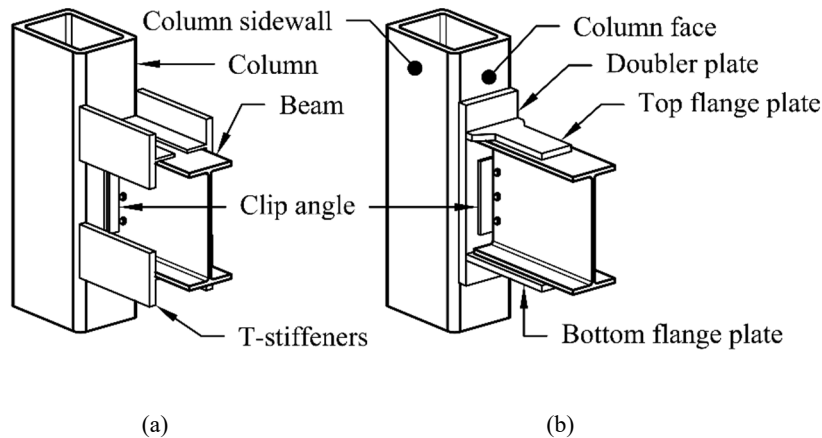
In this study, three connection assemblies were created for each connection type. One assembly was tested under static conditions to determine its yielding, stiffness, and ductility behaviours. Then two connection assemblies were tested under cyclic loading, in accordance with the requirements of CSA S16:19 Clause 27.4.2.1c) and Annex J, to observe their moment vs. rotation behaviour. The results of the experiments were analyzed to assess whether the connections meet the CSA S16:19 pre-qualification requirements for Type LD moment connections, and to compare the low seismic moment connection design requirements of CSA S16:19 and AISC 341-22. This thesis concludes with a summary of the findings, recommendations for CSA S16, and future research.

# Chapter 3: MOMENT CONNECTION DESIGN

## 3.1. CONNECTION DESIGN PHILOSOPHIES

Due to the limited design guidance in CSA S16, the W-section-to-RHS beam-to-column connections for the case study MRF (Section 1.2) were designed using the prescriptive requirements (i.e., for  $M_u$  and  $V_u$ ) in AISC 341-22. It is speculated herein, that these requirements will produce connections that meet or exceed the required performance in AISC 341-22 Section K.2 (and, hence, CSA S16:19 Clause 27.4.4.1c). The two connections designed in this thesis, the T-Stiffener connection and the Doubler Plate connection, have been researched prior but were never tested to meet the requirements on CSA S16 or AISC 341-22 pre-qualification.

Using finite-element analysis, Ting et al. (1993) investigated I-beam to box-column connections with external T-shaped stiffeners. They developed and recommended a design procedure defined in Section 3.1.1 with some additional modifications made according to a discussion on the paper by Iwankiw (1994). Dawe & Grondin (1990) completed tests on full scale connections and identified failure modes discussed in Section 3.1.2. Also discussed in the following section are the four basic failure modes identified by Packer & Henderson (1997). The connection concepts (i.e., the T-Stiffener and Doubler Plate reinforced moment connections) were configured and detailed with the input of a local fabricator in Windsor Junction, NS, to ensure their feasibility for off-site fabrication and on-site erection. As shown in Fig. 3.1, both connections include a 10 mm gap between the beam and column members and a beam clip angle to aid in erection. The clip angle was designed using Table 3-40a in the CISC's Handbook of Steel Construction (CISC 2021) for a required shear strength of  $V_u$ .



**Fig. 3.1.** T-Stiffener (a) and Doubler Plate (b) reinforced moment connections

### 3.1.1. T-STIFFENER CONNECTION

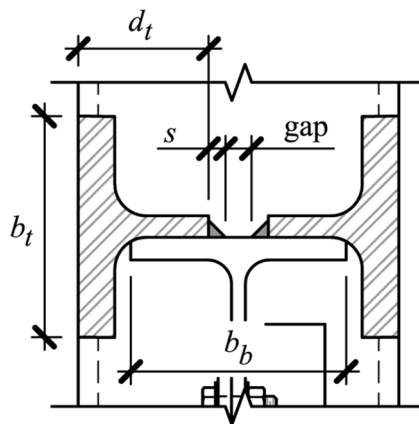
The T-Stiffener reinforced connection was designed based on experimental and finite-element (FE) work by Ting et al. (1991, 1993) and Shanumugan et al. (1991). The theoretical methods were compared to experimental results for 4-way connections (Ting et al. 1993). The stiffeners were shown to serve two main purposes: (1) they increase the moment of inertia of the effective cross-section at that column face [beyond that of the beam ( $I_b$ )] – thereby increasing both strength and stiffness; and (2) they broaden the beam flanges – thereby helping to transfer forces from the beam into the sidewalls (rather than the unsupported face) of the RHS. The connection components are labelled in Fig. 3.1a, shown previously.

#### 3.1.1.1. Stiffener Web Thickness

To prevent premature yielding of the T-stiffener, it has been recommended by Ting et al. (1993) and Packer & Henderson (1997) that the stiffener web thickness ( $w_t$ ) be taken as greater than or equal to  $0.50t_b$  (where  $t_b$  = beam flange thickness).

#### 3.1.1.2. Stiffener Cross Section

The width of the T-stiffener web section is based on the available width of the W-section beam flange. A length ( $d_t$ ) should be chosen so that two fillet welds could be installed on the inside faces on the T-stiffener webs as shown in Fig. 3.2. To ensure that  $1.1R_yZ_b$  of the beam could be transferred through the T-stiffeners into the column the section modulus ( $Z_t$ ) of the four T-stiffeners was set equal to or greater than  $1.1R_yZ_b$ , and this inequality was used to select the T-stiffener flange width ( $b_t$ ). Additionally, the shear and tensile resistances for the weld located on the T-stiffener flanges and web was checked to be sufficient for the given values of  $d_t$  and  $b_t$  which affect the weld area. Appendix A, Section A.4.5 shows detailed calculations.



**Fig. 3.2.** T-Stiffener cross-sectional area and dimensions

### 3.1.1.3. Stiffener Length

If one assumes a load dispersion angle of  $20^\circ$  from the beam flange/T-stiffener junction to the corner of the RHS (Packer & Henderson 1997), the criteria for the minimum T-stiffener length ( $l_s$ ) (to ensure the T-stiffeners are sufficiently stiff) is:

$$l_s \geq \frac{b_0 - b_b}{2 \tan 20^\circ} \quad (3.1)$$

where  $b_0$  = column width and  $b_b$  = beam-flange width.

For strength, Iwankiew (1994), in conjunction with Ting et al. (1993), recommended that for each stiffener, the load on one stiffener should be equal to equal to the net effective strength of the stiffener flange ( $T_1$ ) plus the factored tensile strength of the stiffener web ( $T_2$ ) based on the stress distribution at failure on the beam flanges and stiffeners are as shown in Fig. 3.3.

$$l_s \geq \frac{0.5T_u - (A_{ne})F_{yt}}{\sqrt{3}w_t F_{ut}} \quad (3.2)$$

where  $A_{ne}$  = net effective area for shear lag according to CSA S16:19 Clause 12.3.3.3;  $F_{yt}$  = specified minimum yield stress of the T-stiffener;  $w_t$  = T-stiffener web thickness; and  $F_{ut}$  = specified minimum tensile strength of the T-stiffener. Iwankiew (1994) discussed that it would be reasonable to ignore the contribution of the T-stiffener web in the calculation of  $A_{ne}$  in Eq. (3.2).

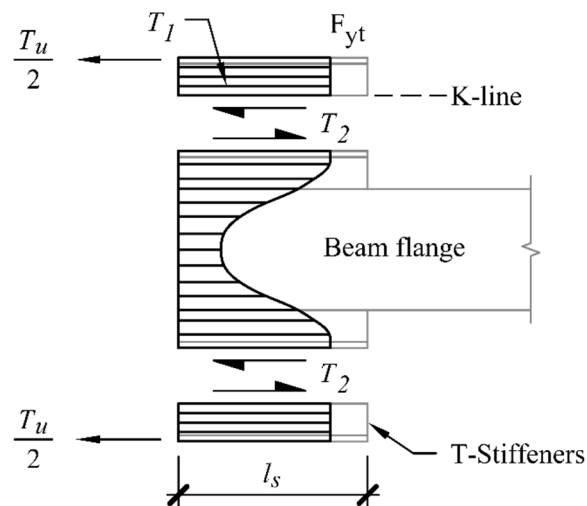


Fig. 3.3. T-Stiffener connection shear distributions at failure

A further criterion for determining  $l_s$  is the required length of the longitudinal weld(s) to connect the T-stiffener to the beam. If fillet welds are used, then according to CSA S16:19:

$$l_s \geq \frac{\sqrt{2} \times T_u}{0.67 \times \phi_w \times s \times X_u (1.00 + 0.50 \sin^{1.5} \theta_w)} \quad (3.3)$$

where  $\phi_w$  = weld metal resistance factor (= 0.67);  $s$  = fillet weld leg size;  $X_u$  = ultimate strength of the weld (nominally 490 MPa for the current study); and  $\theta_w$  = angle (in degrees) between the weld axis and the applied force (= 0° for a longitudinal weld). The weld size,  $s$ , was selected to be the maximum fillet weld size allowed based on the T-stiffener web thickness (i.e.,  $s = w_t - 2$  mm according to CISC's Handbook (2021)).

### 3.1.2. DOUBLER PLATE CONNECTION

The Doubler Plate connection was initially investigated by Dawe & Grondin in 1990, and they reported eight failure modes for the connection. In 1997 Packer & Henderson continued the work started by Dawe & Grondin (1990) and simplified the design process down to four failure modes. This section will outline and compare the different approaches. The connection components (i.e., the flange plates, doubler plate, column sidewalls and column face) are labelled in Fig. 3.1b, shown previously.

#### 3.1.2.1. Dawe & Grondin (1990)

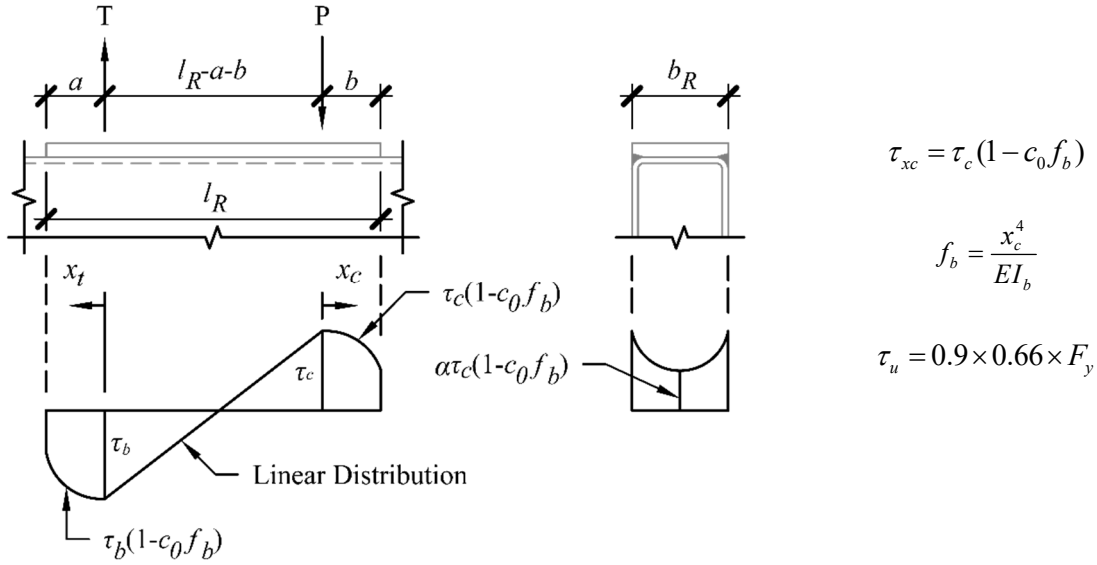
Dawe & Grondin (1990) conducted full scale tests on varying flange plate connections; one set of connections utilized two flange plates and a doubler plate (HW series), and one set of connections that utilized a doubler plate, top flange plate and a seat angle (SL series). Connection designated as HW1 is the type of connection selected for this research project consisting of a web clip angle, a doubler plate and flange plates.

From the full-scale tests, eight failure modes were formulated for the range of connections (i) shear failure of RHS flange, (ii) shear failure of doubler plate, (iii) tension plate failure, (iv) tension flange failure, (v) web crippling of RHS column, (vi) buckling of compression flange plate (vii) web crippling of branch beam, and (viii) Lamellar separation of doubler plate. However, the author considers only the first six failure modes for the HW1 connection. The design equations presented by Dawe & Grondin (1990) are not designer friendly; therefore, Packer & Henderson's (1997) simplification of failure modes were used to design the connections.

The shear distribution presented by Dawe & Grondin (1990) for the first failure mode (i) of shear failure of the RHS flange aided in understanding the development of load within the connection and later provided insight on key locations to instrument the connections during testing. This shear failure is based on the stress that will develop around the perimeter of the doubler plate due to the coupling forces through the flange plates, as seen in Fig. 3.4. This distribution shows that the highest zones of stress will be at the edges of the doubler plate in line with the flange plates. The distribution longitudinally along the length of the doubler plate is



assumed linear between the flange plate action lines, and the outer distributions are calculated using the equation for  $\tau_{xc}$  shown in Fig. 3.4. Transversely along the width of the doubler plate, the distribution is assumed to be parabolic with minimum stress at the midpoint of the doubler plate to be  $\alpha\tau_{xc}$  where  $\alpha = [(b_R - l_R)/b_R]^3$ ,  $b_R =$  the doubler plate width,  $l_R =$  the doubler plate length.



**Fig. 3.4.** Assumed shear distribution around doubler plate

### 3.1.2.2. Packer & Henderson (1997)

Packer & Henderson (1997) refined the work done by Dawe & Grondin (1990) to present four basic failure modes rather than eight and provide connection parameters for validity. The four basic failure modes are presented by Packer & Henderson (1997); (i) effective width rupture of the flange plate(s) or weld, (ii) punching shear of doubler plate, (iii) column sidewall crippling; and (iv) punching shear of column face. Failure mode equations were created by modifying those developed for Plate-to-HSS connections.

#### 3.1.2.2.1. Flange Plates and Welds

Effective width rupture can occur in the tension flange plate or adjacent weld. For the flange plate, the factored moment resistance ( $M_{r1}^*$ ), which is inclusive of a resistance factor, is taken as (Packer & Henderson 1997):

$$M_{r1}^* = h_b F_{yf} t_f b_e \quad (3.4)$$

with

$$b_e = \left( \frac{10}{b_p / t_p} \right) \left( \frac{F_{yp} t_p}{F_{yf} t_f} \right) b_f \leq b_f \quad (3.5)$$

where  $h_b$  = beam height;  $F_{yf}$  = flange plate yield strength;  $t_f$  = flange plate thickness;  $b_f$  = flange plate width;  $b_p$  = doubler plate width;  $t_p$  = doubler plate thickness; and  $F_{yp}$  = doubler plate yield strength. The weld between the flange plate and the doubler plate can be sized by using Eq. (3.5) for the weld effective length in conjunction with Clause 13.13.4.3 of CSA S16:19.

### 3.1.2.2.2. Doubler Plate

Punching shear failure can occur in the doubler plate (on the column face) due to localized loading from the flange plate(s). For this limit state,  $M_{r1}^*$  can be estimated by (Packer & Henderson 1997):

$$M_{r1}^* = 2h_b \frac{F_{yp}}{\sqrt{3}} t_f b_{ef} \quad (3.6)$$

with

$$b_{ef} = \left( \frac{10}{b_p / t_p} \right) b_f \leq b_f \quad (3.7)$$

where  $F_{yb}$  = beam yield strength and  $t_f$  = flange plate thickness.

### 3.1.2.2.3. Column Sidewalls

Web failure of the column sidewall(s) was checked according to the following (Packer & Henderson 1997):

$$M_{r1}^* = 2h_b F_k t_0 (t_b + 5(t_0 + t_p)) \quad (3.8)$$

where  $F_k$  = unit buckling stress of the RHS wall as described by Packer & Henderson (1997) and  $t_0$  = thickness of the RHS column.

### 3.1.2.2.4. Column Face

Punching shear failure of the column face may occur along the doubler plate edge if  $b_p < b_0 - 4t_0$ . For this limit state (Packer & Henderson 1997):

$$M_{r1}^* = 0.25 \left( \frac{F_{y0}}{\sqrt{3}} \right) t_0 (h_p^2 + 2h_p b_p) \quad (3.9)$$

where  $F_{y0}$  = RHS column yield strength and  $h_p$  = doubler plate height.

Packer & Henderson (1997) also recommend checking that  $b_b$  (beam width)  $\leq 0.85b_p$  to avoid premature fracture of the weld between the doubler plate and the column.

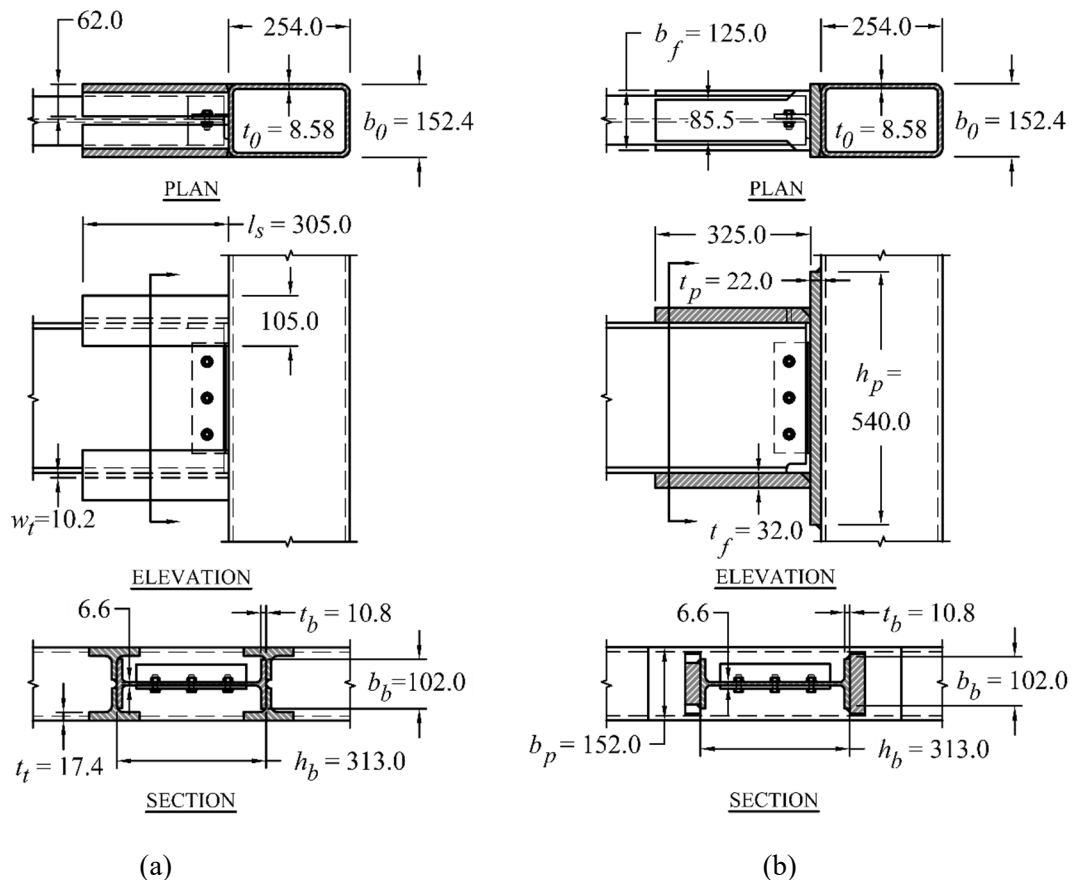
## 3.2. CONNECTION DESIGN SUMMARIES

### 3.2.1. T-STIFFENER CONNECTION

After consultation with local fabricators, W200 × 71 sections were selected for the T-stiffeners so that  $w_t \geq t_b$  to help mitigate local shear failure and allow for large-sized fillet welds to connect each T-stiffener to the beam. A cope was also added to the top flange of the beam to help with on-site erection around the clip angle.

Based on the aforementioned criteria, and accounting for the 10 mm gap between the beam and column (see Section 3.1.1), the T-stiffeners were designed to have a total length ( $l_t$ ) = 305 mm. [Using nominal properties,  $l_s$  required was 69 mm, 37 mm, and 224 mm, respectively, from Eqs. (3.1) – (3.3), detailed calculation in Appendix A].

The T-stiffener webs were attached to the beams using an 8 mm fillet weld along the longitudinal and transverse edges, and a 10 mm partial joint penetration (PJP) flare-bevel groove weld and 10 mm fillet were used to connect the T-stiffener flanges and web, respectively, to the column. A T-stiffener web width of 62 mm was chosen to provide 12 mm gap between the fillet weld toes and a flange width of 105 mm was chosen to provide adequate length of PJP weld to connect the T-stiffeners under tensile loading. The overall layout of the T-stiffener connection is shown in Fig. 3.5a (in which welding symbols have been omitted for clarity).



**Fig. 3.5.** T-Stiffener (a) and Doubler Plate (b) reinforced moment connection design details

### 3.2.2. Doubler Plate Connection

The overall layout of the Doubler Plate connection is shown in Fig. 3.5b and a summary of the  $M_{r,l}^*$  values calculated using nominal connection properties in accordance with Eqs. (3.4) -(3.9) is given in Table 3-1.

**Table 3-1.** Summary of Doubler Plate connection failure moments

Design Criteria	$M_{r,l}^*$ (kNm)
Effective width failure [Eqs. (3.4) & (3.5)]	374
Punching shear failure [Eqs. (3.6) & (3.7)]	434
Column web failure [Eq. (3.8)]	183
Column face failure [Eq. (3.9)]	N/A
Design moment, $M_u$	183

To avoid overhead welding, the top flange plate was tapered (allowing welding on plate edge to beam flange), the bottom flange plate was widened (allowing welding on the beam flange edge to plate), and a fabrication cope was added to the bottom beam flange to allow for the welding of the bottom flange plate to the column. The flange plate length (= 325 mm in Fig. 3.5b) was controlled by the required length of the longitudinal weld between the flange plate and beam (plus the taper, cope, and 10 mm gap) and the flange plate thickness was controlled by the PJP bevel groove weld required to connect the flange plate to the doubler plate. The doubler plate was connected to the column using 10 mm fillets and 10 mm PJP flare-bevel groove welds along its top and side edges, respectively.

## Chapter 4: EXPERIMENTAL PROGRAM

### 4.1. TESTING OVERVIEW

The experimental program of this research was developed to determine if moment connections designed to AISC 341-22 would meet or exceed the performance requirements of CSA S16:19 Clause 27. First, the geometric properties of all six connection assemblies were collected (either at Marid Industries Ltd. during fabrication or on site at the Dalhousie Heavy Structures Lab). Then, the mechanical properties of all materials and heats used for the fabrication were determined through tensile coupon tests and compared to material data sheets obtained from the fabricator (Appendix I).

Initial monotonic quasi-static tests were conducted for each connection type to understand how each connection would behave before applying rotation-controlled cyclic loading to the assemblies. The static tests were conducted in the testing arrangement as detailed in Section 4.5. The static test loading was applied at a constant rate of 4 mm/min until the displacement reached the limit of the actuator (86 mm), and each test took approximately 1 hour to complete.

Then, two cyclic tests were conducted for both the T-Stiffener and Doubler Plate connections in accordance with CSA S16:19 Annex J (see Section 2.3.2) (CSA 2019; AISC 2022a). The same testing arrangement detailed in Section 4.5 was used for the cyclic tests.

Before cyclic tests were conducted, target deflections (Table 4-1) were calculated for the actuator and the string pot (deflection = drift  $\times$  length, where the length was taken from the column face = 1702 mm for the actuator and 1477 mm for the string pot) to control the testing. These values were based off the requirements in CSA S16 Annex J.

In all cases, cyclic testing was initiated with rotation in the positive direction (actuator pushing). Then, once the target string pot deflection was reached, the loading of the actuator was manually reversed to cause rotation in the negative direction (actuator pulling) until the next target deflection. This process was manually controlled and repeated for 32 cycles (target interstorey drift of 0.05 rad) before testing was concluded at the actuator stroke limit.

**Table 4-1.** Cyclic testing string pot target deflection used to control cyclic testing.

Interstorey Drift (rad)	Actuator Deflection (mm)	String Pot Deflection (mm)
0.00375	6.4	5.5
0.005	8.5	7.4
0.0075	12.8	11.1
0.01	17.0	14.8
0.015	25.5	22.2
0.02	34.0	29.5
0.03	51.1	44.3
0.04	68.1	59.1
0.05	85.1	73.9

## 4.2. TEST SPECIMENS

The six connection assemblies (i.e., three for each concept) were fabricated utilizing the details in Fig. 3.5. Each of the assemblies consisted of a single column and a beam attached mid-height on one side. Atlas Tube Ltd. donated the RHS materials ( $HSS254 \times 152 \times 9.5$ ), and all remaining materials were supplied from Russel Metals Inc (via the fabricator). The assemblies were fabricated by Shelden Butler (24 years' experience) and Gordon Densmore (23 years' experience) at Marid Industries Ltd., located in Windsor Junction, Nova Scotia. During the fabrication of each assembly, the doubler plate (where applicable) and the clip angle was first tack welded onto the column, then the beam was lifted using a crane and bolted onto the clip angle. Once the beam was attached, reinforcement elements were aligned snugly to the beam and tack welded onto the beam. This process (Fig. 4.1) ensured all elements fit well once assembled. Finally, when elements were tack welded into their respective locations, the welds designated on the design drawings (Appendix D) were laid. After fabrication, the assemblies were shipped to the Dalhousie Heavy Structure Lab.



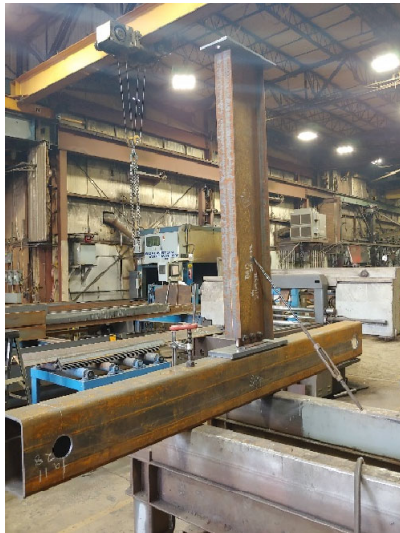
(a) T-stiffeners tack welded



(b) beam fitup



(c) fully welded connection



(d) beam fitup



(e) flange plates tack welded



(f) fully welded connection

**Fig. 4.1.** Fabrication process for the T-Stiffener (a-c) and Doubler Plate (d-f) moment connections

### 4.3. GEOMETRIC PROPERTIES

To ensure accurate dimensions, a distinct notation was assigned to each connection. T-Stiffener prototypes were labeled as T#, while Doubler Plate connections were designated as DP#. Dimensions were collected for the HSS254 × 152 × 9.5 columns, W310 x 33 beams, plates, T-stiffeners, and clip angles and are outlined in Appendix F.



## 4.4. MECHANICAL PROPERTIES

The sections below describe the methods and results of the tensile strength testing as per AISC 341-22 (AISC 2022a) Section K2.6e to satisfy the pre-qualification requirements for both the base metals and the weld metal. Tension testing to fracture (Fig. 4.2) allows the determination of yield strength, yield point elongation, tensile strength, elongation, and cross-section area reduction. All tests were conducted in the 2 MN MTS universal testing machine located in the Dalhousie Heavy Structures Lab at room temperature, 10 °C to 38°C, as defined by ASTM E8/8M-21 (ASTM 2021b). The tensile coupons (TCs) were instrumented with a 50 mm extensometer (Fig. 4.3) to measure the deformation, and the gauge lengths for each TC type were used to determine the strain. All tests had a target run time of 10-30 minutes. A testing rate of 1.5mm/min was used for TC with  $t < 18\text{mm}$  and 2.0mm/min for TC with  $t \geq 18\text{mm}$ . The all weld metal TC's were tested at a rate of 1.0mm/min.



Fig. 4.2. TC post-fracture for base metals and all weld metal

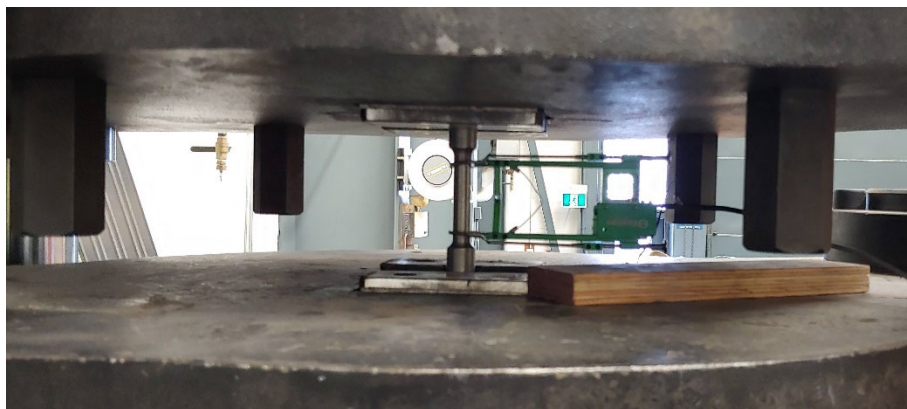


Fig. 4.3. All weld metal TC instrumented and in the 2 MN MTS universal testing machine



#### 4.4.1. BASE METAL TENSILE COUPON TESTS

Marid Industries Ltd. supplied samples of the base material for each heat of each material. The facilities at the Dalhousie Heavy Structures Lab were used to cut these samples into three TCs per each, meeting the requirements of ASTM E8/E8M-21 (ASTM 2021b) sheet-type TCs (Fig. 4.4) recommended to be used for metallic materials with nominal thickness from 13 mm to 19 mm and therefore were used. Fig. 4.5 shows the areas of the sample steel materials for the HSS and W-section that TCs were extracted from.

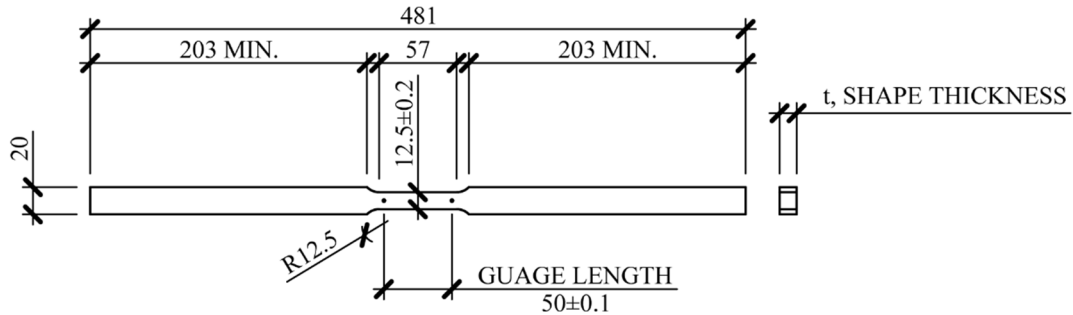


Fig. 4.4. Sheet-type TC from HSS and W-section material

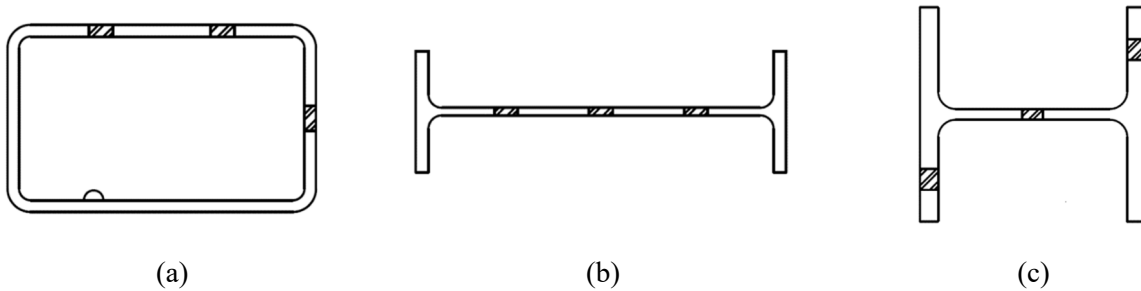
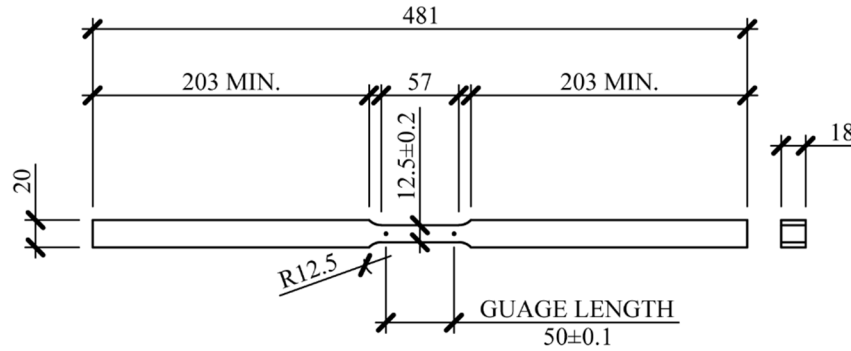


Fig. 4.5. TC location from (a) HSS254 × 152 × 9.5, (b) W310 × 33, and (c) W200 × 71

Sheet-type TCs were also used for the 22 mm and 32 mm thick plate materials. Where the material thickness is outside the recommended range, materials were milled down on top and bottom to a thickness of 18 mm, as shown in Fig. 4.6 and permitted by ASTM E8. Sample materials from Marid Industries Ltd. came in dimensions of plate thickness × 50 mm × 610 mm, and – where possible – multiple coupons were extracted from a sample piece to limit the material waste and amount of work required. Once TCs were cut, the designation and heat numbers were labelled and tracked to ensure coupons were not mixed up.



**Fig. 4.6.** Sheet-type TC from plate material

#### 4.4.2. BASE METAL TENSILE COUPON RESULTS

During the TC tests, both the applied force (by the MTS machine) and elongation (by the extensometer) were recorded. The force was converted into engineering stress by dividing it by the original cross sectional area of the reduced section ( $\sigma = P / A$ , where  $\sigma$  = engineering stress,  $P$  = load from the MTS machine, and  $A$  = original cross-sectional area of the coupon reduced section) and the elongation was converted to engineering strain ( $\varepsilon$ ) using Eq. (4.1):

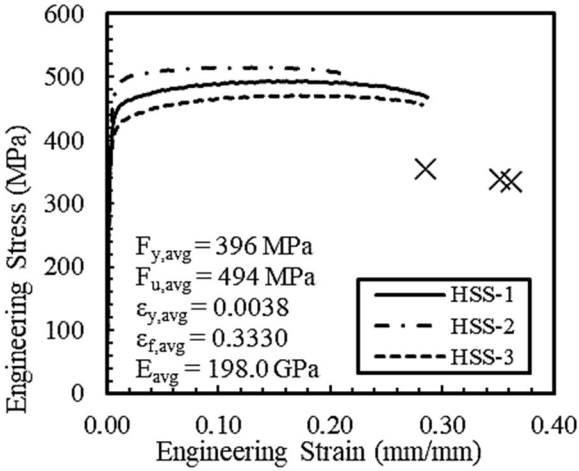
$$\varepsilon = (\Delta L) / L_0 \quad (4.1)$$

where  $\Delta L$  = elongation reading from the extensometer and  $L_0$  = initial gauge length (= 50 mm).

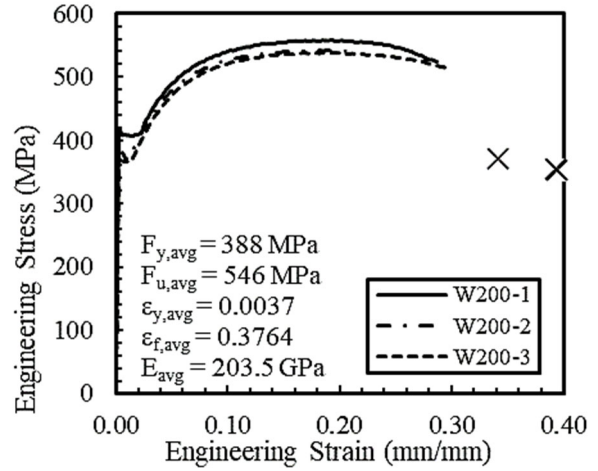
The stress-strain diagrams with three set of data each (one for each coupon) for all base materials for the project are shown in Fig. 4.7. Due to noise being present in the data, a moving average filter was applied to the data to smooth the curves. The yield strength ( $F_y$ ) and yield strain ( $\varepsilon_y$ ) were both determined using the 0.2% offset method. The Young's Modulus ( $E$ ) was then taken as the slope of the 0.2% offset line of the elastic region of the stress-strain curve. The extensometer was removed around a strain of 0.30 mm/mm or when the loading dropped by 30%. The point of fracture (denoted by an  $\times$  on the diagrams) was determined post-testing. The fracture strains ( $\varepsilon_f$ ) were calculated using Eq. (4.2) where  $L_f$  was measured by joining the fractured pieces back together after the tensile coupon failed and remeasured the gauge length. The fracture stresses ( $F_f$ ) were calculated by dividing the final load (i.e., just before rupture) by the original cross-sectional area of the TC. Key average base metal properties are summarized in Table 4-2.

$$\varepsilon_f = (L_f - L_0) / L_0 \quad (4.2)$$

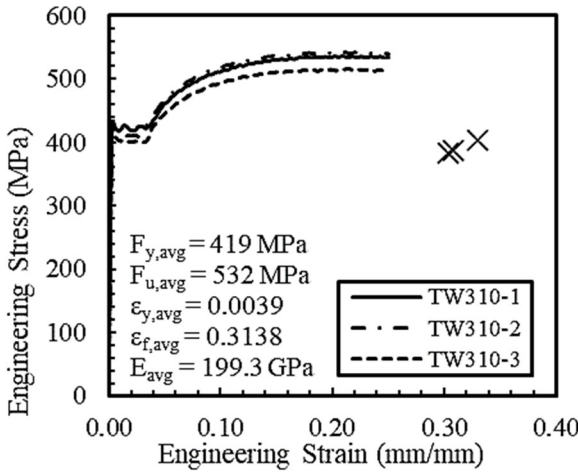
where  $L_f$  is the gage length after failure.



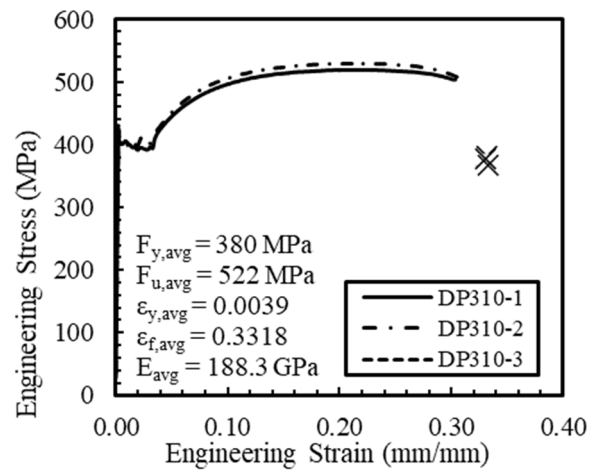
(a) HSS254 × 152 × 9.5



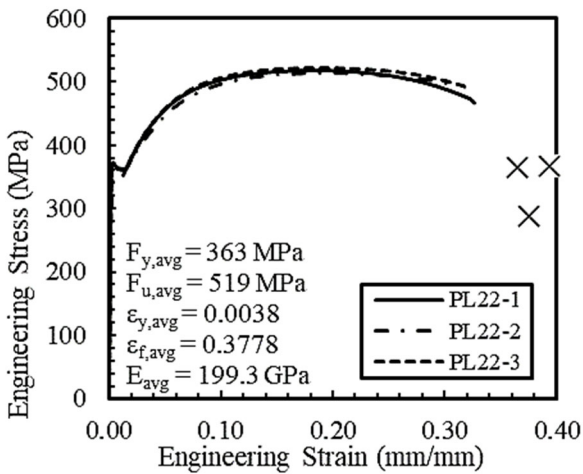
(b) W200 × 71



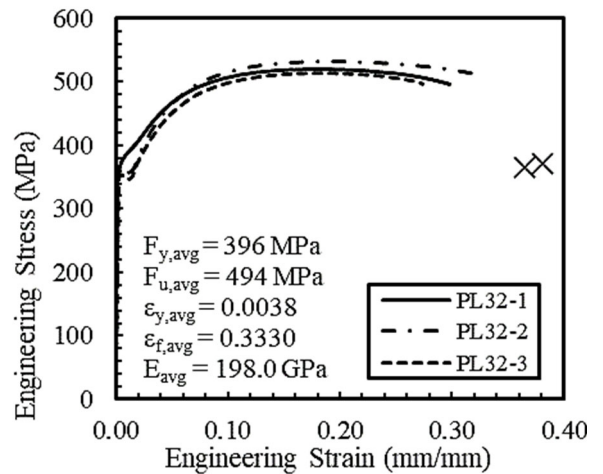
(c) W310 × 33 – HT#D165477



(d) W310 × 33 – HT#D169312



(e) 22 mm PL



(f) 32 mm PL

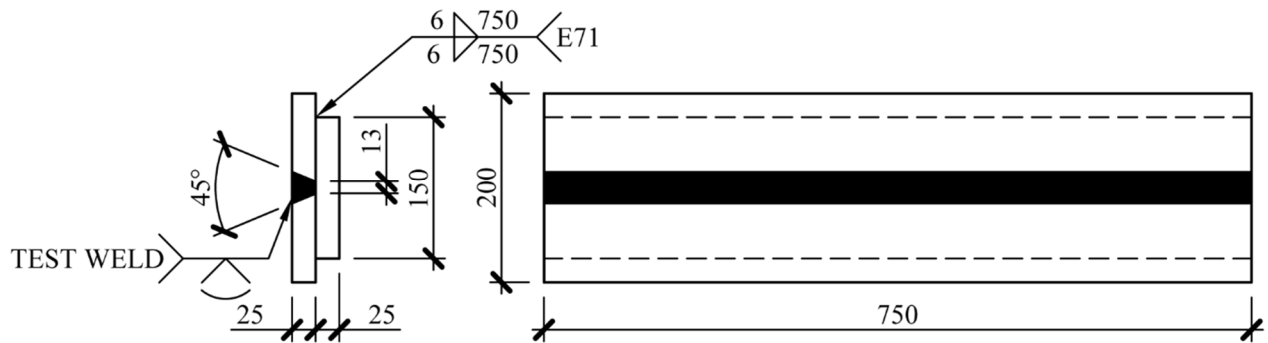
Fig. 4.7. Stress vs. strain curves for base metals

**Table 4-2.** Average base metal property summary

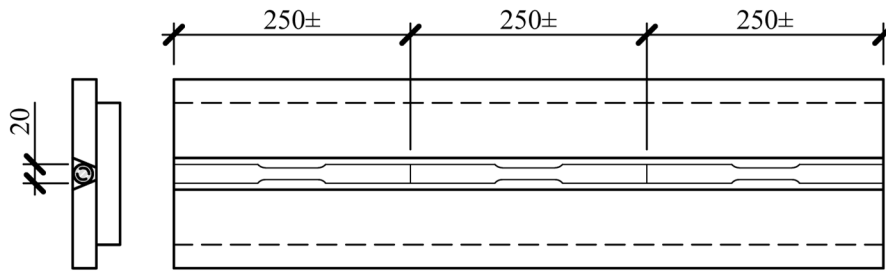
Material	Yield Strength, $F_y$ (MPa)	Ultimate Strength, $F_u$ (MPa)	Yield Strain, $\epsilon_y$ (mm/mm)	Ultimate Strain, $\epsilon_f$ (mm/mm)	Young's Modulus, $E$ (GPa)
HSS254 × 152 × 9.5	396	494	0.0038	0.3330	198.0
W200 × 71	388	546	0.0037	0.3764	203.5
W310 × 33- HT#D165477	419	532	0.0039	0.3138	199.3
W310 × 33- HT#D169312	380	522	0.0039	0.3318	188.3
22 mm PL	363	519	0.0038	0.3778	199.3
32 mm PL	362	523	0.0038	0.3847	195.0

### 4.4.3. ALL WELD METAL TENSILE COUPON TESTS

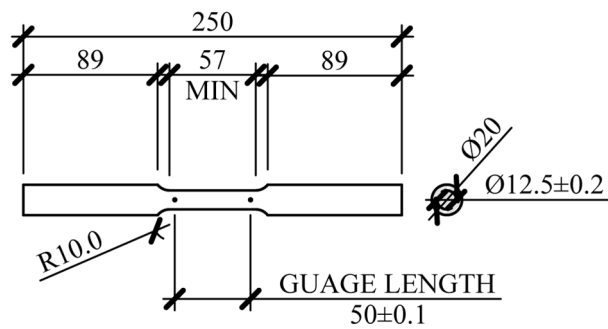
In order to obtain the E491T1 (nominal  $X_u = 490$  MPa) all weld metal samples for TCs, a groove weld was done using multiple passes from the same weld coil (same heat) and under the same conditions as the connections at Marid Industries Ltd. The groove was created by fabricating three plates, as shown in Fig 4.8a and Fig. 4.9, which were then formed into a joint for a V-groove weld. The overall sample was cut into three round TCs, as shown in Fig. 4.8b. Each TC had a minimum length of 250 mm, as requested by the Dalhousie lab technicians for testing in the 2 MN MTS universal testing machine. The round TCs were machined to meet the specifications of ASTM E8/E8M-21 (ASTM 2021b) with a gauge length of four times the nominal diameter, as illustrated in Fig. 4.8c.



(a) All weld metal fabrication arrangement



(b) All weld metal coupon specimen



(c) All weld metal coupon specimen

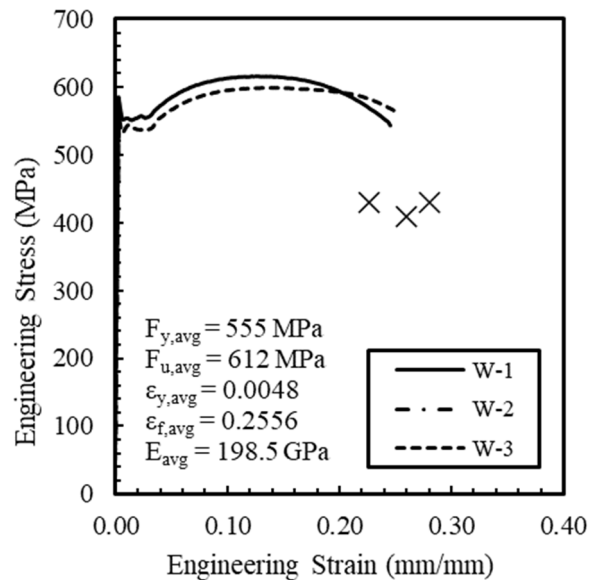
**Fig. 4.8.** Weld metal coupon details



**Fig. 4.9.** All weld metal groove assembly plates fabricated before weld metal added

#### 4.4.4. ALL WELD METAL TENSILE COUPON RESULTS

The stress-strain diagrams for the all weld metal TCs are shown in Fig. 4.10, and – similar to the base material – a moving average filter was applied to smooth the data curves. The values on the graph were calculated using the same process as defined in Section 4.4.2 with the point of fracture determined post-fracture being denoted by the × symbols on the diagram. For test W-2 the extensometer was removed from the coupon at a strain of 0.03 mm/mm and therefore the post-yield behaviour of that coupon is missing from the diagram.



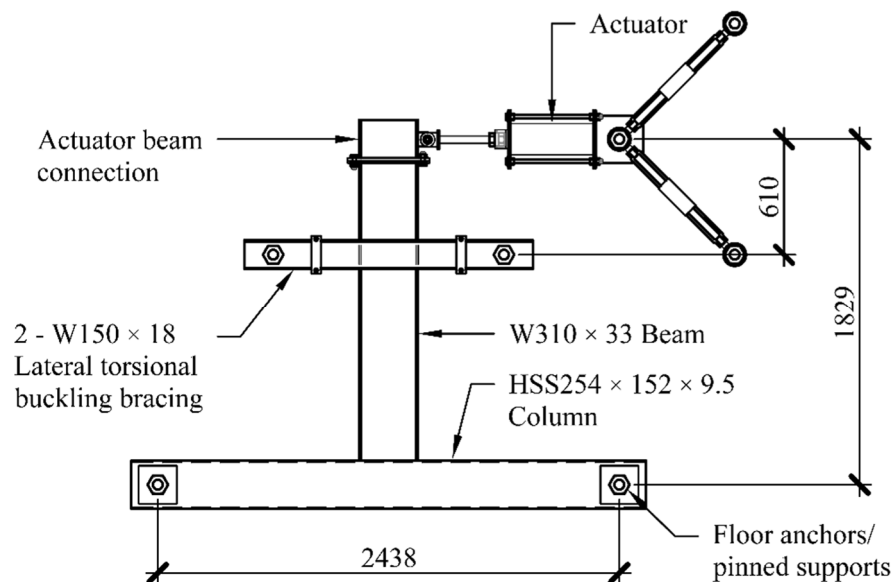
**Fig. 4.10.** Stress vs. strain curves for all weld metal coupons

## 4.5. TEST SETUP AND INSTRUMENTATION

The test setup and instrumentation plan for the large-scale connection tests were created to efficiently use equipment available in the Dalhousie University Heavy Structures Lab. This equipment included a 500 kN actuator, threaded anchor bolts, strain gauges and linear potentiometers.

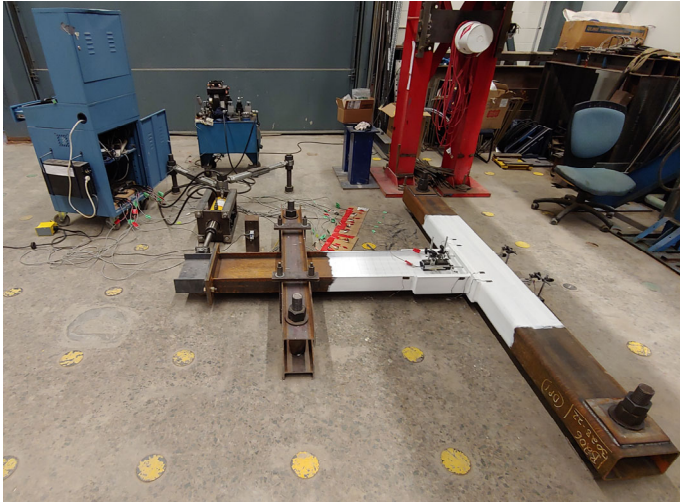
### 4.5.1. TEST SETUP AND ARRANGEMENT

In previous cyclic tests presented in the literature, most were conducted in the vertical orientation (i.e., the column and beam were in a vertical plane) using strong frames or strong walls. However, the tests conducted herein were done in a horizontal orientation to take advantage of the existing 2'-6" thick reinforced strong floor with anchoring locations lined with steel pipes in a 2' × 2' (610 mm × 610 mm) grid. The connection assemblies were then fabricated utilizing the details in Fig. 3.5, and Appendix D. Both assemblies had a column height of 2.7 m and a beam length of 1.8 m. These dimensions were selected to represent the inflection points (points of zero moment) in an MRF with 2.4 m high by 3.6 m long bays. To best mimic the behaviour of a beam located in a moment frame building, the setup required pinned-connected columns and a pivoting connection from the beam to the actuator that would not add any additional torque or strain. The arrangement of the test as shown in Fig. 4.11 and Fig. 4.12a; the column pin connections were created by bolting to the strong floor (Fig. 4.12b) in Dalhousie Heavy Structures Lab.



**Fig. 4.11.** Testing arrangement schematic with dimensions

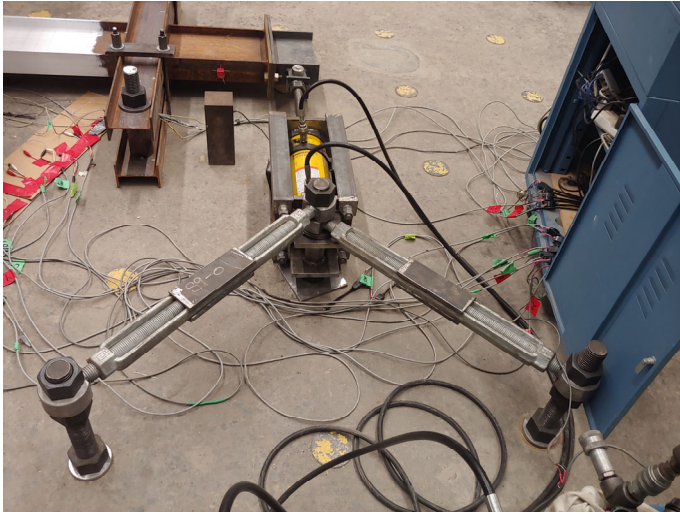




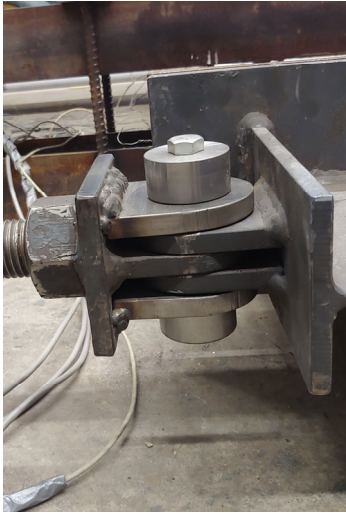
(a)



(b)



(c)



(d)



(e)



(f)

**Fig. 4.12.** Testing arrangement photographs



During fabrication, holes were cut in the HSS on two faces at each end that were slightly larger than required for the bolt; this allowed for some adjustments to be made in the test setup as the anchor locations in the strong floor vary based on location. Additional plates were fabricated to have a bolt hole sized by the recommendations of CSA S16:19 and were welded onto the HSS once in location to ensure snug installation and minimal movement and additional strain would occur during testing. The actuator support, consisting of the actuator casing, three 2" bolts, and two turnbuckles, was also bolted to the strong floor (Fig. 4.12c).

The actuator beam connection was designed to mimic a concentrically applied point load and provide easy reassembly of the test setup. This was accomplished by having a bolted end to the beam to attach at the end where the actuator would apply the loading. Then to prevent additional torsion from being applied by the actuator as loading was applied (during higher rotations), a pinned connection (five interlocking pad eyes with a high-strength steel pin, Fig. 4.12d) was added between the beam and actuator rod.

Finally, the setup was reinforced with two W150 × 18 beams placed 610 mm away from the loading point to prevent lateral torsional buckling (Fig. 4.12e and Fig. 4.12f). During testing, without this bracing, the beams twisted and caused eccentric loading from the actuator. In an actual building system, the attached floor or roofing system would provide lateral bracing. Static and cyclic testing was conducted following the procedures outlined in Section 4.1. Under static loading, the connection assemblies were tested to the actuator's stroke limit. The cyclic test was conducted using a manual deflection control process to meet the testing requirements in CSA S16 Annex J.

#### 4.5.2. INSTRUMENTATION

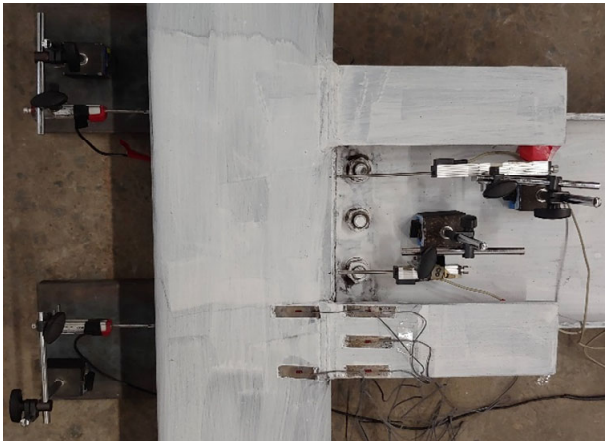
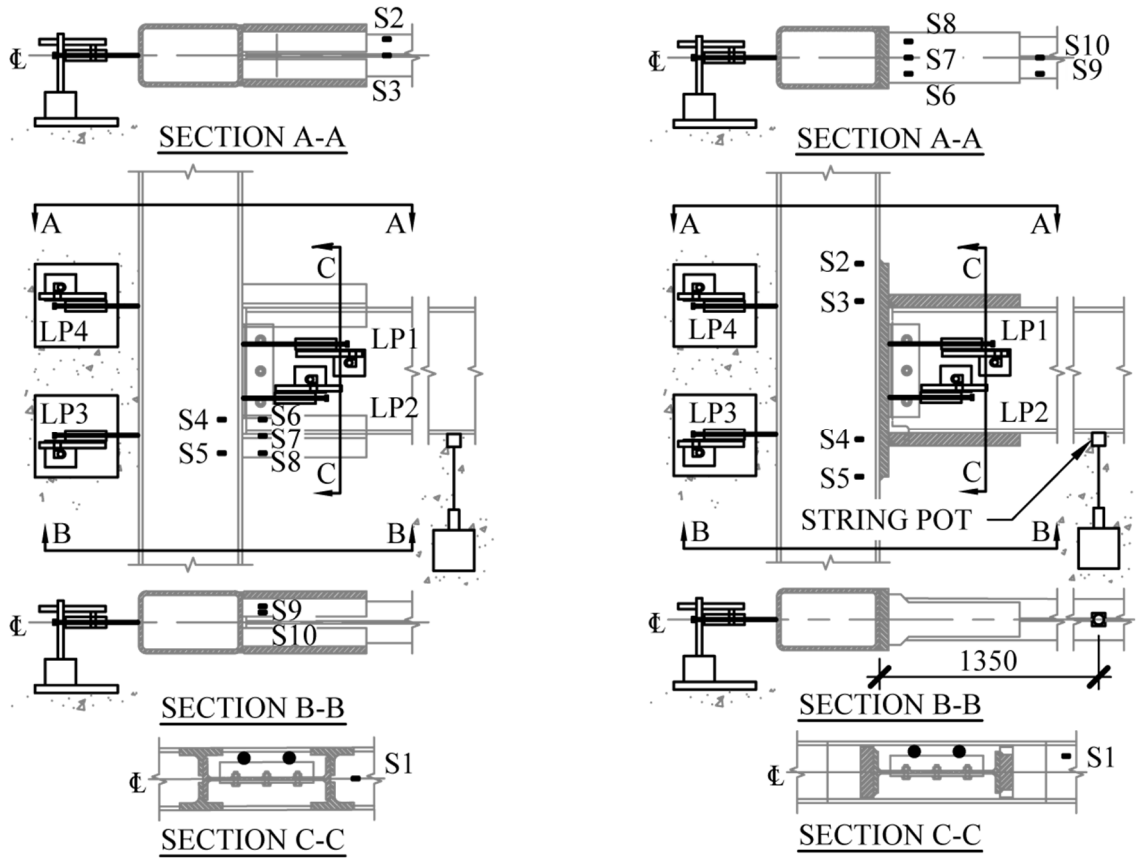
The strain gauge (SG) locations for each prototype varied based on the connection and test type. The static tests, for each of the two connection types, will be instrumented to provide detailed strain readings, and the cyclic tests will include select SGs for comparison of the results to the static test results. Fig. 4.13a and Fig. 4.14a shows the locations of the SGs for the T-Stiffener connections, which are intended to verify: (i) the yielding of the wide flange beam (at the end of the connection); and (ii) the load transfer from the T-stiffeners to the HSS column sidewalls. Fig. 4.13b and Fig. 4.14b shows the locations of the SGs for the doubler-plate connections, which will be used to verify: (i) the yielding of the wide flange beam; (ii) the load transfer from the flange plate(s) to the doubler plate; and (iii) the load transfer from the doubler plate to the column sidewalls.

For the static tests, SGs were installed for the T-Stiffener reinforced connection (see Fig. 4.13a) at the column face above the connection (S1); the beam flanges at the plastic hinge location (S2-S3); the column wall at the T-stiffeners (S4-S5); and the T-stiffeners flanges and web (S6-S10). For the Doubler Plate reinforced connection, SGs were installed: at the column face above the connection (S1); along the doubler plate on the column side wall (S2-S5); on the bottom flange plate (S6-S8); and along the beam flanges at the plastic hinge location (S9-S10) (Fig. 4.13b). The SGs were used to compare experimental strain distributions to those reported in previously in the literature (Ting et al. 1991, Ting et al. 1993, Shanmugan et al. 1991, and Dawe & Grondin 1990).

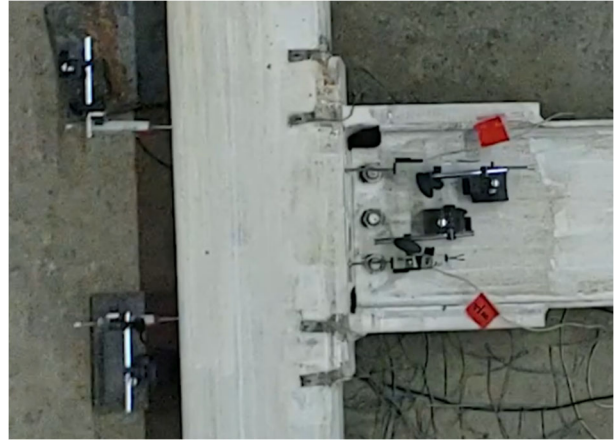
For the cyclic tests SGs were installed for the T-Stiffener reinforced connection (see Fig. 4.14a) at the column wall at the T-stiffeners (S1-S4) and the beam flanges at the plastic hinge locations on both sides of the beam (S5-S6). For the Doubler Plate reinforced connection, SGs were installed: along the doubler plate on the column side wall (S1-S4); on both flange plates (S5 and S7); and along the beam flanges at the plastic hinge location (S6-S8) (Fig. 4.14b).

To determine connection rotation,  $\theta$  (i.e., the relative rotation of the beam with respect to the column), two linear potentiometers (LPs) (LP1 and LP2) were installed on the beam with magnetic bases (see Fig. 4.13 and Fig. 4.14). The LPs were spaced 133 mm apart and centred on the connection work point. Additional LPs (LP3 and LP4) spaced 320 mm apart were anchored to the lab floor (using steel plates and magnetic bases) to calculate the overall column rotation. A string pot anchored on a steel block and connected to the beam flange using a magnetic attachment located 1350 mm from the face of the column (1477 mm from the center of the column) was used to record the beam deflection. The interstorey drift of the connections was calculated using the relationship of drift to the beam's deflection defined by Eq. (4.3) where  $\Delta$  = the deflection reading from the string pot, and  $L$  = the distance from the string pot attachment to the center of the column. Detailed drawings for the detailed instrumentation plan can be found in Appendix E.

$$\text{interstorey drift} = \frac{\Delta}{L} \quad (4.3)$$

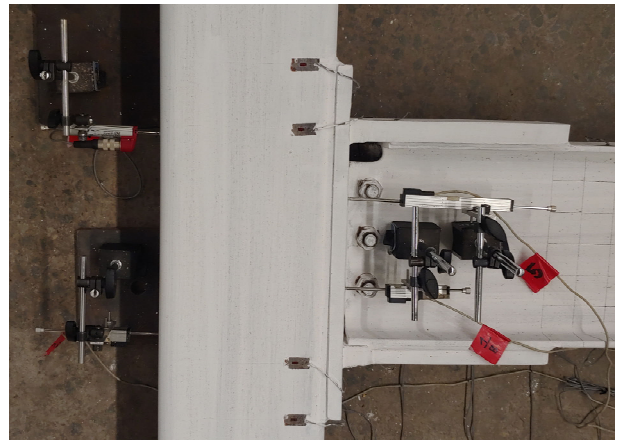
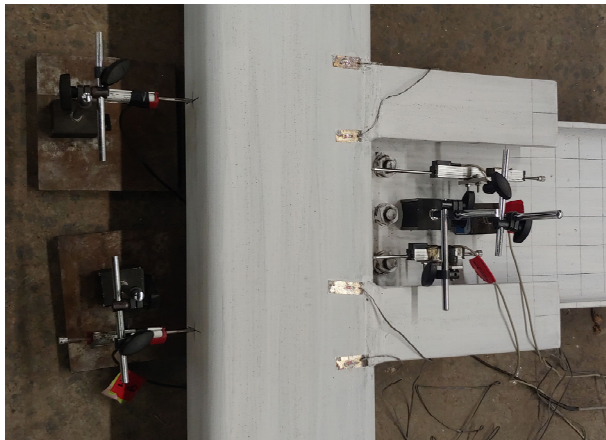
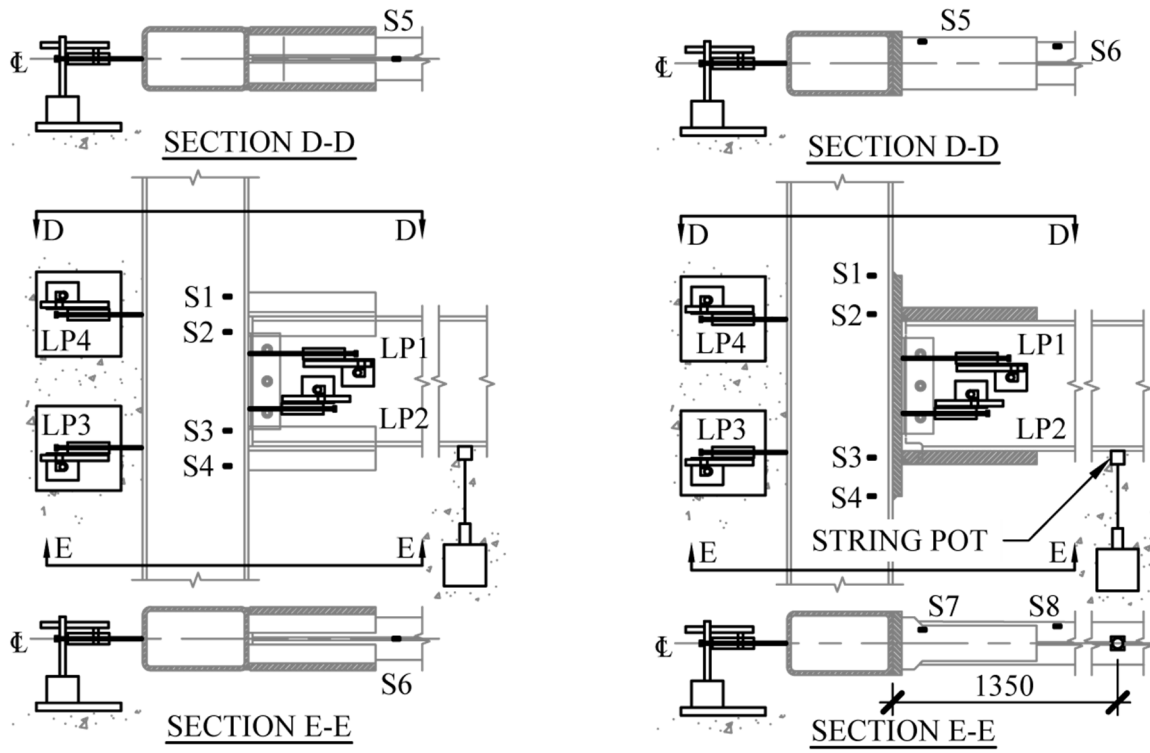


(a)



(b)

**Fig. 4.13.** Instrument locations for static tests (diagram and photographs)



(a)

(b)

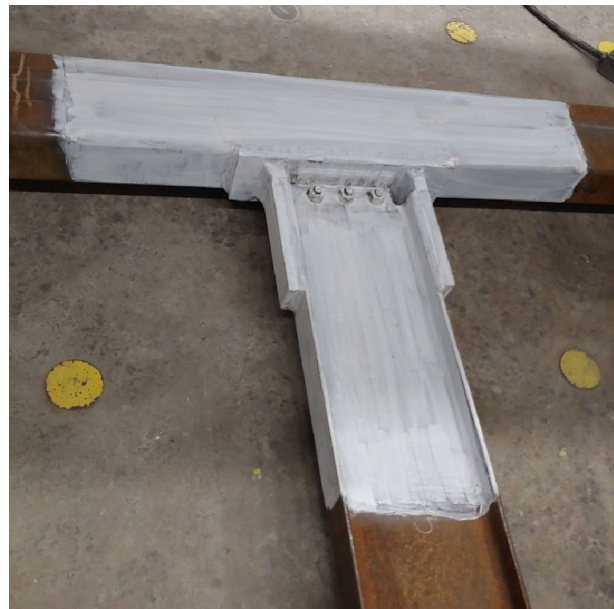
**Fig. 4.14.** Instrument locations for cyclic tests (diagram and photographs)

### 4.5.3. SURFACE TREATMENTS

Before testing the connections, assemblies were cleaned with wire brushes and sanding blocks to remove any accumulated debris or rust. A mechanical sander with various sanding grades was used on local areas for strain gauges. Assemblies were then cleaned with soapy water and rinsed to remove all fine particles remaining in the prepared areas (Fig. 4.15a). Once cleaned, the assemblies were treated with five to six coats of limewash (mixed using the procedure found in Appendix L) until an opaque coverage was achieved (Fig. 4.15b). Lastly, when all limewash coats had been applied and dried completely, a 2" x 2" (50 mm x 50 mm) grid was drawn on the beam web using a pencil to help quantify the yielding/ paint flaking area during testing.



(a)



(b)

**Fig. 4.15.** Photographs of surface treatments applied to connection assembly pre-testing

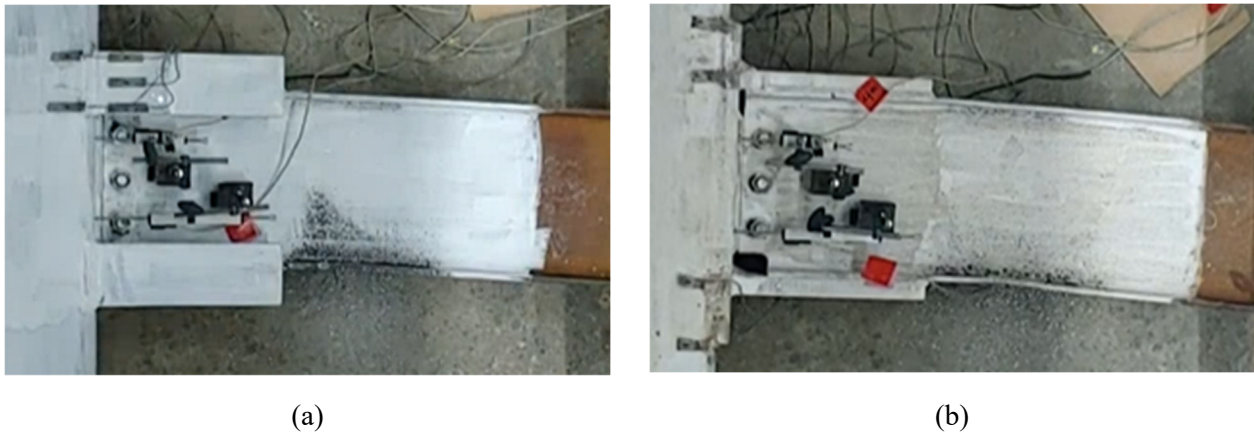
# Chapter 5: EXPERIMENTAL RESULTS

## 5.1. QUASI-STATIC TEST RESULTS

During the static tests, both connections were loaded to a maximum moment of  $M_{max}$  (which corresponded to the actuator stroke limit and not necessarily the ultimate moment of the connection). This section describes the observations and results from the static tests.

### 5.1.1. VISUAL OBSERVATIONS

During both physical tests, yielding began at the end of the connection (i.e., the junction between the T-stiffener or flange plate and the beam) at the extreme fibre (on the compression side) and propagated up towards the neutral axis as loading increased (as indicated by flaking of the limewash) (see Fig. 5.1). Both connections developed a moment of at least  $M_u$  and a shear of at least  $V_u$  at the column face, with plastic hinges evident at distances of 425 mm and 490 mm from the column face for the T-Stiffener and Doubler Plate reinforced connections, respectively. No yielding was observed in the RHS column nor any other elements in the connections.

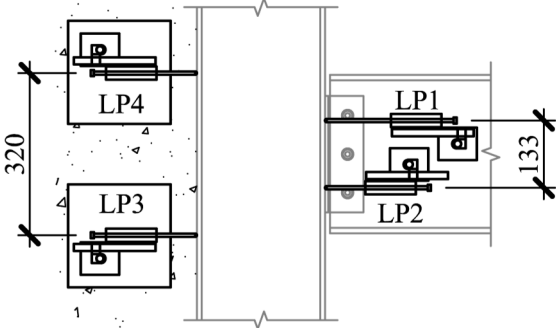


**Fig. 5.1.** Photographs of T-Stiffener (a) and Doubler Plate (b) moment connections (taken after testing)

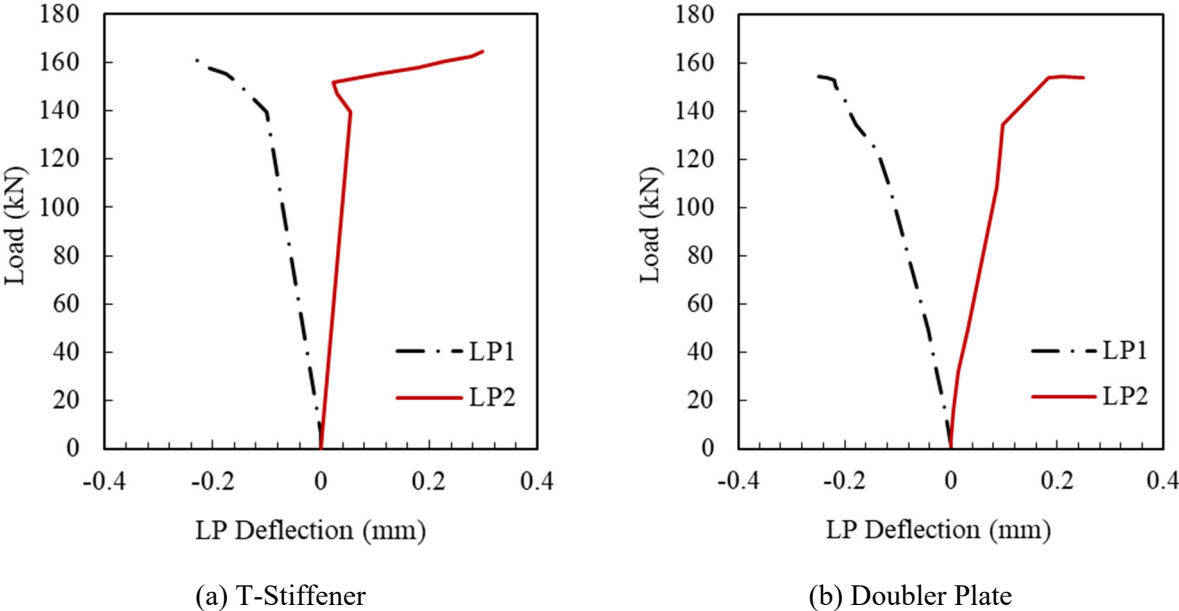


### 5.1.2. INSTRUMENTATION OBSERVATIONS

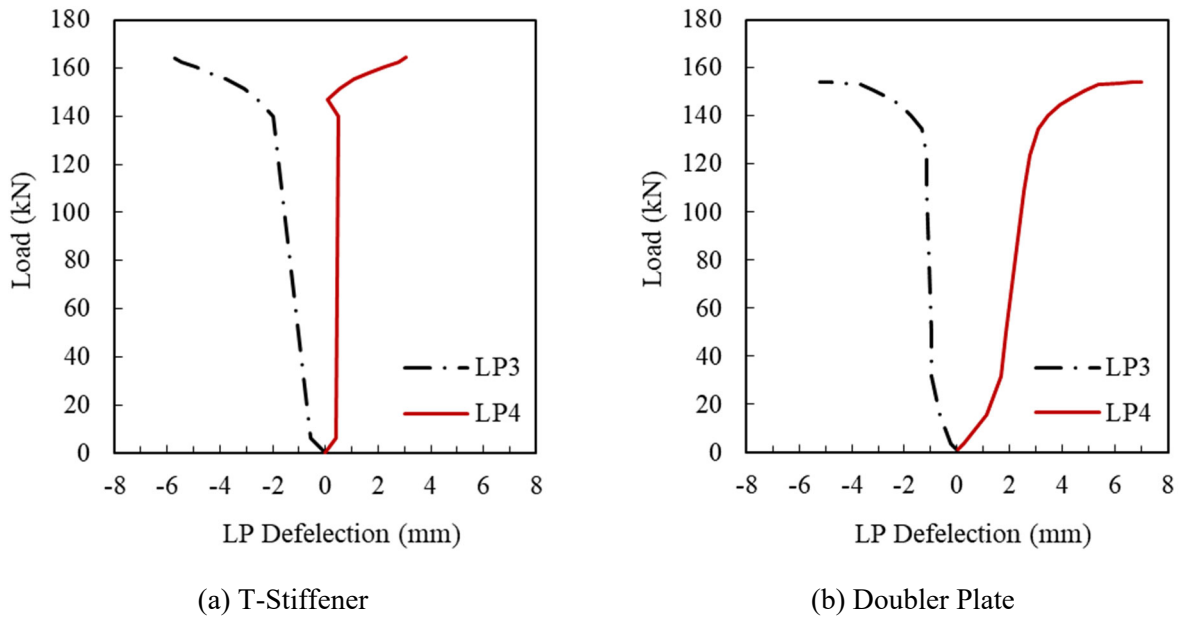
During the static tests, LPs (Section 4.5.2) recorded the deflections of the connection and column at equal distances from the connection work point as shown in Fig. 5.2. As loading was applied to the connection assembly, LP1 and LP3 experienced elongation, while LP2 and LP4 experienced compression. The movement on the connections is shown by Fig. 5.3 and column movement is shown in Fig. 5.4. Additionally, the beam deflection was recorded by the string pot (Fig. 5.5).



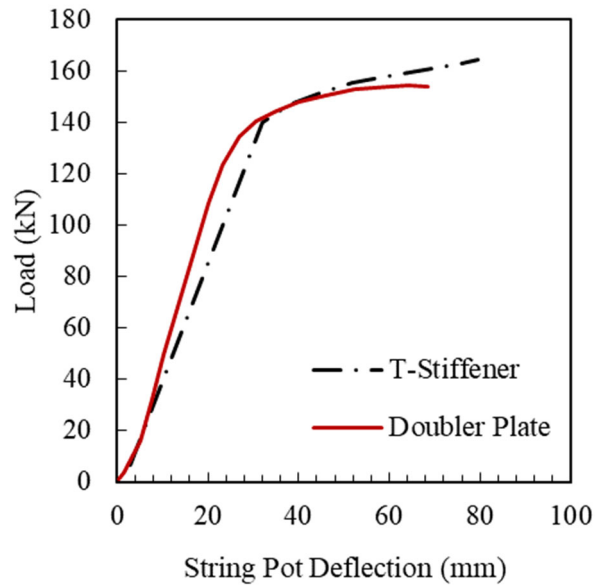
**Fig. 5.2.** Linear potentiometer rotation arm dimensions (used to calculate connection and column rotation)



**Fig. 5.3.** Load vs. linear potentiometer connection deflections (LP1 & LP2) for quasi-static tests



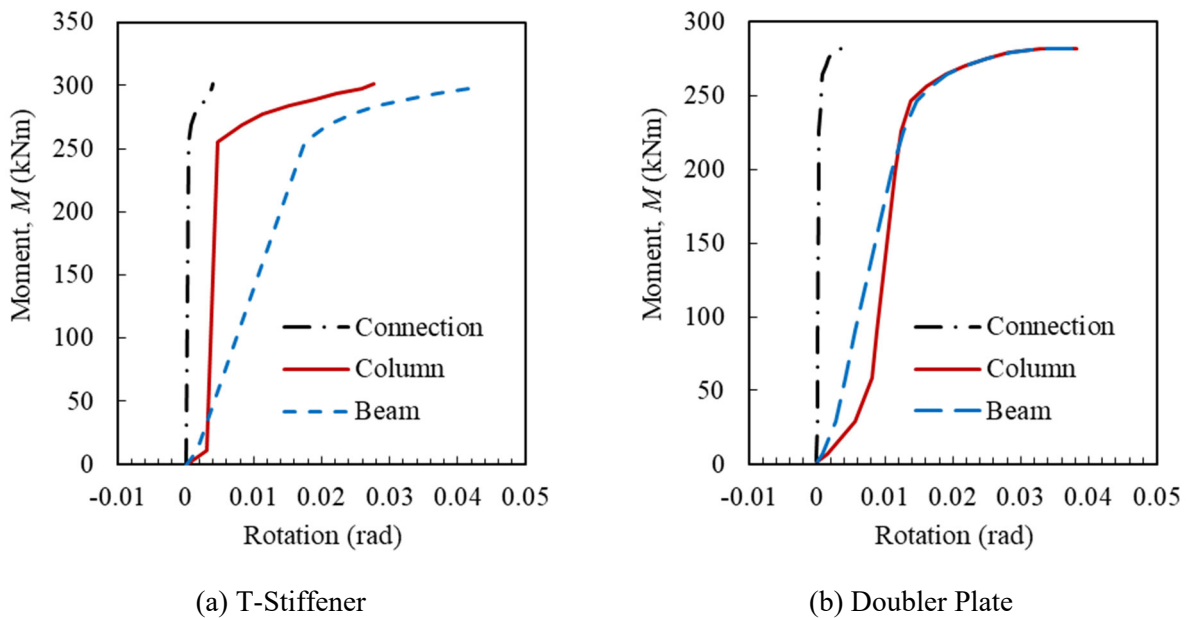
**Fig. 5.4.** Load vs. linear potentiometer column deflections (LP3 & LP4) for quasi-static tests



**Fig. 5.5.** Load vs. string pot deflections for quasi-static tests



Connection rotations  $\theta$  were calculated using the difference in LP readings and the rotation arm (LP2 - LP1 / 133 mm). Similar calculations were completed for the column rotation (LP4 - LP3 / 320 mm). Deflection readings from the string pot were converted to interstorey drift using Eq. (4.3). The test loading was measured as a point load from the actuator and converted to applied moment at the column face post-testing ( $M = P \times L$ , where  $L =$  moment arm to the applied load = 1829 mm). Fig. 5.6 shows the calculated rotations for the connection, column and beam plotted vs. the calculated applied moment at the column face.

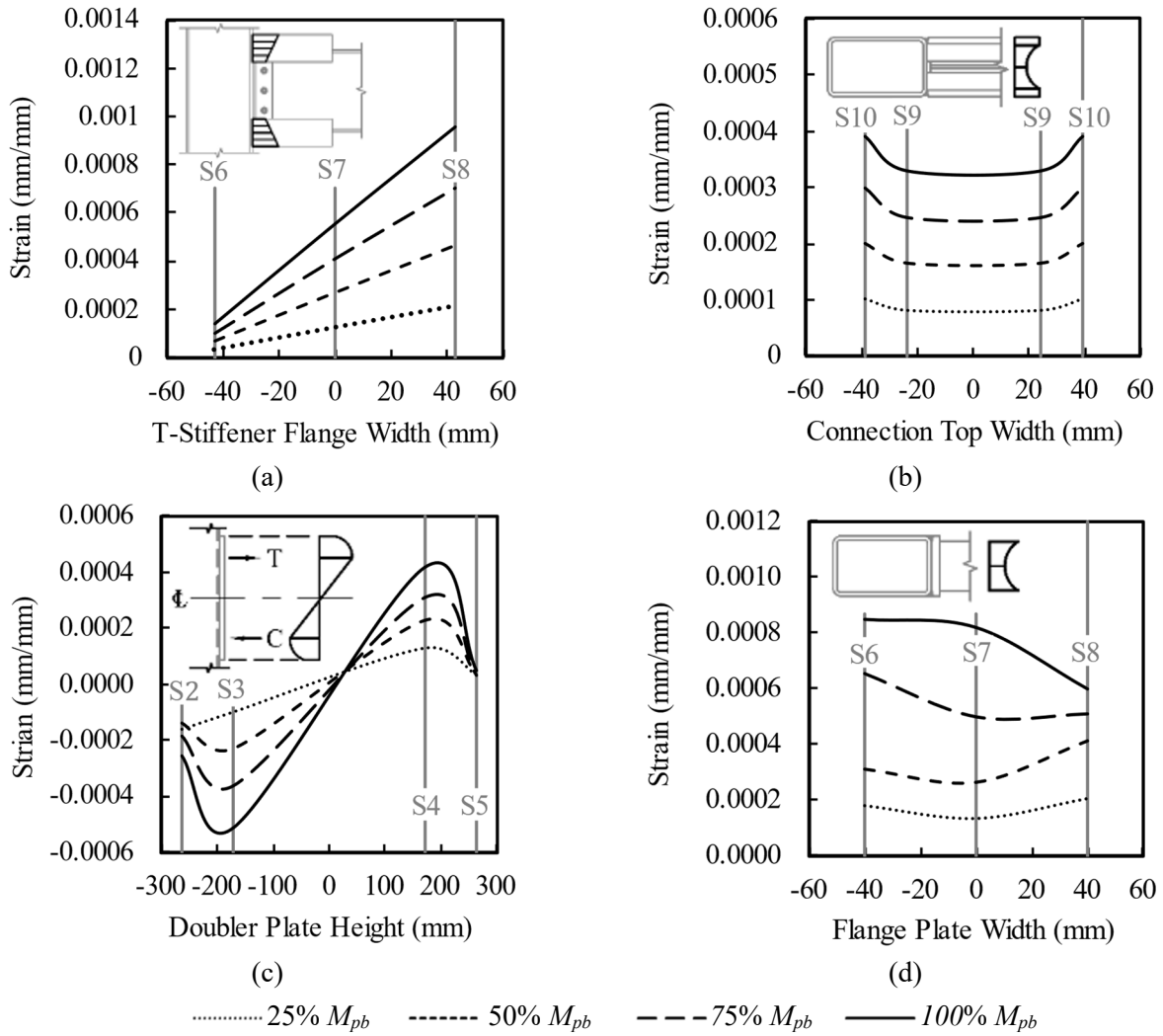


**Fig. 5.6.** Moment vs. connection, column, and beam rotations for quasi-static tests

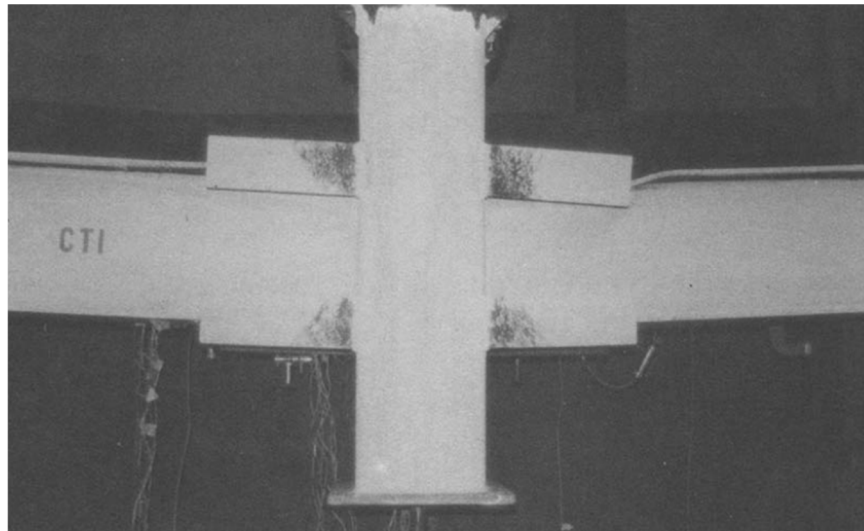
### 5.1.3. STRAIN OBSERVATIONS

SGs S2 and S3 on the T-Stiffener connection (see Fig. 4.13a) verified the yielding of the beam (at the end of the connection), and SGs S4 and S5 verified the load transfer from the T-stiffeners directly into the RHS sidewalls. From S6-S8 (Fig. 5.7a), a strain distribution similar to that reported in previous studies (Shanmugan et al. 1991) was observed (Fig. 5.8). The readings from SGs S9 and S10 (Fig. 5.7b) gave credence to the critical section at failure being at the top of the connection (where the T-stiffeners interact with the beam flanges) (Ting et al. 1993).

SGs S6-S8 (Fig. 5.7d) confirmed the principal design basis for the Doubler Plate connection (namely, the presence of an effective width phenomenon in the doubler plate from Packer & Henderson (1997)), and SGs S2-S5 (Fig. 5.7c) corroborated: (i) the linear distribution of longitudinal shear in the RHS sidewalls between the lines of action of the flange plates; and (ii) the non-linear distribution of this shear stress beyond the flange plates observed by Dawe & Grondin (1997). Moreover, SGs S6-S8 (Fig. 5.7d) showed an approximately parabolic distribution transversely on the doubler plate at the flange plates' location.



**Fig. 5.7.** Strain distributions for the T-Stiffener and the Doubler Plate connections



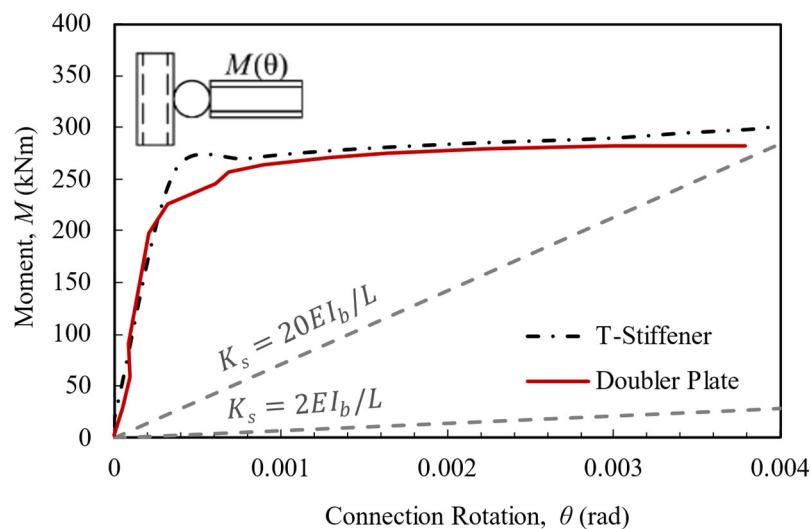
**Fig. 5.8.** Stiffener yielding after failure (Shanmugan et al. 1991)

### 5.1.4. CONNECTION STIFFNESS

According to AISC 360-22, FR connections (as discussed in Section 2.3.3) are those in which the connection's secant stiffness ( $K_S$ ) at service loads is greater than or equal to  $20EI_b/L$ . Using nominal values for  $E$  ( $= 200$  GPa),  $I_b$  ( $= 65 \times 10^6$  mm<sup>4</sup>) and  $L$  ( $= 3658$  mm), the T-Stiffener and Doubler Plate connections require  $K_S \geq 71 \times 10^3$  kNm to be classified as FR. The secant stiffness for both connections were determined through the procedure shown in AISC 360 Fig. C-B3.3 and adapted to reflect the Canadian design requirements in CSA S16:19 Clause 27. A linear relationship between the maximum moment (lesser of  $M_n$  and  $M_{pb}$ ) and 0.02 rad (rotation required for Type LD MRF connection) was plotted and the intersecting data points from the connection lab tests were taken as the moment at service load ( $M_S$ ) and the rotation at service load ( $\theta_S$ ). The secant stiffness at service load was then calculated ( $K_S = M_S / \theta_S$ ) and a summary of tabulated values is shown in Table 5-1. The plots of the  $M$  vs.  $\theta$  for both connections (Fig. 5.9) indicates that both connections meet the requirements for FR.

**Table 5-1.** T-Stiffener and Doubler Plate connection stiffness values

Connection	Rotation at Service Load, $\theta_S$ (rad)	Moment at Service Load, $M_S$ (kNm)	Secant Stiffness, $K_S$ ( $\times 10^3$ kNm)
T-Stiffener	0.00024	201	836
Doubler Plate	0.00020	198	988



**Fig. 5.9.** Connection moment vs. rotation plot for quasi-static tests

### 5.1.5. INTERSTOREY DRIFT

CSA S16:19 Clause 27.4.4.1 requires limited ductility connections to maintain a minimum strength at the column face of 80%  $M_{pb}$  through a minimum interstorey drift of 0.02 radian under cyclic loading (Section 2.3.2). Plots of the ratio of  $M/M_{pb}$  at the column face versus the interstorey drift for both connections are shown in Fig. 5.10, where this requirement was met under quasi-static loading. Using the mechanical properties from the TC tests on the beam materials for the T-Stiffener ( $F_y = 419$  MPa) and Doubler Plate ( $F_y = 380$  MPa) connections, the values of  $M_{pb}$  (= 201 kNm and 183 kNm, respectively) were updated and used herein to normalize the test results.

Thus, the W-section-to-RHS beam-to-column connections designed herein using the prescriptive requirements (i.e., for  $M_u$  and  $V_u$ ) in AISC 341-22 are likely to meet or exceed the required performance in CSA S16:19 Clause 27.4.4.1c). This is verified, however, in the following Chapters.

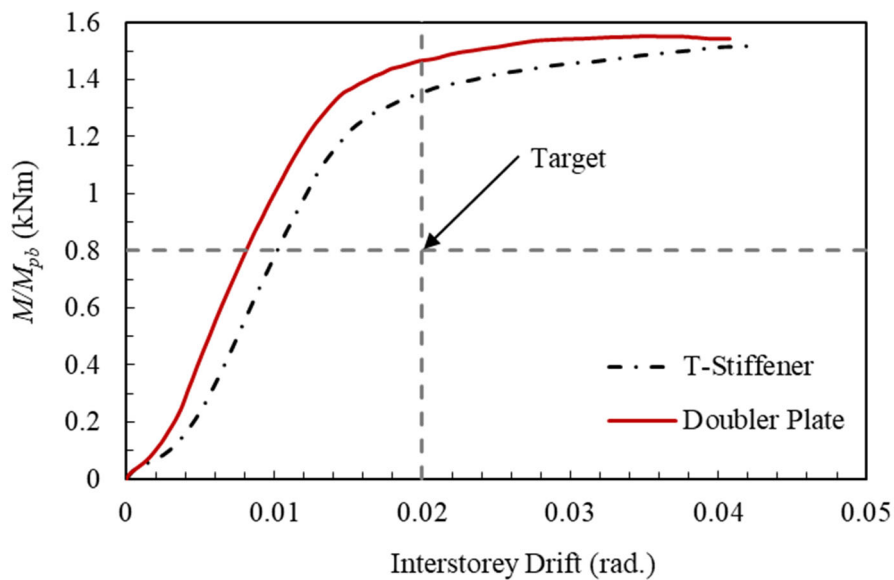


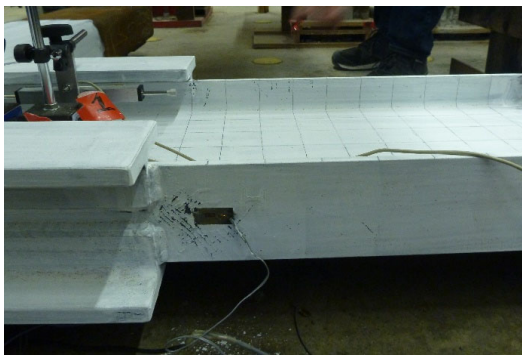
Fig. 5.10. Connection moment vs. interstorey drift plot for quasi-static tests

## 5.2. CYCLIC TEST RESULTS

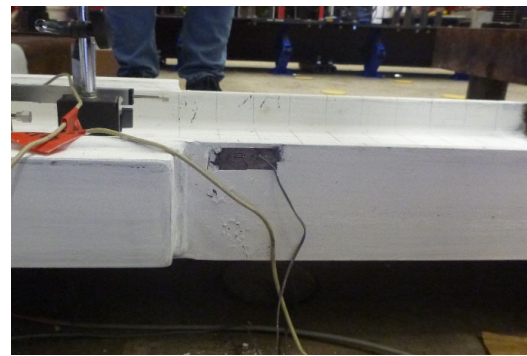
The cyclic test was completed according to Annex J of CSA S16:19 qualification testing provisions for seismic moment connections. The testing procedure was interstorey drift controlled and reached a specified rotation for a defined number of cycles using the test setup described in Section 4.5. This section describes the results of the cyclic tests.

### 5.2.1. VISUAL OBSERVATIONS

For all cyclic tests on both connections, the yielding (seen by flaking of the limewash) started within the first 50 mm from the end of the connection (Fig. 5.11) and propagated down the beam flanges towards the loading point and then into the beam's web. No yielding occurred in the column, or any connection elements until after an interstorey drift of 0.03 radians; then high stress yielding could be seen on the welds connecting the flange plates and T-stiffeners (Fig. 5.12). Both connections developed a moment of at least  $M_u$  and a shear of at least  $V_u$  at the column face, with plastic hinges (Fig. 5.13) evident at distances of 458 mm and 525 mm from the column face for the T-stiffener and Doubler Plate reinforced connections, respectively.



(a)



(b)

**Fig. 5.11.** Initial yielding occurring within the first 50 mm from the ends of the connections



(a)

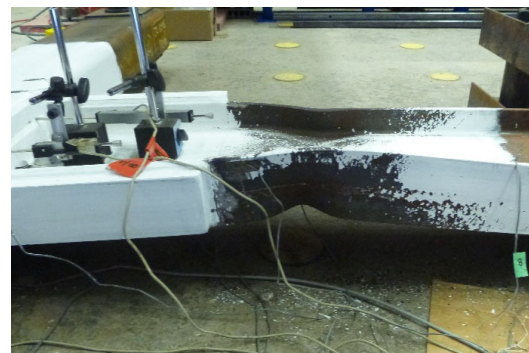


(b)

**Fig. 5.12.** High stress yielding in connection welds after interstorey drift of 0.03 rads



(a)



(b)

**Fig. 5.13.** Plastic hinges of the connection assemblies post-cyclic testing

### 5.2.2. STRAIN OBSERVATIONS

Strain gauges attached to the center of the wide-flange beam 50 mm from the end of the T-stiffeners (S5 and S6) were used to confirm the yielding of the beam in the plastic hinge region using a yield limit of 0.0038 mm/mm (from material testing of W310 × 33 - HT# D165477). During the T2 test, the top flange of the beam (S6) started to yield at a rotation of 0.015 rad and 0.02 rad for the bottom beam flange (S5). The top flange of the beam during the T3 test started to yield at 0.01 rad, and the bottom flange at 0.015 rad.

The load transfer of the connection into the column was recorded by SGs S1-S4 located at each end (top and bottom) of each of the T-stiffeners at the column face. The strain distribution was linear, with the outer edge T-stiffener flange strains greater than the inner edge. When the T-stiffeners are in tension, the strain was positive and negative for compression. The distributions show the coupled load action creating the moment on the connection. This distribution was the same as seen by Shanmugan et al. (1991) and shown in the static test (Section 5.1.2). The strain observed during the T2 test shown in Fig. 5.14a for the negative rotations and Fig. 5.14b for the positive rotations was less than that seen during the T3 test (Fig. 5.14c for negative rotations and Fig. 5.14d for positive rotations), this was likely caused by the connection assembly having a fabrication error of the beam being installed 50 mm off center.

Strain gauges attached to the Doubler Plate connection flange plates 50 mm from the column face (S5 and S7) never reach the yield limit of 0.0038 mm/mm (from material testing of 32 mm thick plate). During the DP1 test, the bottom flange plate and the top plate strain gauge (S6 and S8) reaches the yield limit of 0.0039 mm/mm (from material testing of W310 × 33 - HT# D169312) during the first 0.015 rad cycle. During the DP2 test, the bottom flange plate strain gauge (S6) reaches the yield limit during the first 0.015 rad cycle, and the top flange plate (S8) reaches the yield limit during the first 0.03 rad cycle.

The load transfer of the connection into the column was recorded by SGs S1-S4 at the ends of the doubler plate and at the locations of the flange plates. During the DP1 cyclic test, the strain response while moving toward the positive rotation (Fig. 5.15a) was 50% larger than the strain in the negative rotation direction (Fig. 5.15b). The strain response during the DP2 test toward the positive rotation (Fig. 5.15c) was 30% larger than the strain in the negative rotation direction (Fig. 5.15d), this is hypothesized due to the top and bottom plates not being symmetrical and well as the bottom beam flange cope.

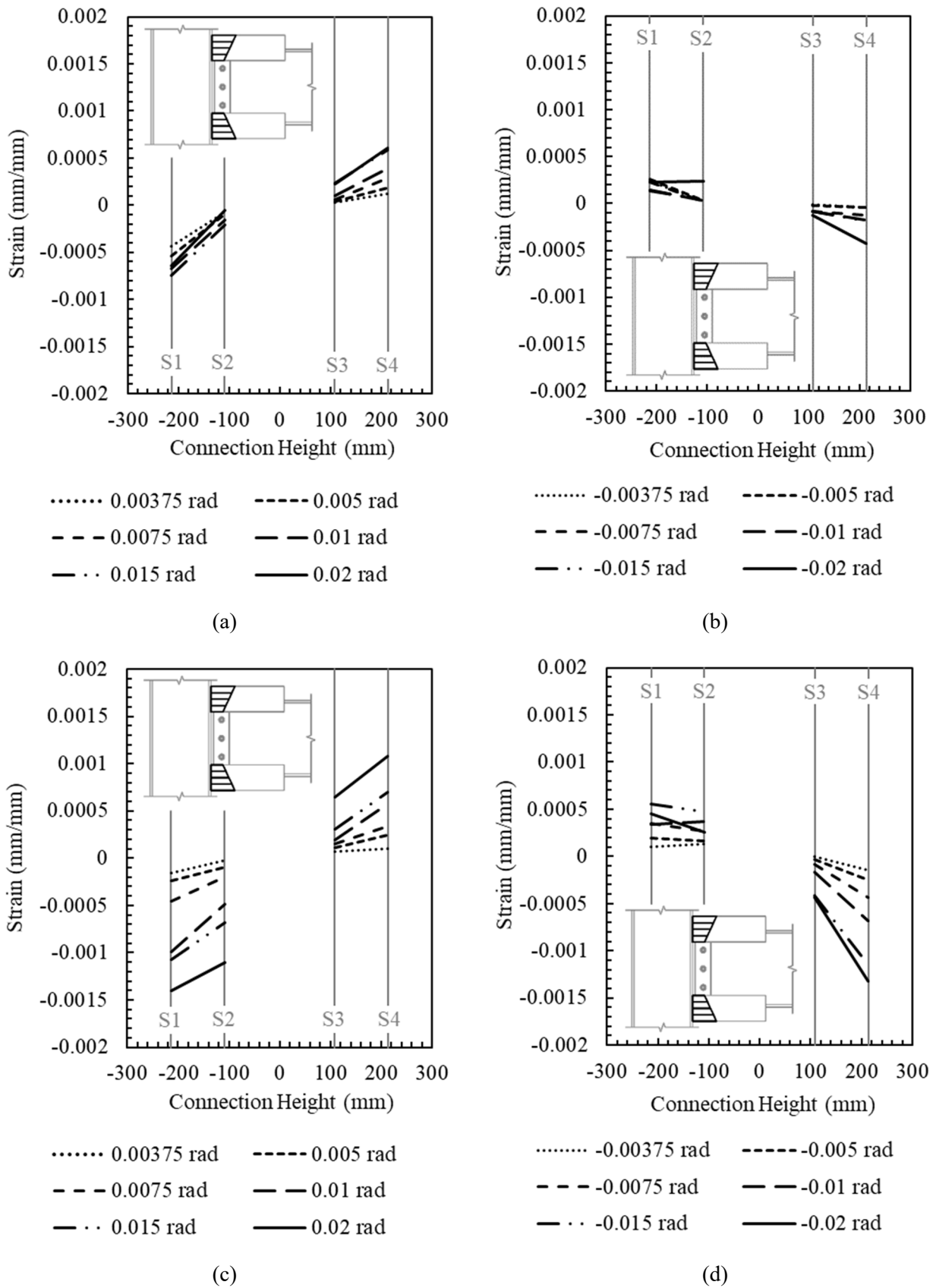
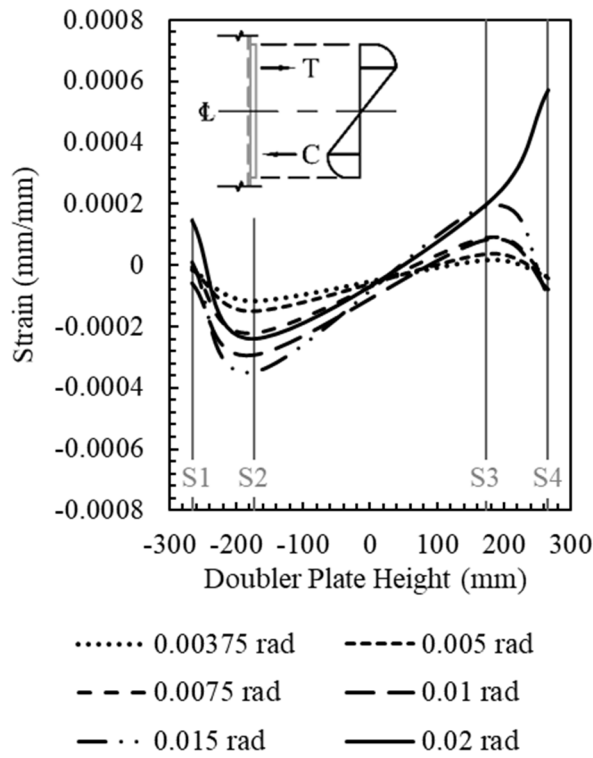
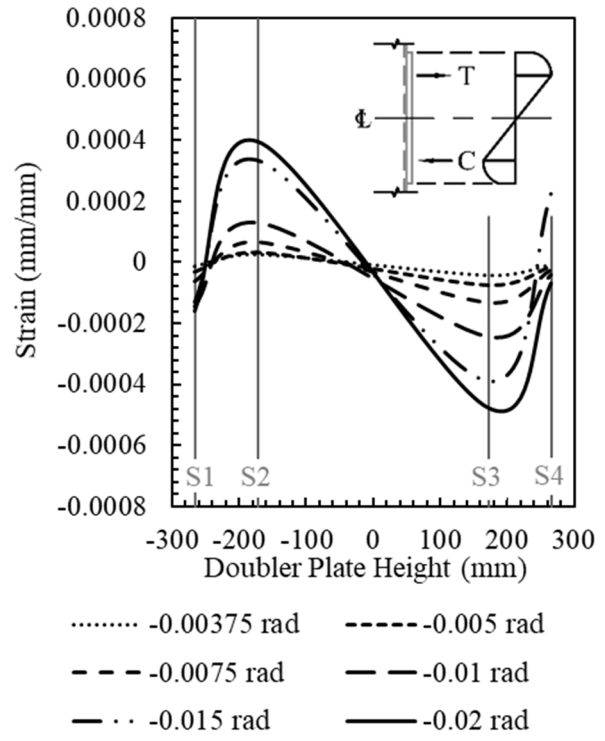


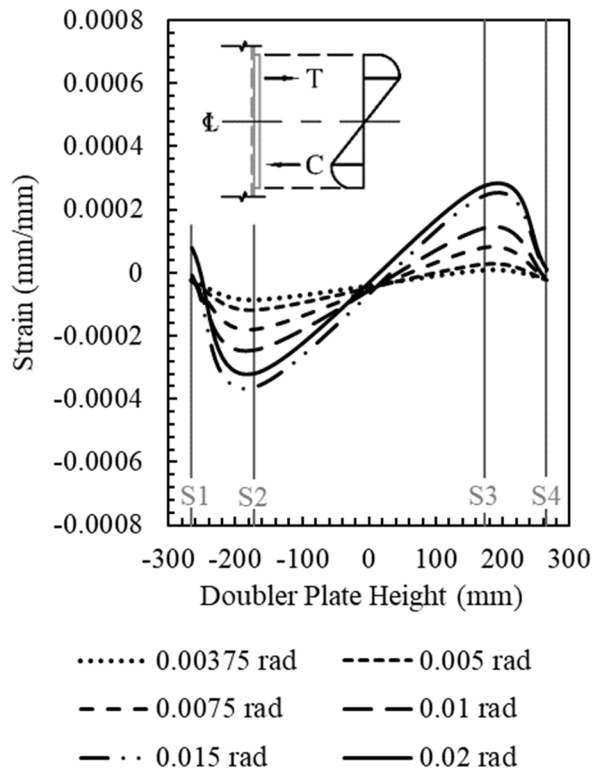
Fig. 5.14. T-Stiffener connection strain distributions



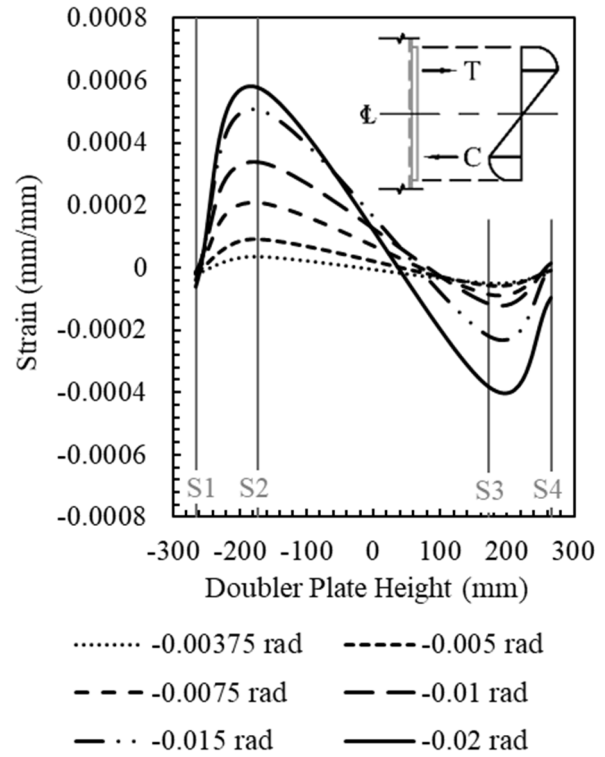
(a)



(b)



(c)



(d)

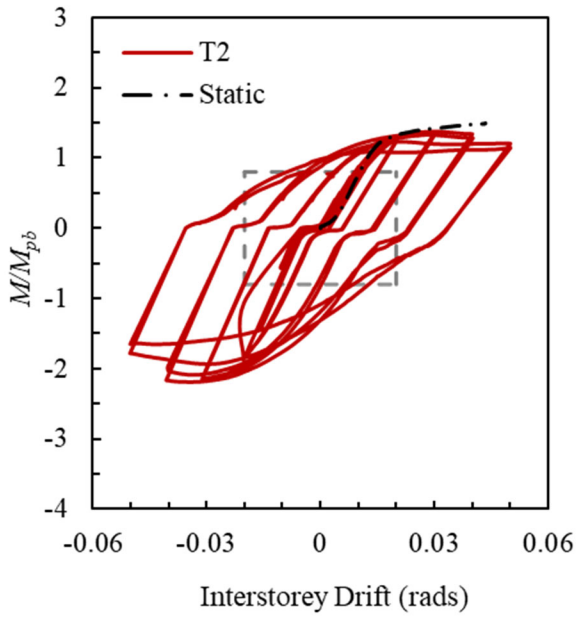
**Fig. 5.15.** Doubler plate connection strain distributions



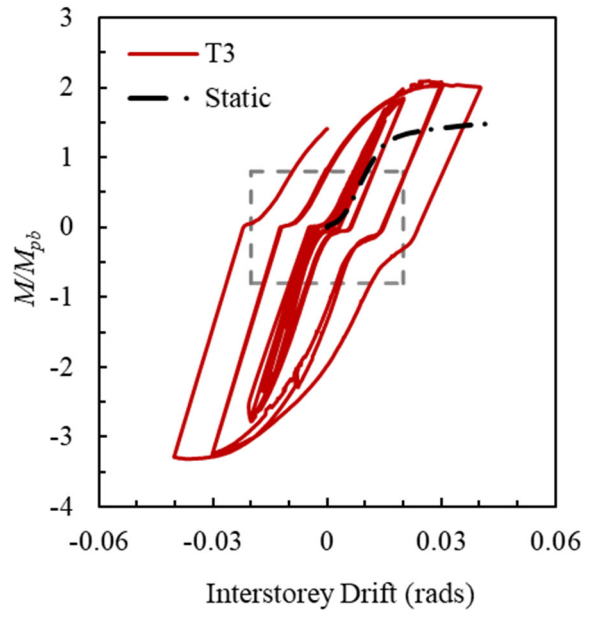
### 5.2.3. HYSTERETIC OBSERVATIONS

Test data was collected as described in Section 4.5.2 and analyzed using the same process identified in for the quasi-static tests (Section 5.1.2). Fig. 5.16 and Fig. 5.17 show normalized moment-interstorey drift hysteretic curves for both the T-Stiffener and Doubler Plate connections, respectively. For three of the four cyclic tests performed, the static test behaviour provided a good indication of the envelope response up to an interstorey drift of 0.04 radians. However, when comparing the cyclic data of test T3 (Fig 5.16b) to the static test data, there appears to be an increase in connection strength in the former (i.e., under cyclic loading). This was believed to have been caused by the beam “biting” into the lateral bracing system and pushing it into the concrete slab, which added additional strength into the system. Another observation made regarding the cyclic tests results was that the areas of the curves around  $M/M_{pb} = 0$  display a period of rotation increase without the addition of load. This is believed to be due to some slip that occurred at the actuator-to-beam connection as a result of oversized bolt holes (Fig.5.18). For comparison to finite-element results in future studies, it is recommended that this slip be removed from the data. Detailed observations and additional data related to the hysteretic response curves are found in Appendix H.

The plots for both connections show the quasi-static testing performance as well as the performance of both quasi-static cyclic tests. The results indicate that both connections perform in accordance with CSA S16 under cyclic testing for Type LD MRF connections as they meet and surpass a load retention of  $0.8M_{pb}$  at an interstorey drift of 0.02 radians (boundary’s shown by the grey dashed lines in Fig. 5.16 & Fig. 5.17). Thus, the W-section-to-RHS beam-to-column connections designed herein using the prescriptive requirements (i.e., for  $M_u$  and  $V_u$ ) in AISC 341-22 meet and exceed the required performance in CSA S16:19 Clause 27.4.4.1c).

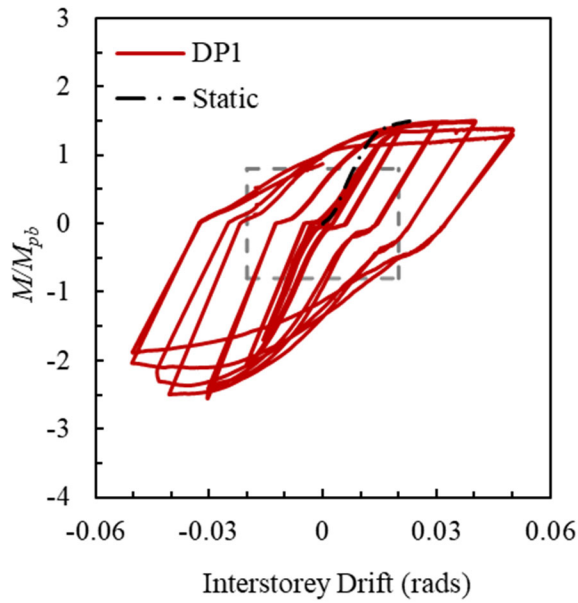


(a) T2

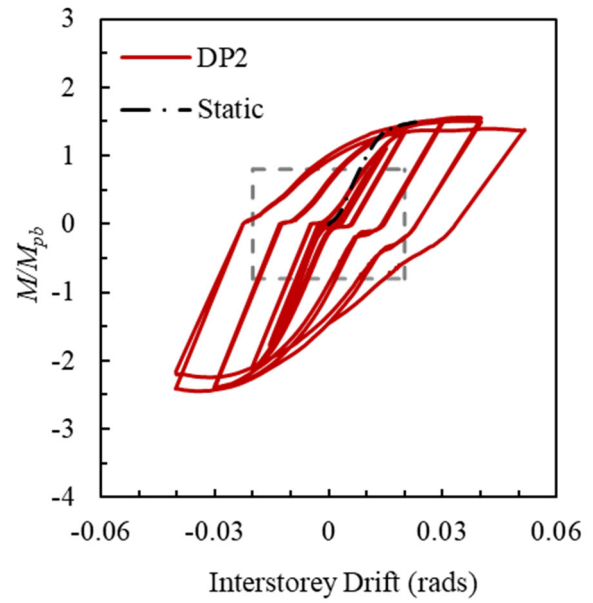


(b) T3

**Fig. 5.16.** T-Stiffener normalized moment-interstorey drift hysteretic curves (T2 & T3 assemblies)



(a) DP1



(b) DP2

**Fig. 5.17.** Doubler Plate normalized moment-interstorey drift hysteretic curves (DP1 & DP2 assemblies)



**Fig. 5.18.** Actuator beam connection

## Chapter 6: CONCLUSIONS AND RECOMMENDATIONS

### 6.1. SUMMARY

Based on the results of two quasi-static tests and four cyclic tests on large-scale moment connection assemblies [i.e., a T-Stiffener reinforced connection (Fig. 3.1a) assembly and a Doubler Plate reinforced connection (Fig. 3.1b) assembly], the following can be concluded:

- The T-Stiffener reinforced connections, experienced plastic hinging 425 mm from the column face (at the end of the T-stiffeners) during the static test and 458 mm during the cyclic tests, and there was no visible damage to the RHS column or any elements of the connection.
- The Doubler Plate reinforced connections, experienced plastic hinging 490 mm from the column face (at the end of the flange plates) during the static test and 525 mm during the cyclic tests, and – similarly – there was no visible damage to the RHS column or any elements of the connection.
- In both connections under static loading, the maximum moment ( $M_{max}$ ) coincided with the development of a moment in excess of  $1.1R_yF_yM_{pb}$  at the column face (as required by AISC 341-22 Section E.1.6b). Under monotonic static loading, both connections reached an interstorey drift of 0.04 radians with a corresponding moment at the column face of  $1.5M_{pb}$ .
- Both connections under cyclic loading maintained and exceeded a moment capacity of at least 80%  $M_{pb}$  at an interstorey drift of 0.02 rads meeting and surpassing the performance requirements for use in a Type LD MRF in Canada.
- Both connections can be classified as full strength and fully rigid (FR) according to the classification system used in AISC 341-22. (Both connections should be modeled as rigid joints in frame-analysis software.)

### 6.2. CONCLUSION

Based on a comparison of the above results to the performance requirements in CSA S16:19, the AISC 341-22 prescriptive design requirements for OMFs (i.e., for  $M_u$  and  $V_u$ ) produce connections that meet or exceed those in CSA S16:19 Clause 27.4.4.1.c) for Type LD MRF connections. Moreover, the results of this study demonstrate the feasibility of having static design criteria for prequalified beam-to-column connections for Type LD MRFs in Canada.

### 6.3. RECOMMENDATIONS AND FUTURE WORK

Recommendations for future work in this area of research are:

- Perform additional, comprehensive tests on alternative connections with RHS columns that are compatible with Type LD MRF connections to broaden the range of connection options.
- Expand the parameters and limits of the current test results and applicability of the connections by completing a parametric study.

## REFERENCES

AISC. (2022a). *Seismic Provisions for Structural Steel Buildings*. ANSI/AISC 341-22. American Institute of Steel Construction. Chicago, IL., USA.

AISC. (2022b). *Prequalified Connections for Special and Intermediate Steel Moment Frames for Seismic Applications*. ANSI/AISC 358-22. American Institute of Steel Construction. Chicago, IL., USA.

AISC. (2022c). *Specification for Structural Steel Buildings*. ANSI/AISC 360-22. American Institute of Steel Construction. Chicago, IL., USA.

Al Hendi, H., & Celik, M. (2015). Behavior of reverse-channel and double-reverse-channel connections to tubular columns with HSS. *Journal of Constructional Steel Research*, 112, 271–281.

ASTM. (2021a). *Standard Specification for High-Strength Low-Alloy Columbium-Vanadium Structural Steel*. A572/A572M-21E01. American Society for Testing and Materials International. West Conshohocken, PA, USA.

ASTM. (2021b). *Standard Test Methods for Tension Testing of Metallic Materials*. E8/E8M- 21. American Society for Testing and Materials International. West Conshohocken, PA, USA.

ASTM. (2022). *Standard Specification for Structural Steel Shapes*. A992/A992M-22. American Society for Testing and Materials International. West Conshohocken, PA, USA.

Blodgett, O. (1976). Section 7.4 Determining Weld Size. *Design of Welded Structures*, James F Lincoln Arc Welding Foundation, 7.4-1-7.4-22

CISC. (2019). Design Module 7. *Moment Connections for Seismic Applications*, 3rd. Canadian Institute of Steel Construction. Toronto, Canada.

CISC. (2021). *Handbook of steel construction*, 12th ed. Canadian Institute of Steel Construction, Toronto, Canada.

CSA. (2018). *General Requirements for Rolled or Welded Structural Quality Steel / Structural Quality Steel*. CSA G40.20-13/G40.21-13 (R2018). Canadian Standards Association, Toronto, Canada.

CSA. (2019). *Design of Steel Structures*. CSA S16:19. Canadian Standards Association. Toronto, Canada.

Dawe, J. L., & Grondin, G. Y. (1990). W-shape beam to RHS column connections. *Canadian Journal of Civil Engineering*, 17(5), 788–797.

Fadden, M., Wei, D., & McCormick, J. (2015). Cyclic Testing of Welded HSS-to-HSS Moment Connections for Seismic Applications. *Journal of Structural Engineering* (New York, N.Y.), 141(2).

Gholami, M., Deylami, A., & Tehranizadeh, M. (2013). Seismic performance of flange plate connections between steel beams and box columns. *Journal of Constructional Steel Research*, 84, 36–48.

Ghosh, S. K. (1995). Observations on the performance of structures in the Kobe earthquake of January 17, 1995. *PCI Journal*, 40(2), 14–22.

Iwankiw, N.R. (1994). Discussion, Design of I-Beam to Box-Column Connections Stiffened Externally. *Engineering Journal*, American Institute of Steel Construction, Vol. 31, pp. 110.

Luttrell, K. (2015). ConXtech Poised for Rapid Growth with Close of \$25 Million Strategic Investment Led by Saudi Aramco Energy Ventures. *PRWeb*. Retrieved March 21, 2022, from <https://www.prweb.com/releases/2015/04/prweb12656942.html>

NBCC. (2020). Division B. Part 4 - Structural Design. *National Building Code of Canada*. National Research Council Canada, Institute for Research in Construction, 54-57.

Packer, J. A., & Henderson, J. E. (1997). Chapter 9 - Beam to HSS Column Connections. In *Hollow Structural Section Connections and Trusses: A Design Guide* (2nd ed., pp. 301–334). Canadian Institute of Steel Construction. Toronto, Canada.

Picard, A., & Giroux, Y.-M. (1976). Moment connections between wide flange beams and square tubular columns. *Canadian Journal of Civil Engineering*, 3(2), 174–185.

Tabuchi, M., Kanatani, H., Tanaka, T., Fukuda, A., Furumi, K., Usami, K., & Murayama, M. (1994). Behaviour of SHS column to H beam moment connections with one side bolts. *Tubular Structures: Sixth International Symposium on Tubular Structures, Melbourne, Australia, 1994 Proceedings*, Melbourne, Australia (1st ed.). Routledge.

Richards, P. W. (2022). Cyclic Behavior of DuraFuse Frames Moment Connections. *Engineering Journal* (New York), 59(2), 135–148.

Shanmugan, N. E., Ting, L. C., & Lee, S. L. (1991). Behaviour of I-Beam to Box-Column Connections Stiffened Externally and Subjected to Fluctuating Loads. *Journal of Constructional Steel Research*, 20(2), 129–148.

Ting, L. C., Shanmugam, N. E., & Lee, S. L. (1991). Box-column to I-beam connections with external stiffeners. *Journal of Constructional Steel Research*, 18(3), 209–226.

Ting, L.C., Shanmugam, N. E., & Lee, S.L. (1993). Design of I-Beam to Box-Column Connections Stiffened Externally. *Engineering Journal*, American Institute of Steel Construction, 141-149.

Tremblay, R., Filiatrault, A., Timler, P., & Bruneau, M. (1995). Performance of steel structures during the 1994 Northridge earthquake. *Canadian Journal of Civil Engineering*, 22(2), 338–360.

Wei, D., & McCormick, J. (2017). Experimental testing of tube-based seismic collar connections under cyclic loads. *Tubular Structures* (XVI), 365-372

# Appendix A: DESIGN CALCULATIONS

## A.1. BEAM AND COLUMN MEMBER PARAMETERS

**Column:** HSS254 x 152 x 9.5, CSA G40.20/G40.21, Grade 350W, Class C

$$b_0 = 152.4 \text{ mm}$$

$$F_{y0} = 350 \text{ MPa}$$

$$h_0 = 254 \text{ mm}$$

$$A_0 = 6490 \text{ mm}^2$$

$$t_0 = 9.53 \text{ mm}$$

**Beam:** W310 x 33, ASTM A992, CSA G40.20/G40.21, Grade 350W

$$b_b = 102 \text{ mm}$$

$$F_{yb} = 350 \text{ MPa}$$

$$h_b = 313 \text{ mm}$$

$$F_{ub} = 450 \text{ MPa}$$

$$t_b = 10.8 \text{ mm}$$

$$Z_b = 480 \times 10^3 \text{ mm}^3$$

$$w_b = 6.6 \text{ mm}$$

$$M_{pb} = \phi_s Z_B F_{yB} = 151.2 \text{ kNm}$$

$$k_b = 24 \text{ mm}$$

$$L_{cf} = 3.66 \text{ m}$$

$$A_b = 4180 \text{ mm}^2$$

## A.2. AISC DESIGN LOADS

$$R_y = 1.1$$

$$\alpha_s = 1.0 \text{ (LRFD)}$$

$$M_u = \frac{1.1 \times R_y \times M_{pb}}{\alpha_s} = 183 \text{ kNm}$$

$$T_{uT\text{-Stiffener}} = C_u = \frac{M_u}{h_B + w_t} = 566 \text{ kN}$$

$$V_u = \frac{2(1.1 \times R_y \times M_{pb})}{L_{cf}} = 100 \text{ kN}$$

$$T_{uDoubler\ Plate} = C_u = \frac{M_u}{h_B + t_f} = 530 \text{ kN}$$

## A.3. CLIP ANGLE DESIGN

### A.3.1. ANGLE AND BOLT PROPERTIES

**Angle:** L76 X 51 x 6.4, CSA G40.20/G40.21, Grade 300W

$$b_a = 50.8 \text{ mm}$$

$$F_{ya} = 300 \text{ MPa}$$

$$d_a = 76.2 \text{ mm}$$

$$F_{ua} = 440 \text{ MPa}$$

$$t_a = 6.35 \text{ mm}$$

$$A_a = 768 \text{ mm}^2$$

$$L_a = 230 \text{ mm}$$

3 bolts/vertical line

**Bolts:** 3/4" Bolts, A325

$$d = 19 \text{ mm}$$

$$F_u = 825 \text{ MPa}$$

$$A_b = 285 \text{ mm}^2$$



### A.3.2. BOLTED CONNECTION DESIGN

Bolted connection to beam: CSA S16:19 Cl. 13.12.1.2

$$\begin{aligned}B_r &= 3\phi_{br}ntdF_u \\ &= 3 \times 0.8 \times 3 \text{ bolts} \times 6.35 \text{ mm} \times 19 \text{ mm} \times 440 \text{ MPa} \\ &= 382 \text{ kN} > V_u \text{ OK}\end{aligned}$$

$$\begin{aligned}V_r &= 0.7(0.60\phi_b n m A_b F_u) \\ &= 0.7(0.60 \times 0.8 \times 3 \text{ bolts} \times 1 \text{ shear plane} \times 285 \text{ mm}^2 \times 825 \text{ MPa}) \\ &= 237 \text{ kN} > V_u \text{ OK}\end{aligned}$$

### A.3.3. WELDED CONNECTION DESIGN

Welded connection to RHS: CSA S16:19 Cl. 13.13.2.2

$$X_u = 490 \text{ MPa}$$

$$s = 5 \text{ mm}$$

$$L_{Trans.} = 2 \times 50 \text{ mm} = 100 \text{ mm}$$

$$\begin{aligned}V_{rTrans.} &= 0.67 \times \phi_w \times \frac{s}{\sqrt{2}} \times l \times X_u (1.00 + 0.5 \sin^{1.5} \theta_w) M_w \\ &= 0.67 \times 0.67 \times \frac{5 \text{ mm}}{\sqrt{2}} \times 100 \text{ mm} \times 490 \text{ MPa} (1.00 + 0.5 \sin^{1.5}(90^\circ)) \times 1.0 \\ &= 117 \text{ kN}\end{aligned}$$

$$L_{Long.} = 2 \times 230 \text{ mm} = 460 \text{ mm}$$

$$\begin{aligned}V_{rLong.} &= 0.67 \times \phi_w \times \frac{s}{\sqrt{2}} \times l \times X_u (1.00 + 0.5 \sin^{1.5} \theta_w) M_w \\ &= 0.67 \times 0.67 \times \frac{5 \text{ mm}}{\sqrt{2}} \times 460 \text{ mm} \times 490 \text{ MPa} (1.00 + 0.5 \sin^{1.5}(0^\circ)) \times 0.85 \\ &= 304 \text{ kN}\end{aligned}$$

$$V_r = V_{rTrans.} + V_{rLong.} = 421 > V_u \text{ OK}$$

### A.4. T-STIFFENER CONNECTION DESIGN

#### A.4.1. STIFFENER WEB THICKNESS

$$w_t \approx 1.0 \times t_b = 10.8 \text{ mm}$$

**T-Stiffener Design Selection:** W200x71 (Two stiffeners cut from one length of beam)

$$b_t = 105 \text{ mm (based on area required)}$$

$$F_{yt} = 350 \text{ MPa}$$

$$t_t = 17.4 \text{ mm}$$

$$d_t = 62 \text{ mm (based on space available)}$$

$$w_t = 10.2 \text{ mm} \approx t_b$$

$$A_t = 2399 \text{ mm}^3$$

#### A.4.2. STIFFENER LENGTH

$$l_s = \frac{b_0 - b_b}{2 \tan(20^\circ)} = \frac{152.4 \text{ mm} - 102 \text{ mm}}{2 \tan(20^\circ)} = 69.2 \text{ mm}$$

#### A.4.3. MINIMUM LENGTH FOR STIFFENER STRENGTH

$$\begin{aligned} \bar{x} &= \frac{1}{2} \left( \frac{b_t d_t t_t}{A_t} + d_t - t_t \right) \\ &= \frac{1}{2} \left( \frac{105 \text{ mm} \times 62 \text{ mm} \times 10.2 \text{ mm}}{2399 \text{ mm}^2} + 62 \text{ mm} - 10.2 \text{ mm} \right) = 39.7 \text{ mm} \end{aligned}$$

$$\begin{aligned} A_{ne} &= \left( 1 - \frac{\bar{x}}{L} \right) w_t t_t, \text{ for } (L_t \geq w_t) \\ &= \left( 1 - \frac{39.7 \text{ mm}}{l_s} \right) \times 10.2 \text{ mm} \times 17.4 \text{ mm} \\ &= 177.48 \text{ mm}^2 - \frac{7045.96 \text{ mm}^3}{l_s} \end{aligned}$$

$$l_s = \frac{0.5 T_u - (A_{ne}) F_{yt}}{\sqrt{3} w_t F_{ut}}$$

$$l_s = \frac{0.5 \times 566 \text{ kN} - \left( 177.48 \text{ mm}^2 - \frac{7045.96 \text{ mm}^3}{l_s} \right) \times 350 \text{ MPa}}{\sqrt{3} \times 10.2 \text{ mm} \times 450 \text{ MPa}}$$

$$l_s = 27.784 \text{ mm} + \frac{310.195 \text{ mm}^2}{l_s}$$

$$l_s^2 - 27.784 \text{ mm} \times l_s - 310.195 \text{ mm}^2 = 0$$

$$l_s = 36.3 \text{ mm}$$

#### A.4.4. MINIMUM LENGTH FOR WELD STRENGTH

$$\begin{aligned} V_{r \text{ Trans.}} &= 0.67 \times \phi_w \times \frac{s}{\sqrt{2}} \times l \times X_u (1.00 + 0.5 \sin^{1.5} \theta_w) \\ &= 0.67 \times 0.67 \times \frac{8 \text{ mm}}{\sqrt{2}} \times 30 \text{ mm} \times 490 \text{ MPa} (1.00 + 0.5 \sin^{1.5} (90^\circ)) \\ &= 56 \text{ kN} \end{aligned}$$

$$l_s = \frac{\sqrt{2} \times ((T_u/2) - V_{r \text{ Transverse}})}{0.67 \times \phi_w \times s \times X_u (1.00 + 0.5 \sin^{1.5} \theta_w) \times M_w}$$

$$\begin{aligned}
&= \frac{\sqrt{2} \times (585 \times 10^3 \text{ N}/2 - 56 \times 10^3 \text{ kN})}{0.67 \times 0.67 \times 8 \text{ mm} \times 490 \text{ MPa} (1.00 + 0.5 \sin^{1.5}(0^\circ)) \times 0.85} \\
&= 224 \text{ mm}
\end{aligned}$$

#### A.4.5.T-STIFFENER TO COLUMN WELD DESIGN

Horizontal weld of T-stiffener (Fillet weld)

$$\begin{aligned}
V_{r \text{ Horiz.}} &= 0.67 \times \phi_w \times \frac{s}{\sqrt{2}} \times l \times X_u (1.00 + 0.5 \sin^{1.5} \theta_w) \\
&= 0.67 \times 0.67 \times \frac{10 \text{ mm}}{\sqrt{2}} \times 50 \text{ mm} \times 490 \text{ MPa} (1.00 + 0.5 \sin^{1.5}(90^\circ)) \\
&= 78 \text{ kN}
\end{aligned}$$

Vertical weld of T-stiffener (Flare bevel butt weld)

$$A_m = 14 \text{ mm} \times 105 \text{ mm} = 1470 \text{ mm}^2$$

$$V_{r \text{ Base Metal}} = 0.67 \phi_w A_m F_u$$

$$V_{r \text{ HSS}} = V_{r \text{ T}} = 0.67 \times 0.67 \times 1470 \text{ mm}^2 \times 350 \text{ MPa} = 231 \text{ kN}$$

$$A_w = \frac{14 \text{ mm}}{\sqrt{2}} \times 105 \text{ mm} = 1039 \text{ mm}^2$$

$$V_{r \text{ Weld}} = 0.67 \phi_w A_w X_u = 0.67 \times 0.67 \times 1039 \text{ mm}^2 \times 490 \text{ MPa} = 229 \text{ kN}$$

$$V_{r \text{ Total}} = 78 \text{ kN} + 229 \text{ kN} = 307 \text{ kN} > \frac{T_u}{2} = 293 \text{ kN} \text{ OK}$$

#### A.4.6.DESIGN SUMMARY

The T-stiffener webs were attached to the beams using an 8 mm fillet weld along the longitudinal and transverse edges, and a 10 mm partial joint penetration (PJP) flare-bevel groove weld and 10 mm fillet were used to connect the T-stiffener flanges and web, respectively, to the column. A cope was also added to the top flange of the beam to help with on-site erection around the clip angle. Based on the aforementioned criteria, and accounting for the 10 mm gap between the beam and column (see Section 3), the T-stiffeners were designed to have a total length ( $l_s$ ) = 305 mm.

## A.5. DOUBLER PLATE CONNECTION

### A.5.1. CONNECTION VALIDITY

#### Beam Class

$$\frac{h_b}{w_b} = \frac{313 \text{ mm}}{6.6 \text{ mm}} = 47.4 \leq \frac{1100}{\sqrt{345}} = 59.2 \text{ (Class 1)} \quad \text{Class 1}$$

**OK**

#### Column Class

$$b_{el} = 254 \text{ mm} - 4(9.53 \text{ mm}) = 216 \text{ mm} \leq \frac{420}{\sqrt{350}} = 22.4 \text{ (Class 1)} \quad \text{Class 2}$$
$$\frac{b_{el}}{t_b} = \frac{216 \text{ mm}}{9.53 \text{ mm}} = 22.7 \leq \frac{525}{\sqrt{350}} = 28.1 \text{ (Class 2)} \quad \text{OK}$$

#### Dimension Checks

$$\beta = \frac{b_b}{b_0} = \frac{102 \text{ mm}}{152.4 \text{ mm}} = 0.67 \quad \beta \geq 0.25 \quad \text{OK}$$

$$\frac{h_b}{b_0} = \frac{313 \text{ mm}}{152.4 \text{ mm}} = 2.1 \quad \frac{h_b}{b_0} \geq 0.25 \quad \text{OK}$$

$$\frac{b_b}{t_b} = \frac{102 \text{ mm}}{10.8 \text{ mm}} = 9.4 \quad \frac{b_b}{t_b} \geq 50 \quad \text{OK}$$

$$\frac{h_b}{t_b} = \frac{313 \text{ mm}}{10.8 \text{ mm}} = 29.0 \quad \frac{h_b}{t_b} \geq 50 \quad \text{OK}$$

$$\frac{b_0}{t_0} = \frac{152.4 \text{ mm}}{9.53 \text{ mm}} = 16.0 \quad 10 \leq \frac{b_0}{t_0} \leq 35 \quad \text{OK}$$

$$\frac{h_0}{t_0} = \frac{254 \text{ mm}}{9.53 \text{ mm}} = 26.7 \quad 10 \leq \frac{h_0}{t_0} \leq 35 \quad \text{OK}$$

$$\frac{e}{h_0} = \frac{0 \text{ mm}}{254 \text{ mm}} = 0 \quad -0.55 \leq \frac{e}{h_0} \leq 0.25 \quad \text{OK}$$

## A.5.2.PLATE MEMBER PARAMETERS

### Doubler Plate

$$b_p = 152 \text{ mm}$$

$$t_p = 22 \text{ mm}$$

$$h_p = 530 \text{ mm}$$

$$F_{yp} = 300 \text{ MPa}$$

### Flange Plate

$$b_f = 125 \text{ mm}$$

$$t_f = 32 \text{ mm}$$

$$b'_f = 85 \text{ mm}$$

$$F_{yf} = 345 \text{ MPa}$$

$$d_f = 325 \text{ mm}$$

## A.5.3.FLANGE PLATES AND WELDS (“EFFECTIVE WIDTH” RUPTURE)

$$\begin{aligned} b_e &= \left( \frac{10}{b_p/t_p} \right) \left( \frac{F_{yp}t_p}{F_{yf}t_f} \right) b_f \leq b_f \\ &= \left( \frac{10}{152 \text{ mm}/22 \text{ mm}} \right) \left( \frac{300 \text{ MPa} \times 22 \text{ mm}}{300 \text{ MPa} \times 32 \text{ mm}} \right) \times 125 \text{ mm} \leq b_f \\ &= 124.4 \text{ mm} \leq b_f \end{aligned}$$

$$\begin{aligned} M_{r1}^* &= h_b F_{yf} t_f b_e \\ &= 313 \text{ mm} \times 300 \text{ MPa} \times 32 \text{ mm} \times 124.4 \text{ mm} \\ &= 374 \text{ kNm} > M_u \text{ OK} \end{aligned}$$

## A.5.4.DOUBLER PLATE (PUNCHING SHEAR)

$$\begin{aligned} b_{ef} &= \left( \frac{10}{b_p/t_p} \right) b_f \leq b_f \\ &= \left( \frac{10}{152 \text{ mm}/22 \text{ mm}} \right) \times 125 \text{ mm} \leq b_f \\ &= 180 \text{ mm} \leq b_f \\ &= b_f = 125 \text{ mm} \end{aligned}$$

$$\begin{aligned} M_{r1}^* &= 2h_b \frac{F_{yp}}{\sqrt{3}} t_f b_{ef} \\ &= 2 \times 313 \text{ mm} \times \frac{300 \text{ MPa}}{\sqrt{3}} \times 32 \text{ mm} \times 125 \text{ mm} \\ &= 434 \text{ kNm} > M_u \text{ OK} \end{aligned}$$

### A.5.5.COLUMN SIDEWALLS (WEB CRIPPLING OF COLUMN)

$$n = 1.34$$

$$\frac{KL}{r} = 3.46 \left( \frac{h_0}{t_0} - 2 \right) \left( \frac{1}{\sin \theta} \right)^{0.5} = 3.46 \left( \frac{254}{9.53} - 2 \right) \left( \frac{1}{\sin 90^\circ} \right)^{0.5} = 85.3$$

$$F_e = \frac{\pi^2 E}{\left( \frac{KL}{r} \right)^2} = \frac{\pi^2 \times 200\,000 \text{ MPa}}{(85.3)^2} = 271.3 \text{ MPa}$$

$$\lambda = \sqrt{\frac{F_{y0}}{F_e}} = \sqrt{\frac{350 \text{ MPa}}{271.3 \text{ MPa}}} = 1.136$$

$$C_r = \frac{\phi A F_{y0}}{(1 + \lambda^{2n})^{\frac{1}{n}}} = \frac{0.9 \times 6490 \times 350 \text{ MPa}}{(1 + 1.136^{2 \times 1.34})^{\frac{1}{1.34}}} = 1061.4 \text{ kN}$$

$$F_k = \frac{C_r}{\phi A} = \frac{1061.4 \times 10^3 \text{ N}}{0.9 \times 6490 \text{ mm}^2} = 182 \text{ MPa}$$

$$\begin{aligned} M_{r1}^* &= 2h_b F_k t_0 (t_b + 5(t_0 + t_p)) \\ &= 2 \times 313 \text{ mm} \times 182 \text{ MPa} \times 9.53 \text{ mm} \times (10.8 \text{ mm} + 5(9.53 \text{ mm} + 22 \text{ mm})) \\ &= 183 \text{ kNm} = M_u \text{ OK} \end{aligned}$$

### A.5.6.COLUMN FACE (PUNCHING SHEAR OF COLUMN)

$$M_{r1}^* = 0.25 \frac{F_{y0}}{\sqrt{3}} t_0 (h_p^2 + 2h_p b_p)$$

Note: not applicable as the doubler plate width is equal to the column width, done based on a recommendation by the fabricator to make the attachment of the plate better.

### A.5.7.ADDITIONAL FLANGE PLATE CHECKS

Top flange plate checked; bottom flange plate strength is greater due to constant width. Plate thickness made the same for both flange plates to keep details simplistic.

Flange Plate Tension Resistance (CSA S16:19 Cl.13.2)

$$A_g = t_p b'_f = 32 \text{ mm} \times 85 \text{ mm} = 2720 \text{ mm}^2$$

$$T_r = \phi_s A_g F_y = 0.9 \times 2720 \text{ mm}^2 \times 300 \text{ MPa} = 734 \text{ kN} > T_u \text{ OK}$$

Flange Plate Compression Resistance (CSA S16:19 Cl.13.3)

$$n = 1.34$$

$$I = \frac{bh^3}{12} = \frac{85 \text{ mm}(32 \text{ mm})^3}{12} = 232107 \text{ mm}^4$$

$$A = b \times h = 85 \text{ mm} \times 32 \text{ mm} = 2720 \text{ mm}^2$$

$$r = \sqrt{\frac{I}{A}} = \sqrt{\frac{232107 \text{ mm}^4}{2720 \text{ mm}^2}} = 9.2 \text{ mm}$$

$$\frac{KL}{r} = \frac{1.0 \times 250 \text{ mm}}{9.2 \text{ mm}} = 26.3$$

$$F_e = \frac{\pi^2 E}{\left(\frac{KL}{r}\right)^2} = \frac{\pi^2 \times 200\,000 \text{ MPa}}{(26.3)^2} = 2854 \text{ MPa}$$


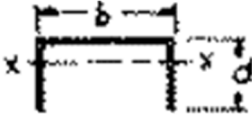

$$\lambda = \sqrt{\frac{F_{y0}}{F_e}} = \sqrt{\frac{300 \text{ MPa}}{2854 \text{ MPa}}} = 0.32$$

$$C_r = \frac{\phi A F_{y0}}{(1 + \lambda^{2n})^{\frac{1}{n}}} = \frac{0.9 \times 2720 \text{ mm}^2 \times 300 \text{ MPa}}{(1 + 0.32^{2 \times 1.34})^{\frac{1}{1.34}}} = 710 \text{ kN} > T_u \text{ OK}$$

### A.5.8.DOUBLER PLATE TO COLUMN WELD DESIGN

Design was completed using Omar Blodgett Method for checking moment and shear loading on a weld. Two different method of sharing loading was checked for adequacy. The first method was that the moment and shear was shared over the entire area of the weld around the doubler plate. The second method was that the top and bottom portions of the weld (u-shaped) will resist the moment only and a portion of the side welds resist shear only.

**Table A-1.** Properties of weld treated as a line (Blodgett 1967)

Outline of Welded Joint b = width      d = depth	Bending (about horizontal axis x-x)
	$S_w = bd + \frac{d^2}{3}$
	$S_w = \frac{2bd + d^2}{3} = \frac{d^2(2b + d)}{3(b + d)}$
	$S_w = \frac{d^2}{3}$

$$\begin{aligned}
 F_{y\text{Weld}} &= 0.67\phi_w X_u \\
 &= 0.67 \times 0.67 \times 490 \text{ MPa} \\
 &= 220 \text{ MPa}
 \end{aligned}$$

Design Method No. 1 (Box)

Shear

$$l_w = 2(b + d) = 2(152 \text{ mm} + 530 \text{ mm}) = 1364 \text{ mm}$$

$$F_{\parallel} = \frac{V}{l_w} = \frac{102 \text{ kN}}{1364 \text{ mm}} = 74.78 \text{ N/mm}$$

Moment

$$S_w = bd + \frac{d^2}{3} = 152 \text{ mm} \times 530 \text{ mm} + \frac{530 \text{ mm}^2}{3} = 174193 \text{ mm}^2$$

$$F_{\perp} = \frac{M}{S} = \frac{183 \text{ kNm}}{174193 \text{ mm}^2} = 1050 \text{ N/mm}$$

$$F_r = \sqrt{(F_{\parallel})^2 + (F_{\perp})^2} = \sqrt{(74.78 \text{ N/mm})^2 + (1050 \text{ N/mm})^2} = 1053 \text{ N/mm}$$

$$w = \frac{F_r}{F_{y\text{Weld}}} = \frac{1053 \text{ N/mm}}{220 \text{ N/mm}^2} = 5 \text{ mm (minimum)}$$



Design Method No. 2 (2U for moment and || for shear)

*Design weld size to 10mm was used based on weld size recommendations in CSA Handbook for a plate 22 mm thick.*

### Shear

$$F_{\parallel} = w \times F_{y \text{ weld}} = 10 \text{ mm} \times 220 \text{ N/mm}^2 = 2200 \text{ N/mm}$$

$$l_w = \frac{V}{F_{\parallel}} = \frac{102000 \text{ N}}{2200 \text{ N/mm}} = 47 \text{ mm (23.5 mm each side)}$$

### Moment

$$I_{w1} = \frac{bd^3}{12} = \frac{(152 \text{ mm} - 2(10 \text{ mm}))(10 \text{ mm})^3}{12} = 11000 \text{ mm}^4$$

$$A_{w1} = bd = (152 \text{ mm} - 2(10 \text{ mm}))(10 \text{ mm}) = 1320 \text{ mm}^2$$

$$y_{w1} = \frac{530 \text{ mm}}{2} - \frac{10 \text{ mm}}{2} = 260 \text{ mm}$$

$$d_2 = \frac{530 \text{ mm} - 23.5 \text{ mm}}{2} = 253 \text{ mm}$$

$$I_{w2} = \frac{bd^3}{12} = \frac{(10 \text{ mm})(253 \text{ mm})^3}{12} = 13.5 \times 10^6 \text{ mm}^4$$

$$A_{w2} = bd = (10 \text{ mm})(253 \text{ mm}) = 2530 \text{ mm}^2$$

$$y_{w2} = \frac{530 \text{ mm}}{2} - \frac{253 \text{ mm}}{2} = 138.5 \text{ mm}$$

$$I_w = \sum I_{wi} + A_i d_i^2$$

$$I_w = 2 \times [(11000 \text{ mm}^4) + (1320 \text{ mm}^2)(260 \text{ mm})^2] \\ + 4 \times [(13.5 \times 10^6 \text{ mm}^4) + (2530 \text{ mm}^2)(138.5 \text{ mm})^2]$$

$$I_w = 2 \times (89.2 \times 10^6 \text{ mm}^4) + 4 \times (62.0 \times 10^6 \text{ mm}^4)$$

$$I_w = 426.6 \times 10^6 \text{ mm}^4$$

$$y = 265 \text{ mm}$$

$$S_w = \frac{I_w}{y} = \frac{426.6 \times 10^6 \text{ mm}^4}{265 \text{ mm}} = 1610 \times 10^3 \text{ mm}^3$$

$$S_{required} = \frac{M}{F_{yWeld}} = \frac{183 \times 10^6 \text{ Nmm}}{220 \text{ N/mm}^2} = 832 \times 10^3 \text{ mm}^3 < S_w \text{ OK}$$

#### A.5.9.FLANGE PLATE TO DOUBLER PLATE WELD DESIGN

Design of the PJP bevel groove weld was completed using CSA S16-19 Clause 13.13.2.1

$$t = 32 \text{ mm} \quad \theta_{groove} = 45^\circ \quad R_f = 4 \text{ mm} (R_f \text{ limit} \geq 3 \text{ mm})$$

$$S = 28 \text{ mm} \quad E = 28 \text{ mm} \quad L = 125 \text{ mm}$$

$$A_m = E \times l_w = 28 \text{ mm} \times 125 \text{ mm} = 3500 \text{ mm}^2$$

$$V_{r \text{ base}} = 0.67 \phi_w A_m F_u = 0.67 \times 0.67 \times 3125 \text{ mm}^2 \times 440 \text{ MPa} = 690 \text{ kN}$$

$$A_w = \frac{E}{\sqrt{2}} \times l_w = \frac{28 \text{ mm}}{\sqrt{2}} \times 125 \text{ mm} = 2475 \text{ mm}^2$$

$$V_{r \text{ weld}} = 0.67 \phi_w A_w X_u = 0.67 \times 0.67 \times 2475 \text{ mm}^2 \times 490 \text{ MPa} = 544 \text{ kN}$$

$$V_r = \min(V_{r \text{ base}}, V_{r \text{ weld}}) = 544 \text{ kN} > T_u \text{ OK}$$

#### A.5.10.FLANGE PLATE TO BEAM FLANGE WELD DESIGN

Top flange plate weld connection checked; bottom flange plate weld connection strength is greater due to the longitudinal weld lengths equal for both plates, but the transverse weld is longer.

$$s = 8 \text{ mm}$$

$$L_{Trans.} = 85 \text{ mm}$$

$$\begin{aligned} V_{r \text{ Trans.}} &= 0.67 \times \phi_w \times \frac{s}{\sqrt{2}} \times l \times X_u (1.00 + 0.5 \sin^{1.5} \theta_w) M_w \\ &= 0.67 \times 0.67 \times \frac{8 \text{ mm}}{\sqrt{2}} \times 85 \text{ mm} \times 490 \text{ MPa} (1.00 + 0.5 \sin^{1.5}(90^\circ)) \times 1.0 \\ &= 159 \text{ kN} \end{aligned}$$

$$L_{Long.} = 275 \text{ mm} \times 2 = 550 \text{ mm}$$

$$\begin{aligned} V_{r \text{ Long.}} &= 0.67 \times \phi_w \times \frac{s}{\sqrt{2}} \times l \times X_u (1.00 + 0.5 \sin^{1.5} \theta_w) M_w \\ &= 0.67 \times 0.67 \times \frac{8 \text{ mm}}{\sqrt{2}} \times 550 \text{ mm} \times 490 \text{ MPa} (1.00 + 0.5 \sin^{1.5}(0^\circ)) \times 0.85 \\ &= 582 \text{ kN} \end{aligned}$$

$$V_{r \text{ Total}} = V_{r \text{ Trans.}} + V_{r \text{ Long.}} = 740 \text{ kN} > T_u \text{ OK}$$

#### A.5.11.DESIGN SUMMARY

To avoid overhead welding, the top flange plate was tapered (allowing welding on plate edge to beam flange), the bottom flange page was widened (allowing welding on the beam flange edge to plate), and a fabrication cope was added to the bottom beam flange to allow for the welding of the bottom flange plate to the column. The flange plate length (= 324.5 mm) was controlled by the required length of the longitudinal weld between the flange plate and beam (plus the taper, cope, and 10 mm gap) and the flange plate thickness was controlled by the PJP bevel groove weld required to connect the flange plate to the doubler plate. The doubler plate was connected to the column using 10 mm fillets and 10 mm PJP flare-bevel groove welds along its top and side edges, respectively.

## Appendix B: FABRICATION DESIGN CONSIDERATIONS

A set of initial designs based on the design procedures defined in Chapter 3 were developed, as shown in Appendix C. It is important to note that the goal of these connections was to produce practical and economical connections (stated in Section 1.3). To accomplish this, fabricators were involved early in the design process to avoid unnecessary work and costs for fabrication.

### B.1. INITIAL COMMENTS

On December 3<sup>rd</sup>, 2021, a consultation with Marid Industries Ltd. was conducted to review the preliminary connection designs to ensure the connections were feasible and economical. This review from the fabricators identified a few fabrication issues and challenges. The identified issues and corrections were:

#### General Comments:

1. The clip angle bolt spacings originally 35 mm – 80 mm – 80 mm – 35 mm (according to Table 3-40a (CISC 2021)) were changed to 39 mm – 76 mm – 76 mm – 39 mm to match the typical spacing used in industry. Utilized existing templates made fabrication more economical as they removed the requirement for the machining process to be modified.
2. Due to the connections being welded (and thus not having much adjustability on site), design drawings should state, “confirm plate-to-plate or column-to-column dimensions prior to fabrication.”

#### For the T-Stiffener Connection Design:

1. Marid Industries Ltd. identified, based on previous experience, that the T-stiffener is designed per Section 3.1.2. (long and thin sections) would be susceptible to shear lag in the T-stiffener web and lateral torsional buckling of the T-stiffener flange. It was recommended that a stockier section be chosen such that the web thickness was equal to or greater than the beam’s flange thickness.
2. From an architectural point of view, it was pointed out by Marid Industries Ltd. that the vertical element(s) of the T-stubs in the T-stub connection could inadvertently interfere with a floor system. The use of angles (i.e., as tested by Picard & Giroux (1976)) could remedy this issue; however, Picard & Giroux (1976) demonstrated that angles performed less satisfactorily than T-stubs; thus, this recommendation was taken only under advisement.

For the Doubler Plate Connection Design:

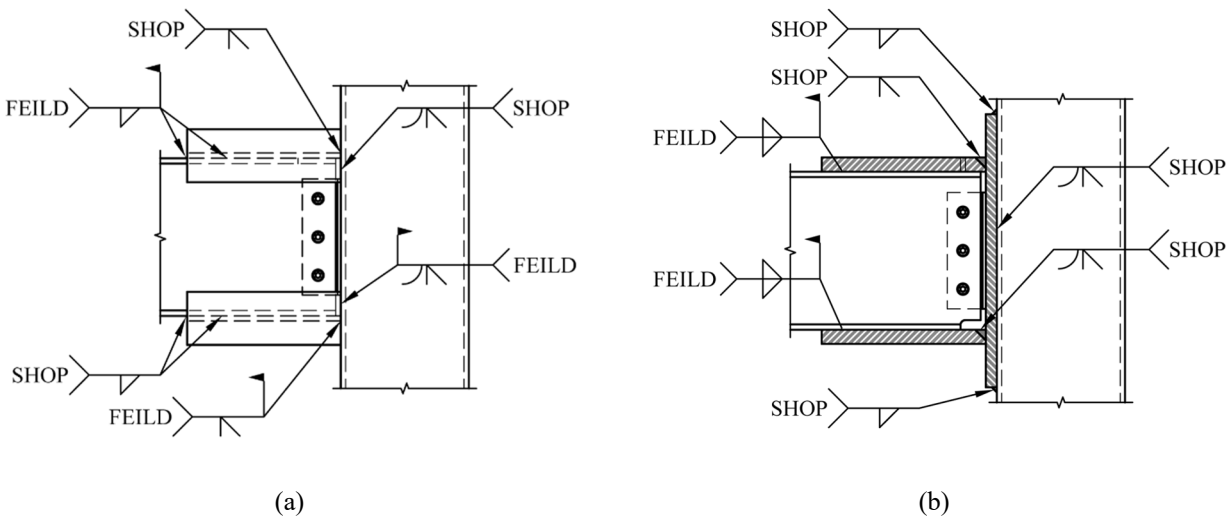
1. Originally, a CJP weld was used to connect the sides of the doubler plate to the HSS column face (see Appendix C). A more economical approach, as recommended by the fabricator, was to widen the doubler plate and utilize the existing corner of the HSS to produce a PJP V-groove weld with a 15-degree bevel. This type of weld is pre-qualified by CSA W59-18.
2. For the bottom flange plate, two recommendations were made to avoid overhead welding onsite. The first, increasing the bottom flange plate to a width of at least 125 mm to ensure adequate space for an 8 mm fillet weld on each side. The second, add a bottom beam flange cope to allow access to the areas required for the PJP weld connecting the flange plate to the doubler plate.

## B.2.FINAL COMMENTS

Following an initial round of revisions, additional recommendations regarding the ideal onsite fabrication concerns were provided by Marid Industries Ltd via email (on April 28<sup>th</sup>, 2022).

For the T-Stiffener Connection Design:

1. Marid Industries Ltd. recommends that a cope be added to the top flange of the beam to clear the clip angle during erection, allowing the beam to be lifted vertically into place rather than lifted and moved horizontally onto the clip angle requiring more equipment and time.
2. Regarding practical construction of the T-Stiffener connection in the shop and onsite, Marid Industries Ltd. provided their recommend approach shown in Fig. B.1.a. The top T-stiffeners should be welded to the column face in the shop, and the bottom stiffeners to the beam bottom flanges. During erection, the top T-stiffener is to be field welded to the beam top flanges and then the bottom T-stiffeners to the column face.



**Fig. B.1.** Recommended construction weld types

For the Doubler Plate Connection Design:

1. The practical shop and onsite welding recommendation from Marid Industries Ltd. for the Doubler Plate connection are shown in Fig. B.1.b. The doubler plate welds and the welds connecting the flange plates to the doubler plate should be completed in the shop. Then during the erection process, after the beam is slipped into place, the fillet welds connecting the flange plate to the beam should be completed.
2. Marid Industries Ltd. also indicated that from a fabrication and construction perspective, the Doubler Plate connection is the easier of the two connections to erect.

# Appendix C: INITIAL DESIGN DRAWINGS

Initial design drawings sent to Marid Industries Ltd. for consultation.

**FABRICATION NOTES:**

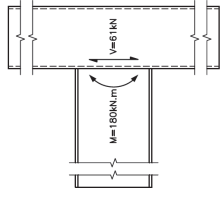
1. REPRESENTATIVE FROM DALHOUSIE UNIVERSITY MUST BE ON-SITE FOR THE DURATION OF THE WORK.
2. FABRICATION TO BE COMPLETED IN ACCORDANCE WITH CSA W59 OR AWS D1.1, REQUIRED FOR A CHEMICAL STUDY CONCERNED WITH LIMITED DUCTILITY MOMENT CONNECTIONS TO RHS.
3. FABRICATOR TO PROVIDE ALL MATERIAL MILL SHEETS FOR ALL STEEL SHAPES, PLATES AND WELD METALS USED.
4. FABRICATOR RESPONSIBLE FOR CUTTING AND WELDING THE STEEL SHAPES AND PLATE MATERIAL TO THE DIMENSIONS SHOWN ON THE DRAWINGS (SEE DET. 1 AND 2/SO1).
5. FABRICATOR TO PROVIDE ONE OFF-CUT OF STEEL SHAPES FOR EACH VARYING SIZE AND MILL HEAT TO THE DIMENSIONS SHOWN ON DET. 5/SO1 SUCH THAT MATERIAL PROPERTIES OF THE STEEL SHAPES CAN BE DETERMINED (BY TENSILE COUPON TESTS, HEREIN REFERRED TO AS TC TESTS, AT DALHOUSIE UNIVERSITY).
6. THE FABRICATOR TO PROVIDE CUT SAMPLES FROM PLATE MATERIAL (TO THE DIMENSIONS SHOWN ON DET. 6/SO1) REPRESENTING MATERIAL PROPERTIES OF THE TEST SPECIMEN PLATES CAN BE DETERMINED (BY TC TESTS, AT DALHOUSIE UNIVERSITY).
7. ALL WELDING WILL BE PERFORMED USING A SINGLE WELD COIL OF 600 MPa (71 ksi) FLUX-CORED ELECTRODE (SUCH THAT EACH OF THE WELDS HAS CONSISTENT MATERIAL PROPERTIES).
8. THE FABRICATOR WILL PROVIDE ONE ALL-WELD-METAL TO TEST SPECIMEN (SEE DET. 7/SO1), USING THE AGREED-UPOON WELDING PARAMETERS SUCH THAT THE MATERIAL PROPERTIES OF THE WELD METAL CAN BE DETERMINED (BY TC TESTS AT DALHOUSIE UNIVERSITY).

**GENERAL NOTES:**

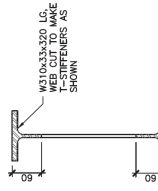
1. DRAWINGS ARE NOT FINAL AND SHOULD BE USED ONLY FOR ESTIMATING PURPOSES ONLY.
2. SEND RFI'S AND QUOTES, BY EMAIL, TO REBECCA.CHAMBERDALCA (CC: KYLIE.TOUSIGNANT@DALCA).
3. ALL UNITS ARE SHOWN IN MILLIMETERS UNLESS NOTED OTHERWISE.
4. DESIGN FORCES FOR CONNECTIONS SHOWN ON DET. 3/SO1.

**STRUCTURAL STEEL:**

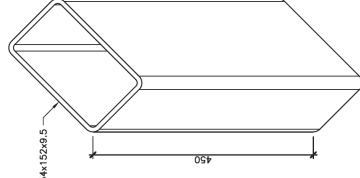
1. ALL STRUCTURAL STEEL SHALL BE NEW STOCK & CONFORM TO THE FOLLOWING GRADES & STANDARDS:
  1. STEEL SECTIONS - G40.20-13/G40.21-13 (R2018), GRADE 350W OR ASTM A572/A572M-18, GRADE 345 MPa WHERE APPLICABLE
  2. ANGLES & PLATES - G40.20-13/G40.21-13 (R2018), GRADE 300W.
2. ALL PLATE MATERIAL OF EQUAL THICKNESS TO ORIGINATE FROM THE SAME MILL HEAT.
3. ALL WIDE-FLANGE SHAPES TO ORIGINATE FROM THE SAME MILL HEAT.
4. ALL HSS TO ORIGINATE FROM THE SAME MILL HEAT. HSS MATERIAL WILL BE SUPPLIED BY ATLAS TUBE.
5. ALL ANGLES TO ORIGINATE FROM THE SAME MILL HEAT.
6. ALL STRUCTURAL STEEL SHALL BE FABRICATED IN ACCORDANCE WITH CSA S16-19.
7. ALL WELDING & WELD MATERIALS TO CONFORM WITH CSA W59-18, & BE PERFORMED BY A FABRICATOR FULLY APPROVED UNDER CSA W47.119, DIVISIONS NO. 1 & NO. 2.
8. ALL BOLTS, NUTS & WASHERS FOR STRUCTURAL STEEL CONNECTIONS SHALL CONFORM TO ASTM F3125/F3125M-1992 (BOLTS) GRADE A325, ASTM A563-15 (NUTS) & ASTM F436/F436M-19 (WASHERS).
9. ALL BOLT HOLES SHALL BE NEATLY DRILLED OR PLASMA CUT AND SHALL NOT BE BURIED.
10. MARK MATERIALS IN ACCORDANCE WITH CAN/CSA-G40.20.



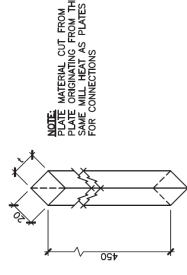
**3 DETAIL—CONNECTION FORCES**  
S01 N.T.S.



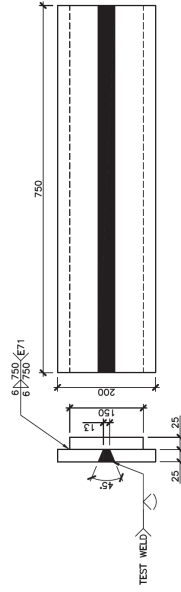
**4 DETAIL—T-STIFFENER**  
S01 1:5



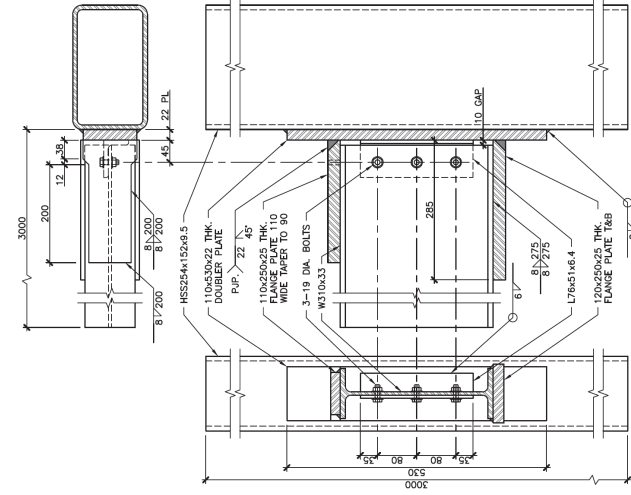
**5 DETAIL—MATERIAL OFF-CUT FOR TENSILE COUPONS**  
S01 1:5 QTY 1/EACH/HEAT



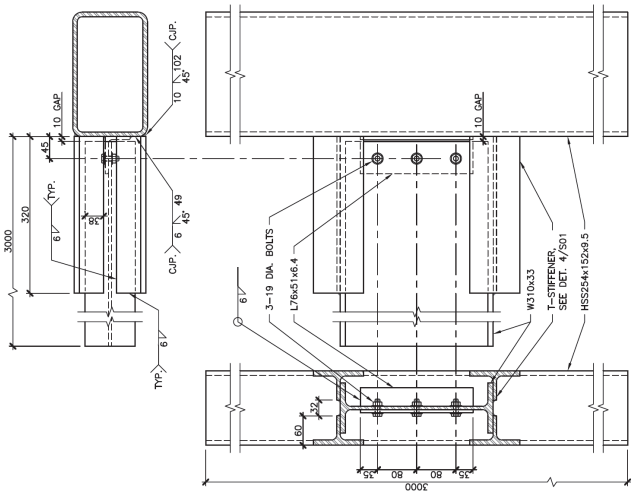
**6 DETAIL—PLATE MATERIAL TENSILE COUPON (TC)**  
S01 1:2 QTY 3/THICKNESS/HEAT



**7 DETAIL—ALL-WELD-METAL TENSILE COUPON (TC)**  
S01 1:5 QTY 1/EACH TYPE



**2 DETAIL—DOUBLER PLATE CONNECTION**  
S01 1:5 QTY 3



**1 DETAIL—T-STIFFENER CONNECTION**  
S01 1:5 QTY 3

No.	REVISION/ISSUE	DATE

**ISSUED FOR QUOTE**

PROJECT : LIMITED DUCTILITY MOMENT CONNECTIONS TO RHS COLUMNS.

DRAWING TITLE : CONNECTION FABRICATION DRAWINGS

SCALE :	AS SHOWN & CLARIFY
DRAWN BY :	
DATE :	04/01/2021
SHEET :	1 OF 1

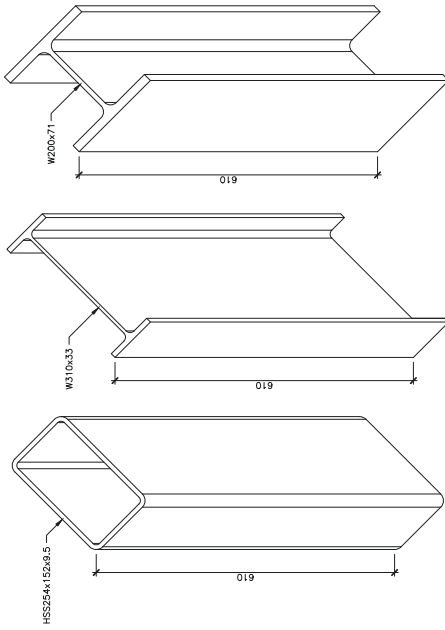
S01



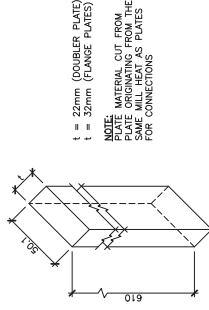
# Appendix D: SPECIMEN AND METAL COUPON FABRICATION DRAWINGS

Connection fabrication drawings, tensile coupon, machining details.

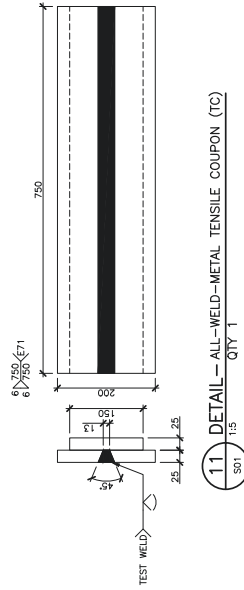




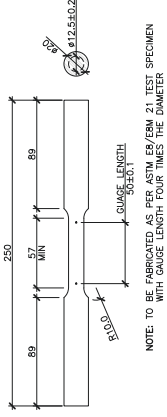
**9** **DETAIL — MATERIAL OFF-CUT FOR TENSILE COUPONS**  
 QTY 1/EACH/HEAT



**10** **DETAIL — PLATE MATERIAL TENSILE COUPON (TC)**  
 QTY 3/THICKNESS/HEAT

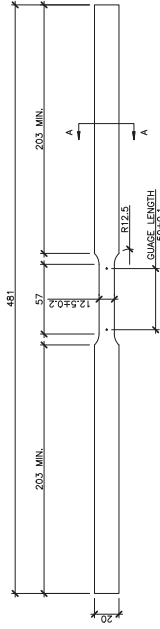


**11** **DETAIL — ALL-WELD-METAL TENSILE COUPON (TC)**  
 QTY 1



NOTE: TO BE FABRICATED AS PER ASTM E8/E8M 21 TEST SPECIMEN WITH GAUGE LENGTH FOUR TIMES THE DIAMETER

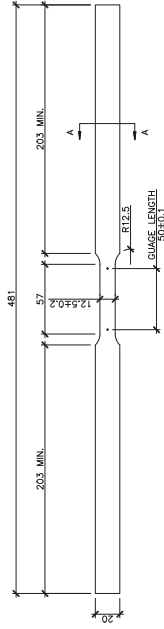
**14** **DETAIL — ALL-WELD-METAL TENSILE COUPON**  
 QTY 3/HEAT



L-SHAPE THICKNESS  
 3 x W305x65x6.5  
 3 x W310x33  
 3 x W200x71  
 SECTION A-A

NOTE: TO BE FABRICATED AS PER ASTM E8/E8M 21 SHEET-TYPE TENSILE COUPON SPECIMEN

**15** **DETAIL — TYPICAL TENSILE COUPON**  
 QTY 3/THICKNESS/HEAT



L-SHAPE THICKNESS  
 3 x FROM 22 THK. PLATE (HT# E18692)  
 3 x FROM 32 THK. PLATE (HT# A20305)  
 SECTION A-A

NOTE: TO BE FABRICATED AS PER ASTM E8/E8M 21 SHEET-TYPE TENSILE COUPON SPECIMEN

**16** **DETAIL — PLATE TENSILE COUPON**  
 QTY 3/HEAT

No.	REVISION/ISSUE	DATE
A	ISSUED FOR THESE	07/23

ISSUED FOR FABRICATION

PROJECT : LIMITED DUCTILITY MOMENT CONNECTIONS TO RHS COLUMNS.

DRAWING TITLE : TENSILE COUPON MACHINING DETAILS

SCALE:	AS SHOWN
DRAWN BY:	R. GUJANE
DATE:	11/07/2023
SHEET:	2 OF 4

# Appendix E: TEST SETUP AND INSTRUMENTATION

Testing layout, machining, and instrumentation details.



No.	ISSUED FOR THIS REVISION/ISSUE	DATE
A		07/23

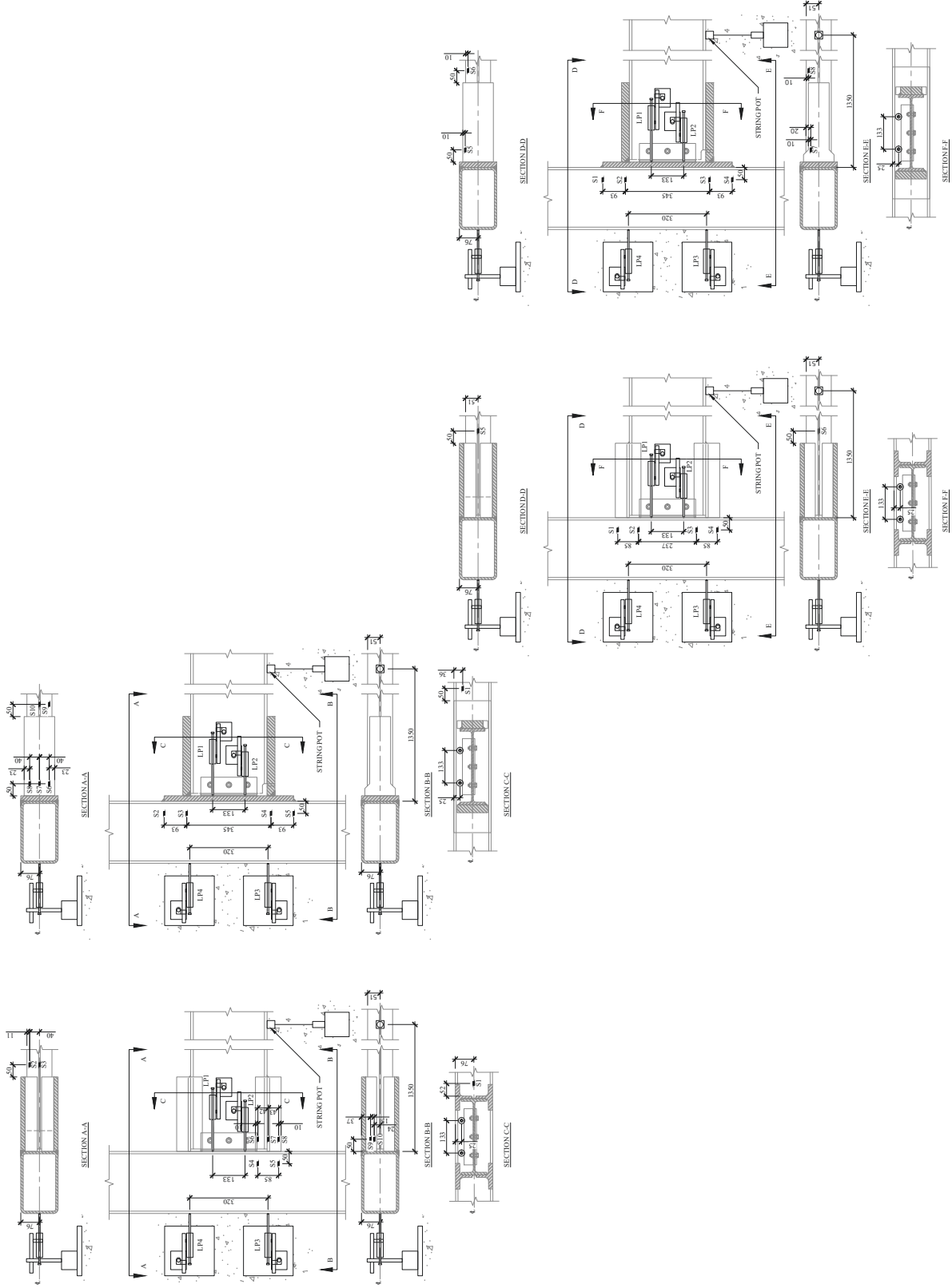
ISSUED FOR FABRICATION

PROJECT : LIMITED DUCTILITY MOMENT CONNECTIONS TO RHS COLUMNS.

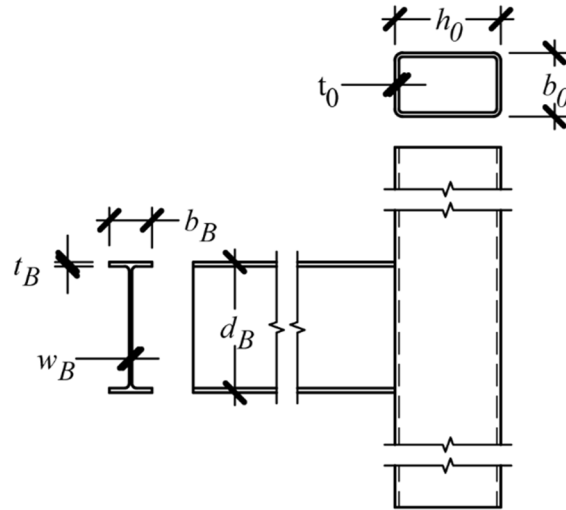
DRAWING TITLE : INSTRUMENTATION DETAILS

SCALE :	AS SHOWN
DRAWN BY :	R. CAHANE
DATE :	10/07/2023
SHEET :	4 OF 4

S04



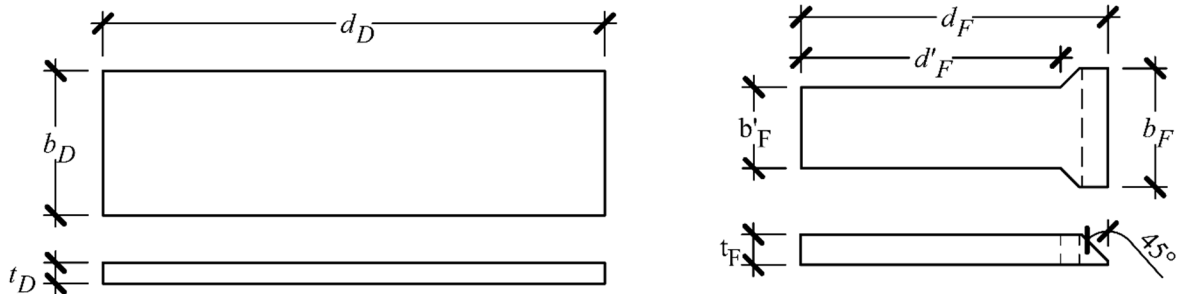
# Appendix F: GEOMETRIC PROPERTIES



**Fig. F.1.** Dimensions of HSS and W-section members

**Table F-1.** Dimensions of HSS and W-section members

Prototype	$b_0$ (mm)	$h_0$ (mm)	$t_0$ (mm)	$b_b$ (mm)	$w_b$ (mm)	$h_b$ (mm)	$t_b$ (mm)
Nominal	152.4	254.0	8.58	102.0	6.6	313.0	10.80
T1	155.5	254.5	9.50	103.0	6.67	313.0	10.22
T2	155.0	255.0	9.57	103.0	6.96	314.0	10.10
T3	154.5	254.0	9.39	102.0	6.70	313.5	9.95
DP1	155.5	253.0	9.53	105.0	6.74	312.0	10.24
DP2	154.0	253.5	9.50	102.5	6.88	312.0	10.26
DP3	154.0	253.5	9.24	104.0	6.69	312.0	10.32



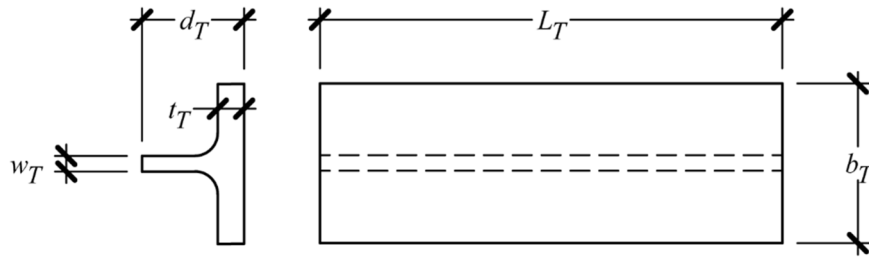
(a) Doubler plate

(b) Top flange plate (bottom similar)

**Fig. F.2.** Dimensions of doubler and flange plates

**Table F-2.** Dimensions of doubler and flange plates

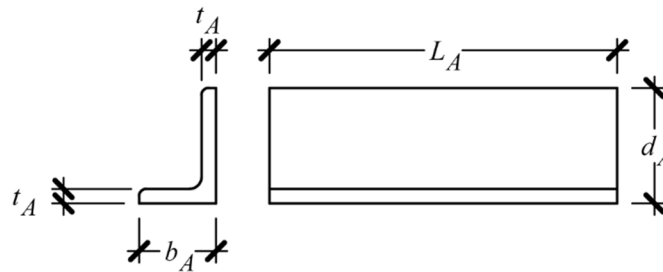
Prototype	$b_p$ (mm)	$d_p$ (mm)	$t_p$ (mm)	$b_f$ (mm)	$b'_f$ (mm)	$d_f$ (mm)	$t_f$ (mm)
Nominal	152.0	540.0	22.00	125.0	85.0	325.0	32.00
DP1	153.0	530.5	22.47	125.0	85.0	325.0	32.00
DP2	153.0	531.0	22.23	126.0	85.0	323.0	32.00
DP3	152.0	531.0	22.37	126.0	85.5	324.5	32.00



**Fig. F.3.** Dimensions of T-stiffeners

**Table F-3.** Dimensions of T-stiffeners

Prototype	$b_t$ (mm)	$w_t$ (mm)	$d_t$ (mm)	$t_t$ (mm)	$l_t$ (mm)
Nominal	105.0	10.20	62.0	17.40	325
T1	109.0	10.55	62.5	17.54	325
T2	108.5	10.41	62.1	17.29	325
T3	108.6	10.33	62.9	17.24	325



**Fig. F.4.** Dimensions of clip angle



**Table F-4.** Dimensions of clip angle

Prototype	$b_a$ (mm)	$d_a$ (mm)	$t_a$ (mm)	$l_a$ (mm)
Nominal	50.8	76.2	6.40	230
T1	52.0	76.0	6.49	230
T2	51.0	76.0	6.48	230
T3	50.5	75.0	6.51	230
DP1	51.0	75.5	6.52	230
DP2	51.0	76.0	6.50	230
DP3	50.0	75.0	6.50	230

# Appendix G: MATERIAL PROPERTY TEST RESULTS

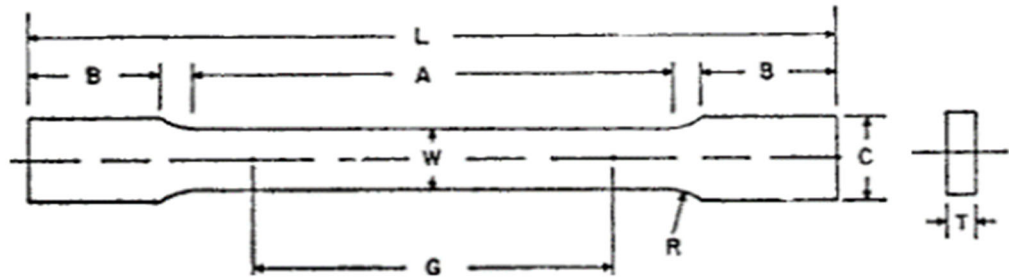
Three tensile coupons were cut from each material type and heat used for the connection assemblies, totaling 7 sets (21 coupons). All coupons cut from steel shapes or plates were fabricated according to ASTM E8/E8M-21 sheet-type specifications, and all weld metal coupons were fabricated to ASTM E8/E8M-21 test specimens with a gauge length four times the diameter. Yield strengths reported on the follow pages were calculated using the offset method at 0.002 mm/mm strain.



Fig. G.1. Tensile coupons (post-testing)

HSS254x152x9.5

Test Date: 2022-12-05 Test Time: 9:00am-9:45am  
 Test Rate: 1.5 mm/min Data Rate: 1 Hz



Testing Loads		
$\Delta L$ (mm)	Yielding Force (kN)	Ultimate Force (kN)
17	52.5	61.2

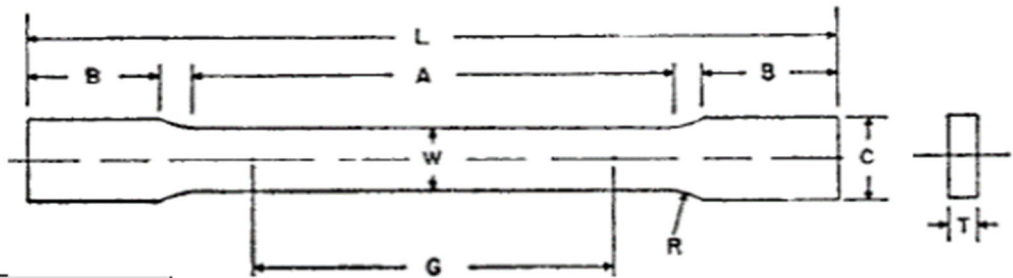
Pre-Test Dimensions							
	L (mm)	B (mm)	A (mm)	W (mm)	G (mm)	C (mm)	T (mm)
Nominal	481	203	57	12.5	50	20	9.53
HSS-1	510	215	60.2	12.5	50	20	9.5
HSS-2	510	215	55	12.6	50.2	20.2	9.5
HSS-3	515	217.5	56	12.4	50	20	9.6

Post-Test Dimensions					
	T (mm)	W (mm)	G (mm)		G avg (mm)
HSS-1	5.6	8.1	68.0	67.7	67.6
HSS-2	5.5	8.3	65.6	65.5	64.5
HSS-3	5.7	7.7	67.6	68.3	68.1

Nominal vs. Actual Properties							
	Yield Strength $F_y$ (Mpa)	Yield Strain $\epsilon_y$ (mm/mm)	Ultimate Strength $F_u$ (Mpa)	Ultimate Strain $\epsilon_u$ (mm/mm)	Fracture Strength $F_f$ (Mpa)	Fracture Strain $\epsilon_f$ (mm/mm)	Young's Modulus $E$ (Gpa)
HSS-1	400.74	0.0040	494.67	0.145	339.35	0.352	200.2
HSS-2	409.15	0.0037	516.50	0.122	355.40	0.285	194.2
HSS-3	379.13	0.0037	472.10	0.172	334.49	0.362	199.6
Average	396	0.0038	494	0.1460	343	0.3330	198.0

W200x71

Test Date: 2022-12-05 Test Time: 10:40am-11:40am  
 Test Rate: 1.5 mm/min Data Rate: 1 Hz



Testing Loads		
$\Delta L$ (mm)	Yielding Force (kN)	Ultimate Force (kN)
14	51.3/87.5	68.7/117.1

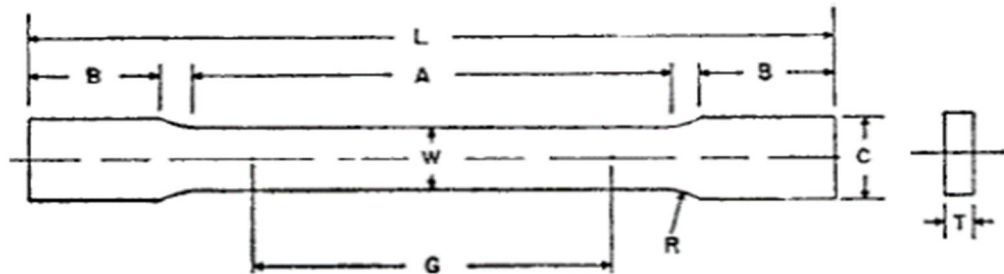
Tensile Coupon Measurements							
	L (mm)	B (mm)	A (mm)	W (mm)	G (mm)	C (mm)	T (mm)
Nominal	481	203	57	12.5	50	20	10.2
W200-1	510	217	56	12.6	50	20.3	10
W200-2	508	217	55.4	12.6	50	19.8	17.2
W200-3	511	215	56.7	12.4	50	20.3	17.5

Post-Test Dimensions					
	T (mm)	W (mm)	G (mm)	G avg (mm)	
W200-1	6.4	8.2	66.8	67.4	67.1
W200-2	10.1	7.5	70.0	69.2	70.0
W200-3	10.8	7.4	69.8	69.6	69.5

Nominal vs. Actual Properties							
	Yield Strength $F_y$ (Mpa)	Yield Strain $e_y$ (mm/mm)	Ultimate Strength $F_u$ (Mpa)	Ultimate Strain $e_u$ (mm/mm)	Fracture Strength $F_f$ (Mpa)	Fracture Strain $e_f$ (mm/mm)	Young's Modulus $E$ (Gpa)
W200-1	413.25	0.0037	558.23	0.193	371.96	0.342	203.5
W200-2	369.90	0.0037	542.99	0.189	353.56	0.395	206.3
W200-3	379.83	0.0038	537.49	0.202	354.86	0.393	200.8
Average	388	0.0037	546	0.1948	360	0.3764	203.5

W310x33 - HT# D165477 (T-Stub)

Test Date: 2022-12-05 Test Time: 9:50am-10:35am  
 Test Rate: 1.5 mm/min Data Rate: 1 Hz



Testing Loads		
$\Delta L$ (mm)	Yielding Force (kN)	Ultimate Force (kN)
13	35.4	43.8

Tensile Coupon Measurements							
	L (mm)	B (mm)	A (mm)	W (mm)	G (mm)	C (mm)	T (mm)
Nominal	481	203	57	12.5	50	20	6.6
TW310-1	508	214	56.1	12.4	50	20.1	6.8
TW310-2	509	215	56.8	12.5	50	20.2	6.7
TW310-3	510	216	56.9	12.8	50	20.1	6.8

Post-Test Dimensions						
	T (mm)	W (mm)	G (mm)		G avg (mm)	
TW310-1	4.1	8.5	65.2	64.2	66.8	
TW310-2	4.1	9.2	67.0	66.3	66.2	
TW310-3	4.1	9.2	63.8	65.2	66.5	

Nominal vs. Actual Properties							
	Yield Strength $F_y$ (Mpa)	Yield Strain $\epsilon_y$ (mm/mm)	Ultimate Strength $F_u$ (Mpa)	Ultimate Strain $\epsilon_u$ (mm/mm)	Fracture Strength $F_f$ (Mpa)	Fracture Strain $\epsilon_f$ (mm/mm)	Young's Modulus $E$ (Gpa)
TW310-1	430.67	0.0039	537.77	0.209	386.96	0.308	200.7
TW310-2	418.40	0.0039	542.14	0.211	404.18	0.330	197.3
TW310-3	408.65	0.0038	515.90	0.214	383.61	0.303	200.0
Average	419	0.0039	532	0.2114	392	0.3138	199.3



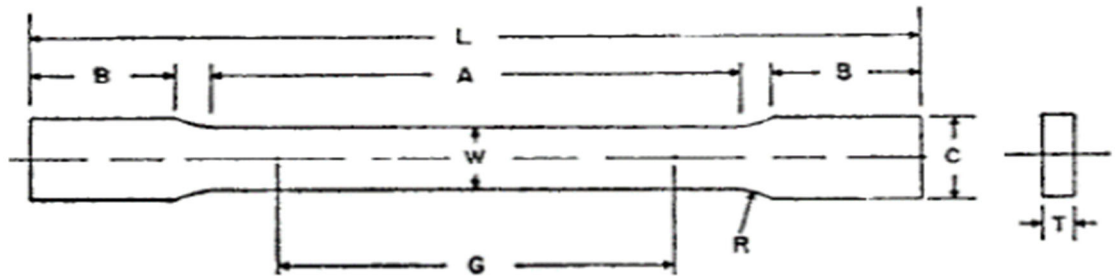
W310x33 - HT# D169312 (Doubler Plate)

Test Date:

Test Time:

Test Rate: 1.5 mm/min

Data Rate: 1 Hz



Testing Loads		
$\Delta L$ (mm)	Yielding Force (kN)	Ultimate Force (kN)
11	34.9	45.6

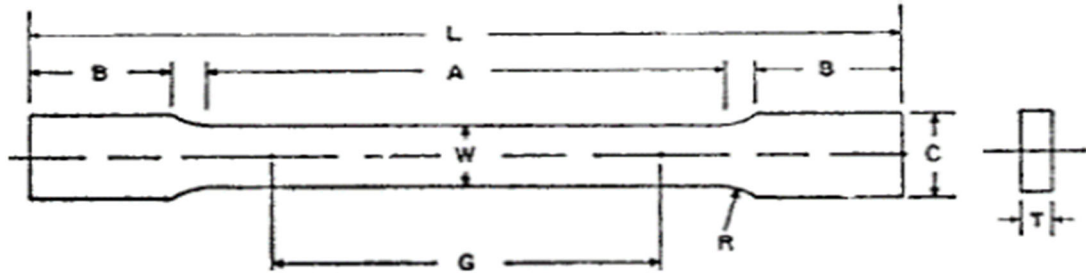
Tensile Coupon Measurements							
	L (mm)	B (mm)	A (mm)	W (mm)	G (mm)	C (mm)	T (mm)
Nominal	481	203	57	12.5	50	20	6.6
W310-1	545	232	65.0	12.5	50	20.4	6.7
W310-2	545	233	65.0	12.5	50	20.2	6.7
W310-3	545	232	64.3	12.8	50	20.3	6.7

Post-Test Dimensions						
	T (mm)	W (mm)	G (mm)			G avg (mm)
W310-1	4.4	8.6	66.4	66.9	66.4	66.6
W310-2	4.4	8.8	66.6	66.8	66.6	66.7
W310-3	4.1	8.9	66.4	66.2	67.00	66.5

Nominal vs. Actual Properties							
	Yield Strength $F_y$ (Mpa)	Yield Strain $\epsilon_y$ (mm/mm)	Ultimate Strength $F_u$ (Mpa)	Ultimate Strain $\epsilon_u$ (mm/mm)	Fracture Strength $F_f$ (Mpa)	Fracture Strain $\epsilon_f$ (mm/mm)	Young's Modulus $E$ (Gpa)
DPW310-1	396.20	0.0040	521.34	0.208	381.70	0.331	190.0
DPW310-2	356.66	0.0039	531.62	0.215	367.35	0.333	183.3
DPW310-3	388.09	0.0038	512.86	0.199	377.42	0.331	191.7
Average	380	0.0039	522	0.2076	375	0.3318	188.3

22mm Plate

Test Date: 2022-12-06      Test Time: 8:30 am - 9:15am  
 Test Rate: 2 mm/min      Data Rate: 1 Hz



Testing Loads		
$\Delta L$ (mm)	Yielding Force (kN)	Ultimate Force (kN)
19	86.4	109.6

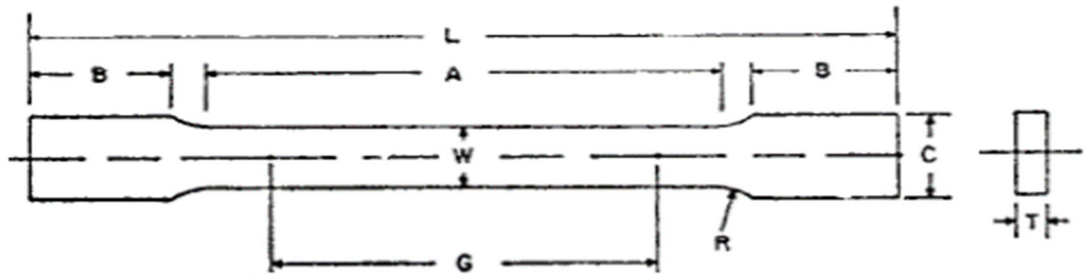
Tensile Coupon Measurements							
	L (mm)	B (mm)	A (mm)	W (mm)	G (mm)	C (mm)	T (mm)
Nominal	481	203	57	12.5	50	20	18
22PL-1	511	219	57.2	12.5	50	20.2	18
22PL-2	510	220	56.4	12.7	50	20.2	18
22PL-3	511	217	56.8	12.4	50	20.3	18

Post-Test Dimensions					
	T (mm)	W (mm)	G (mm)		G avg (mm)
22PL-1	12	7.6	68.4	67.9	69.9
22PL-2	11.5	7.8	69.4	69.1	70.5
22PL-3	11.6	7.6	68.6	68.7	67.5

Nominal vs. Actual Properties							
	Yield Strength $F_y$ (Mpa)	Yield Strain $\epsilon_y$ (mm/mm)	Ultimate Strength $F_u$ (Mpa)	Ultimate Strain $\epsilon_u$ (mm/mm)	Fracture Strength $F_f$ (Mpa)	Fracture Strain $\epsilon_f$ (mm/mm)	Young's Modulus $E$ (Gpa)
22PL-1	372.02	0.0037	518.74	0.187	288.75	0.375	201.3
22PL-2	345.73	0.0038	514.95	0.192	366.38	0.393	189.3
22PL-3	370.67	0.0038	522.92	0.187	347.61	0.365	207.3
Average	363	0.0038	519	0.1889	334	0.3778	199.3

32mm Plate

Test Date: 2022-12-06      Test Time: 9:15am-10am  
 Test Rate: 2 mm/min      Data Rate: 1 Hz



Testing Loads		
$\Delta L$ (mm)	Yielding Force (kN)	Ultimate Force (kN)
12	79.1	114.8

Tensile Coupon Measurements							
	L (mm)	B (mm)	A (mm)	W (mm)	G (mm)	C (mm)	T (mm)
Nominal	481	203	57	12.5	50	20	18
32PL-1	512	216	57.3	12.5	50	20.3	18.3
32PL-2	511	214	58	12.4	50	20.1	17.9
32PL-3	510	219	57.4	12.5	50	20.1	18

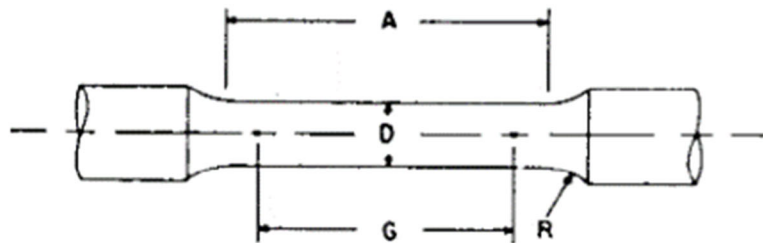
Post-Test Dimensions						
	T (mm)	W (mm)	G (mm)			G avg (mm)
32PL-1	12.6	8	69.1	69.2	68.8	69.0
32PL-2	11.6	7.5	70.7	70.1	70.5	70.4
32PL-3	12.6	7.5	68.6	68	68.1	68.2

Nominal vs. Actual Properties							
	Yield Strength $F_y$ (Mpa)	Yield Strain $\epsilon_y$ (mm/mm)	Ultimate Strength $F_u$ (Mpa)	Ultimate Strain $\epsilon_u$ (mm/mm)	Fracture Strength $F_f$ (Mpa)	Fracture Strain $\epsilon_f$ (mm/mm)	Young's Modulus $E$ (Gpa)
32PL-1	366.98	0.0038	521.09	0.181	371.21	0.381	193.2
32PL-2	362.64	0.0036	531.80	0.184	377.34	0.409	208.7
32PL-3	355.37	0.0039	515.18	0.174	364.50	0.365	183.1
Average	362	0.0038	523	0.1797	371	0.3847	195.0



Weld Metal

Test Date: 2022-12-01      Test Time: 9:00am-10:10am  
 Test Rate: 1 mm/min      Data Rate: 1 Hz



Testing Loads		
$\Delta L$ (mm)	Yielding Force (kN)	Ultimate Force (kN)
61	56.5	75.2

Tensile Coupon Measurements					
	L (mm)	A (mm)	G (mm)	D (mm)	d (mm)
Nominal	250	56	50	12.5	20
W-1	249	56.8	50	12.4	20.1
W-2	252	55.9	50	12.5	20
W-3	248	56.1	50	12.4	20

Post-Test Dimensions					
	D (mm)		G (mm)		G avg (mm)
W-1	7	61	62	61	61.3
W-2	7.4	64	65	63	64.0
W-3	7.2	64	62	63	63.0

Nominal vs. Actual Properties							
	Yield Strength $F_y$ (Mpa)	Yield Strain $\epsilon_y$ (mm/mm)	Ultimate Strength $X_u$ (Mpa)	Ultimate Strain $\epsilon_u$ (mm/mm)	Fracture Strength $F_f$ (Mpa)	Fracture Strain $\epsilon_f$ (mm/mm)	Young's Modulus $E$ (Gpa)
W-1	566.66	0.0046	618.19	0.128	430.53	0.227	199.2
W-2	N/A*	N/A*	614.60	N/A*	430.53	0.280	199.9
W-3	543.31	0.0050	601.71	0.139	409.64	0.260	196.2
Average	555	0.0048	612	0.1334	424	0.2556	198.5

\* During test extensometer was taken off early and data points were not collected to define these values

## Appendix H: EXPERIMENTAL TEST DATA

Tests were conducted in the Dalhousie Heavy Structure Lab located on Sexton Campus. Test were completed at a testing rate of approximately 2 mm/min for static tests and 6 mm/min for cyclic tests. A data collection rate of 1 Hz was used for all tests.

## H.1.STATIC TEST RESULTS FOR CONNECTION ASSEMBLY T1

This test was conducted on February 8th, 2023, from 9:00 am to 9:30 pm. In the first third of the test some yielding/paint chipping occurred at the welded connection for the top T-stiffener but did not continue to propagate or worsen as testing continued.

### H.1.1.ROTATIONS

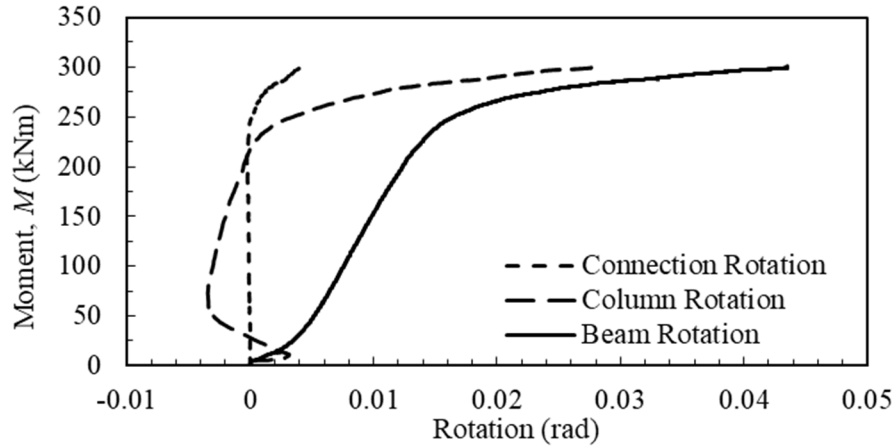


Fig. H.1. T-Stiffener static test rotations

### H.1.2.MOCK CYCLIC RESPONSE

After conducting the static tests, the connection and test setup were subjected to cyclic loading (0.04 radians in the positive rotation direction and 0.02 radians in the negative rotation direction).

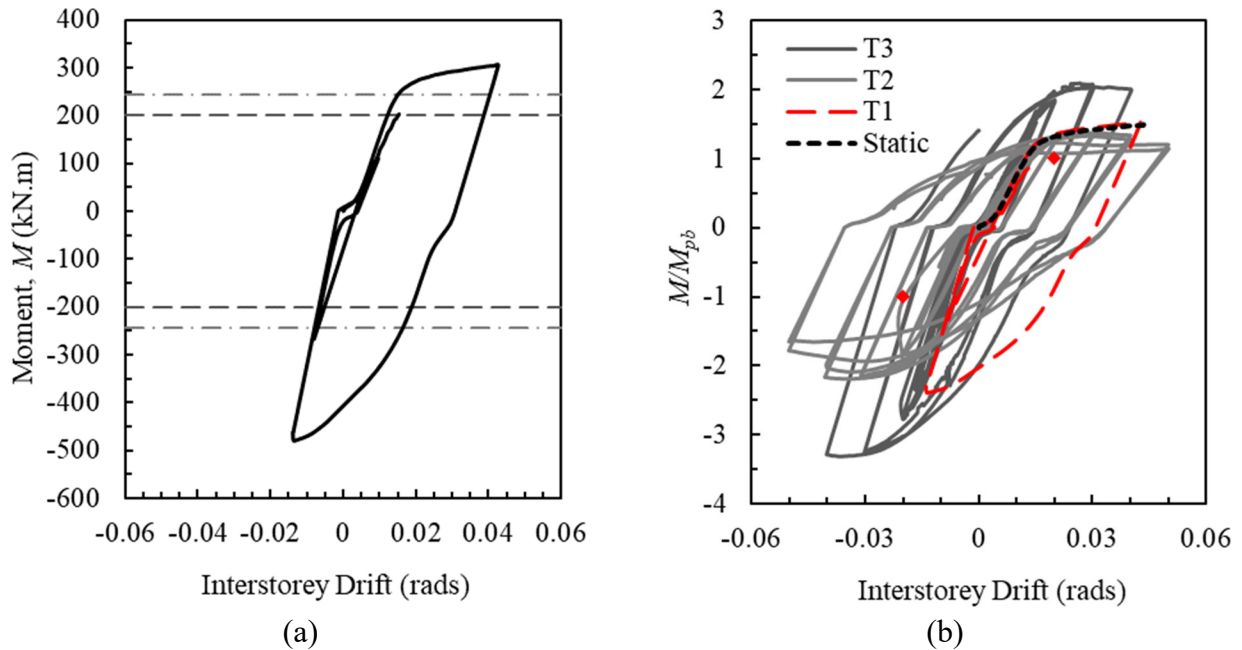
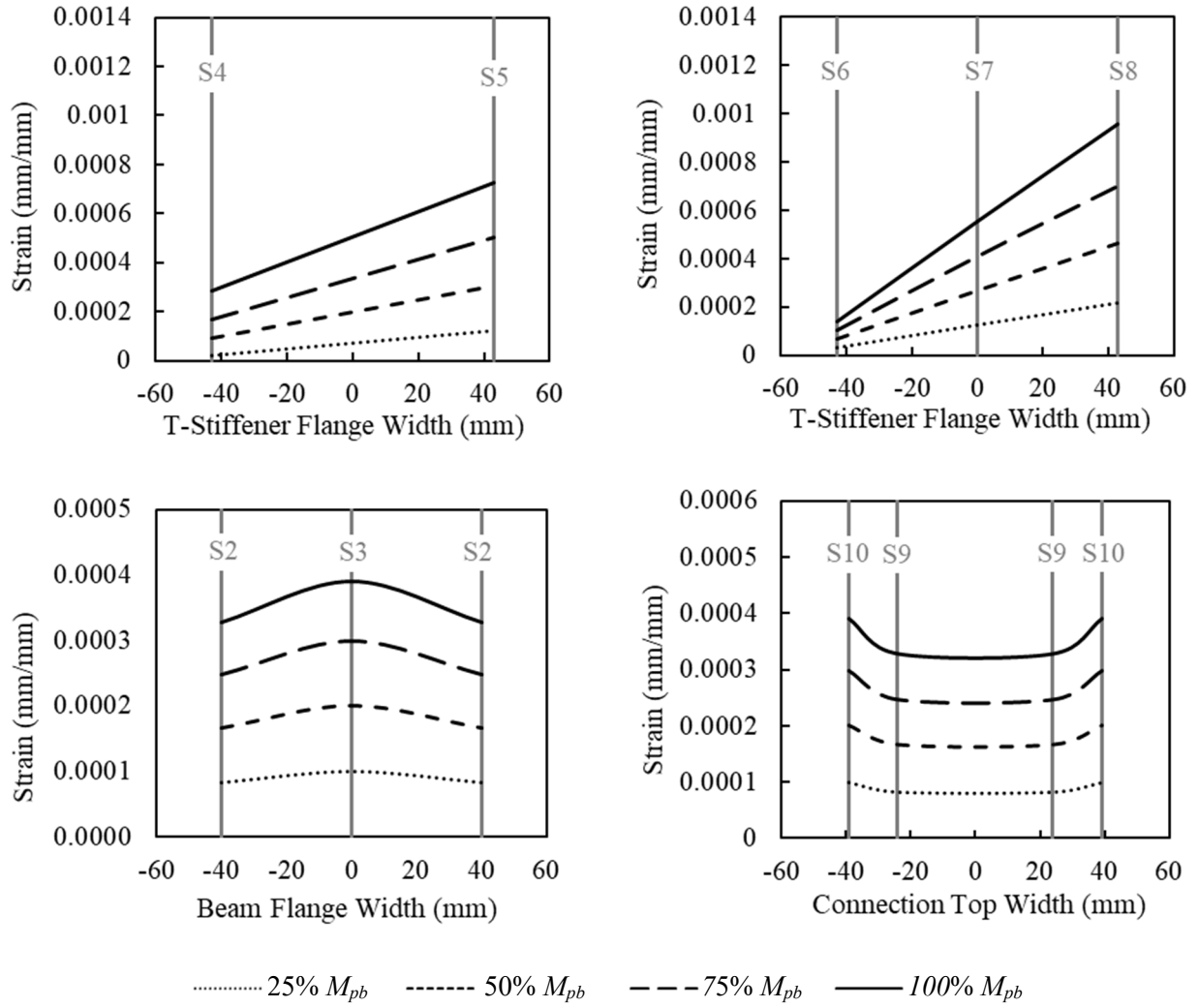


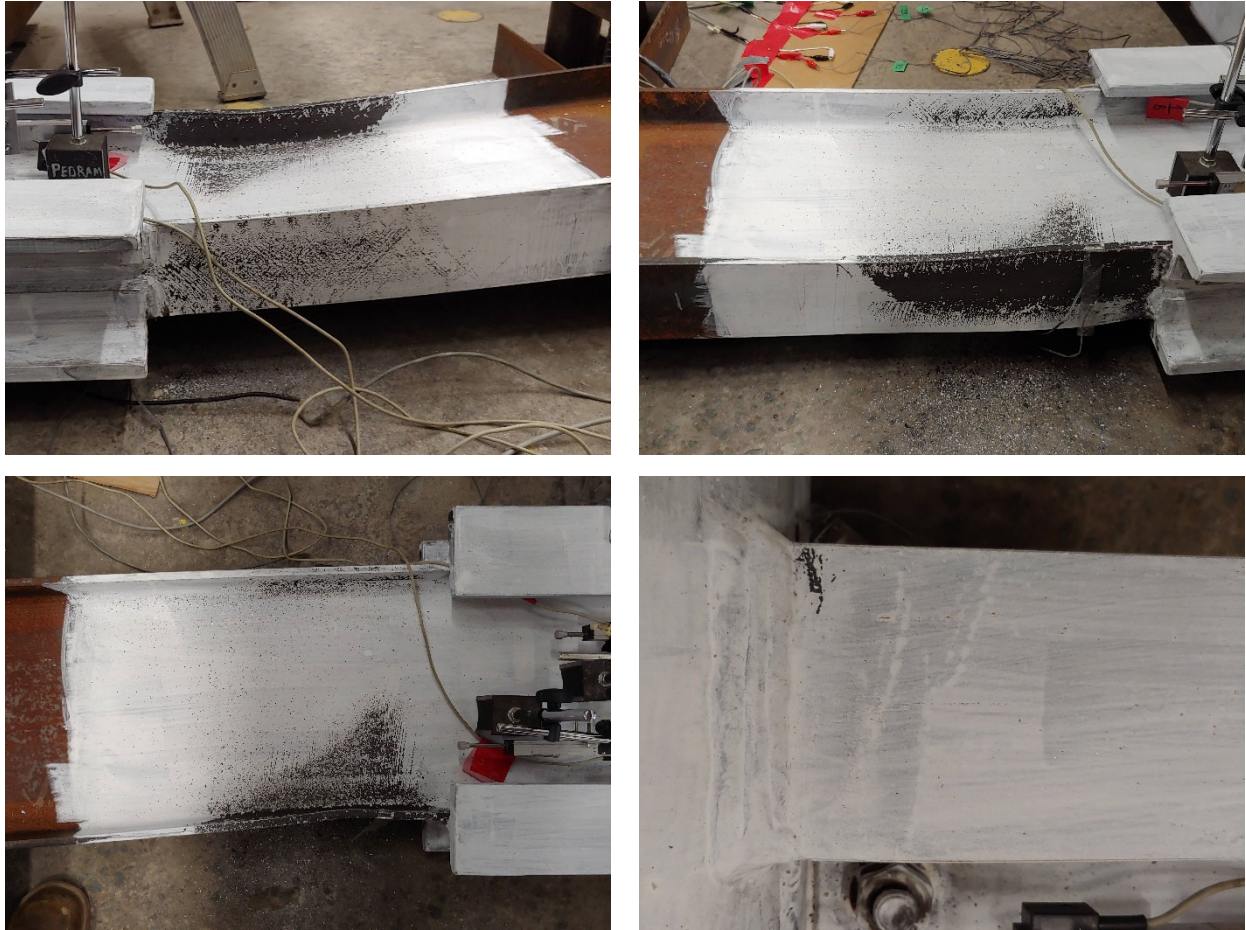
Fig. H.2. T-Stiffener mock cyclic response

### H.1.3. STRAIN GAUGE RESULTS



**Fig. H.3.** T-Stiffener static test strain response

#### H.1.4. TESTING PHOTOS



**Fig. H.4.** T-Stiffener post-testing photos

## H.2.STATIC TEST RESULTS FOR CONNECTION ASSEMBLY DP3

Test initially attempted on December 8<sup>th</sup> but experiment was stopped after 25kN applied due to twisting in the beam and deflection being applied to the actuator. Learning from the first attempt the actuator support system was reinforced, and lateral torsional buckling bracing was added. The official test was conducted on January 18<sup>th</sup>, 2023, from 9:00 am to 9:30 am.

### H.2.1.ROTATIONS

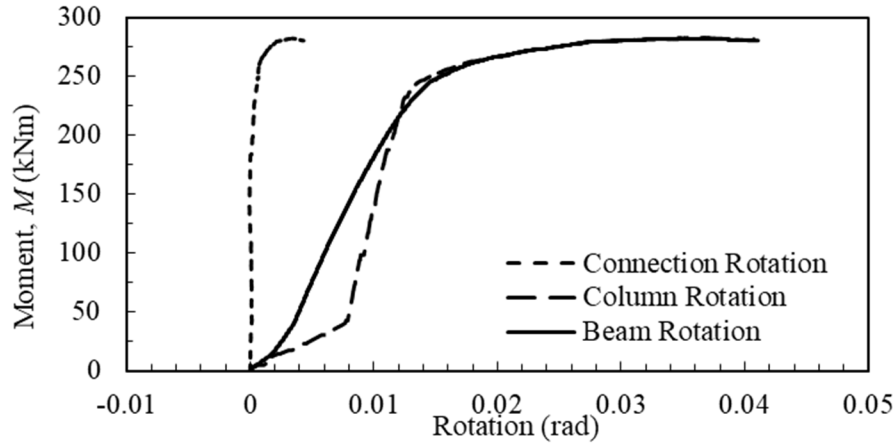


Fig. H.5. Doubler Plate static test rotations

### H.2.2.MOCK CYCLIC RESPONSE

After conducting the static tests, the connection and test setup were subjected to cyclic loading (0.04 radians in the positive rotation direction and 0.02 radians in the negative rotation direction).

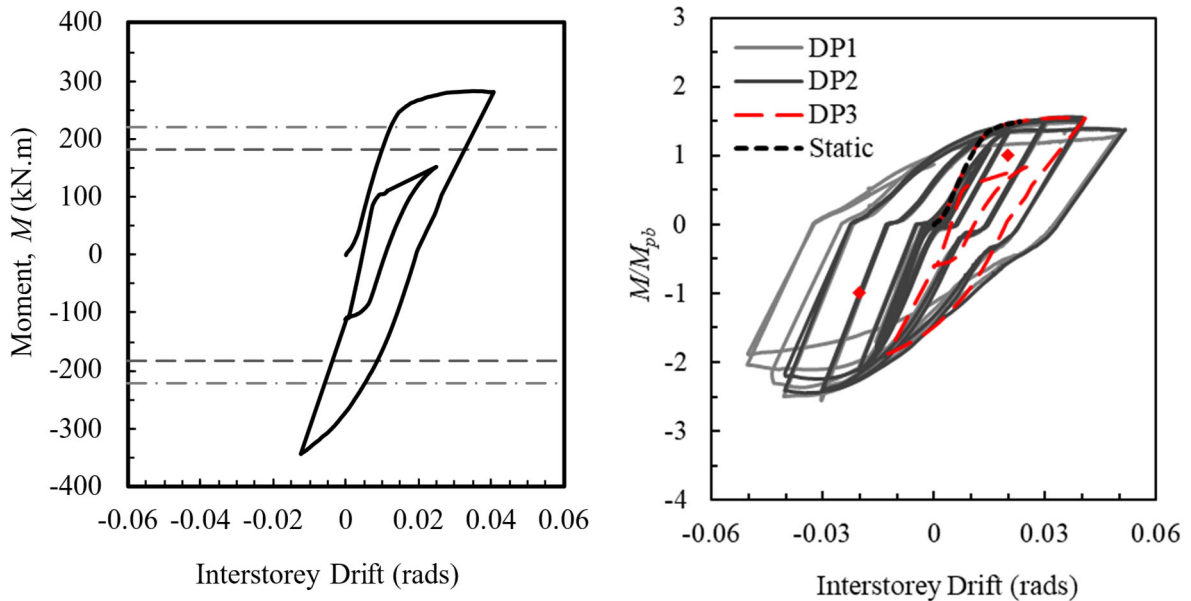
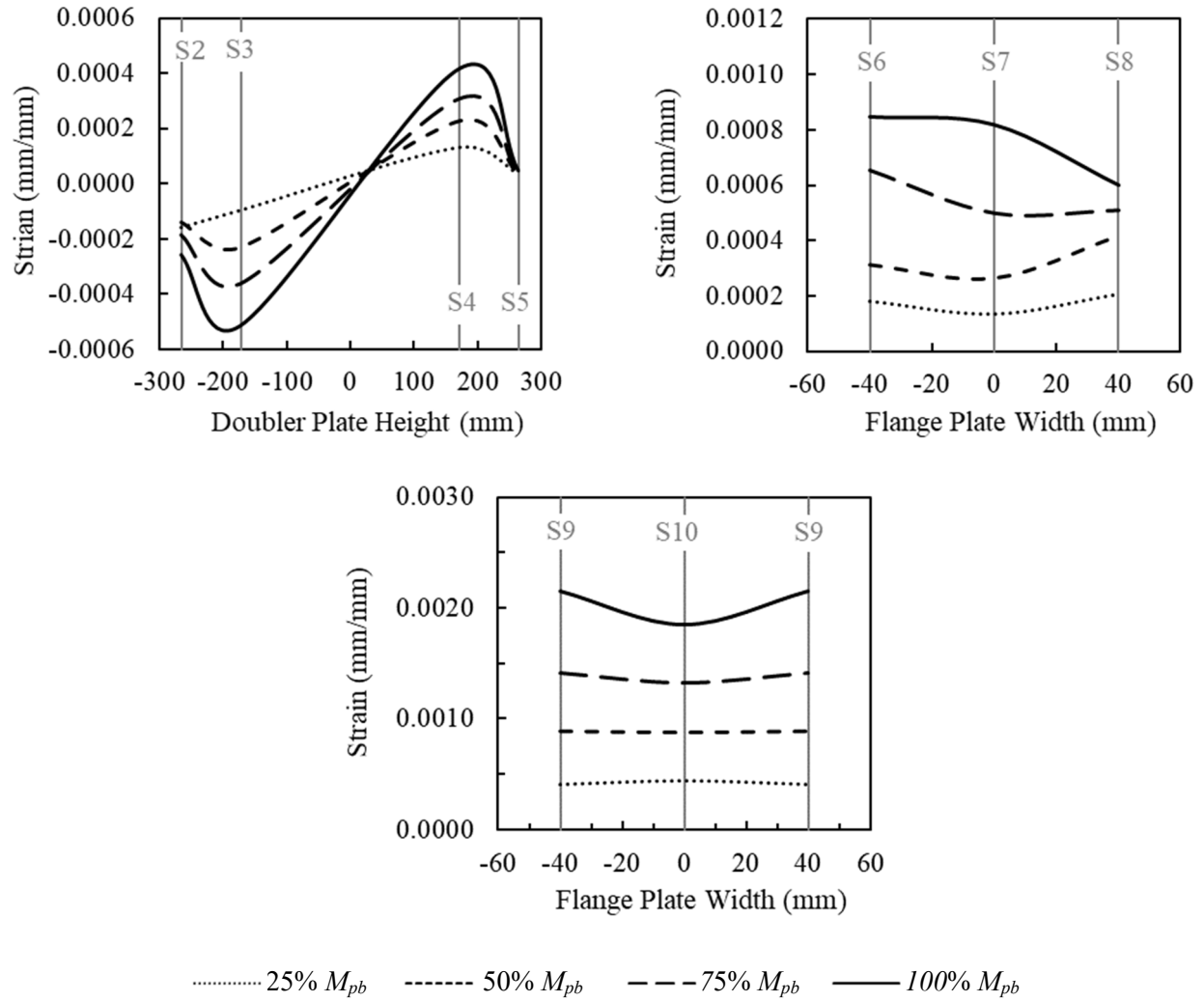


Fig. H.6. Doubler Plate mock cyclic response

### H.2.3. STRAIN GAUGE RESULTS



**Fig. H.7.** Doubler Plate static test strain response



## H.2.4. TESTING PHOTOS



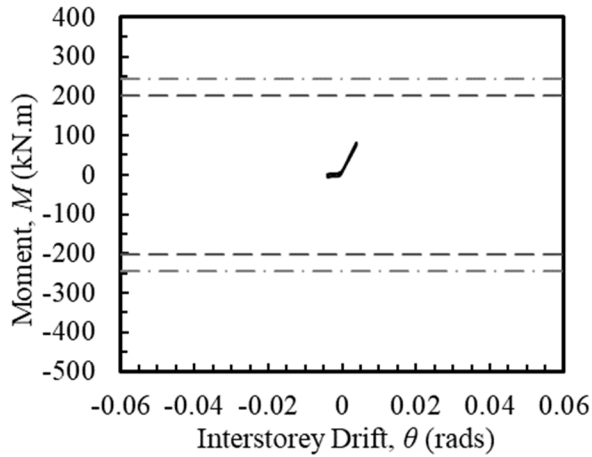
**Fig. H.8.** Doubler Plate post-testing photos



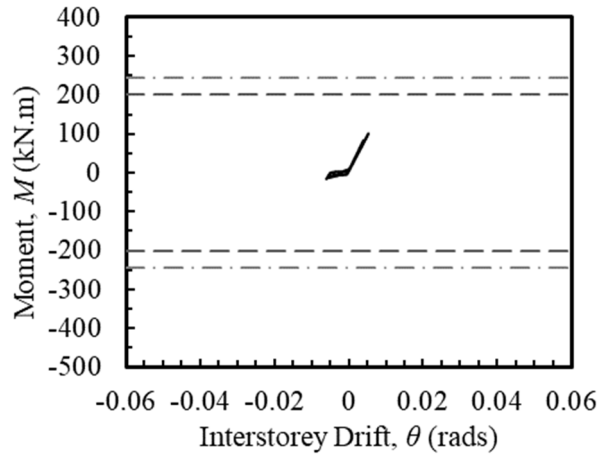
### H.3.CYCLIC RESULTS FOR CONNECTION ASSEMBLY T2

Test conducted on April 13th, 2023, from 8:30 am to 12:30 pm. Early chipping (on beam flange at T-stiffener connection) of limewash occurred at cycle 7 and normal chipping began at cycle 20. The T2 connection assembly had the beam attached 50mm (2 inches) off center and was not caught during fabrication.

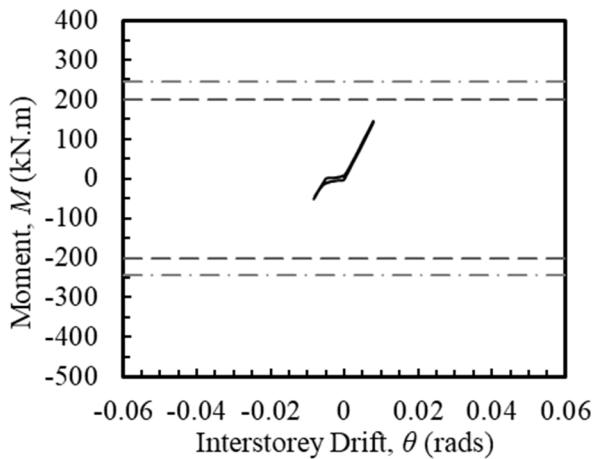
#### H.3.1.HYSTERETIC CURVES



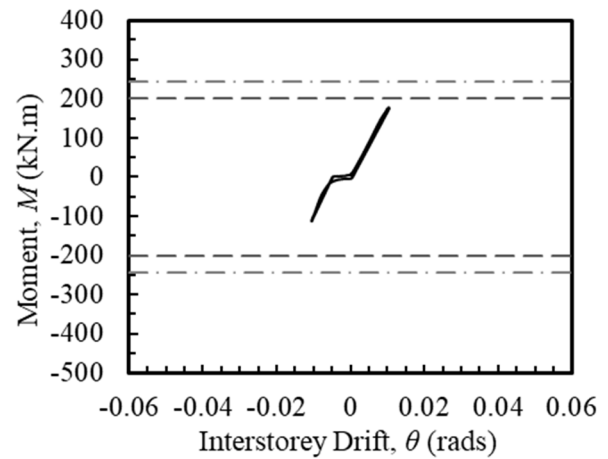
(a) 0.00375 rad



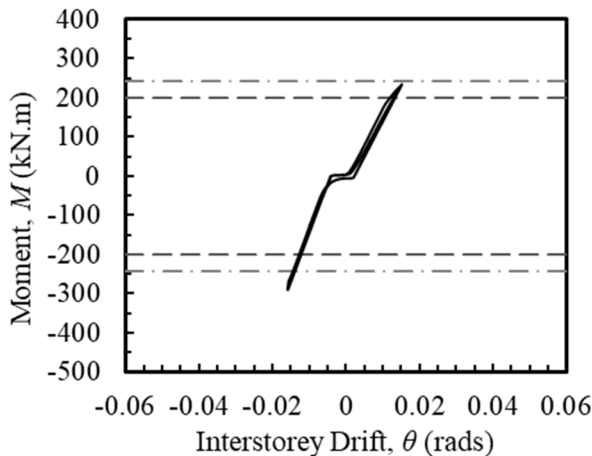
(b) 0.005 rad



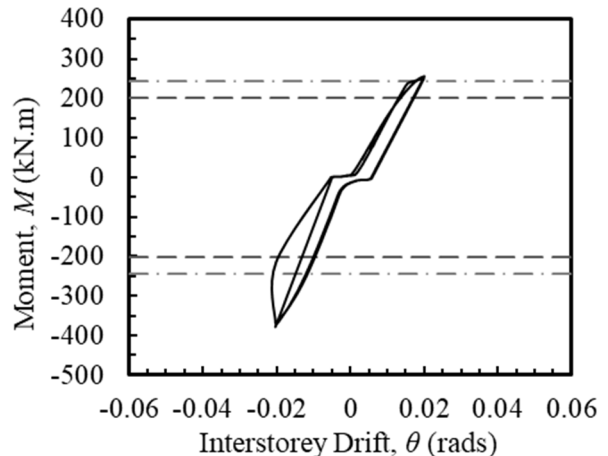
(c) 0.0075 rad



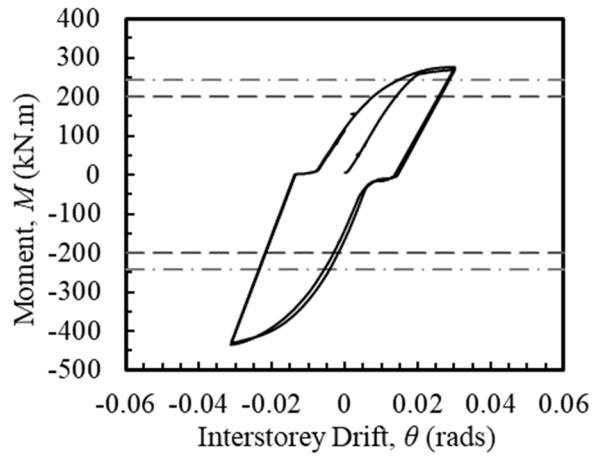
(d) 0.01 rad



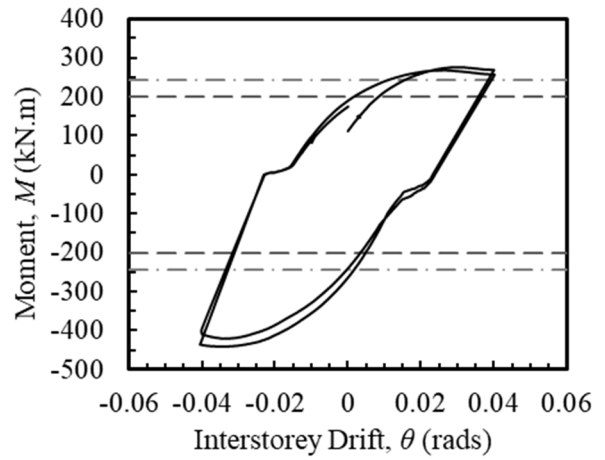
(e) 0.015 rad



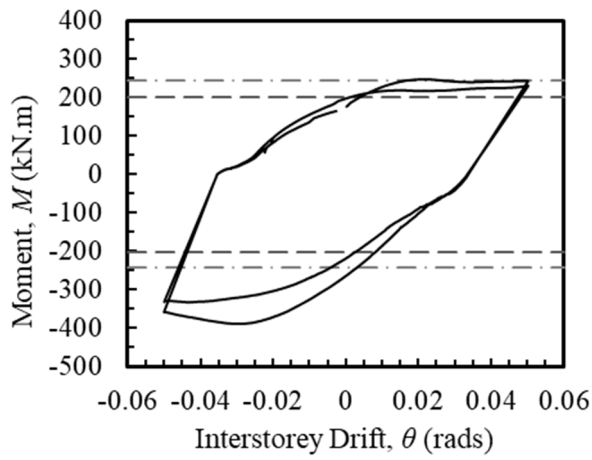
(f) 0.02 rad



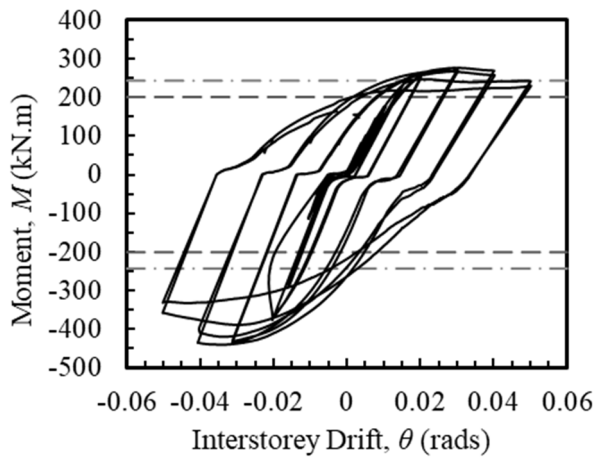
(g) 0.03 rad



(h) 0.04 rad



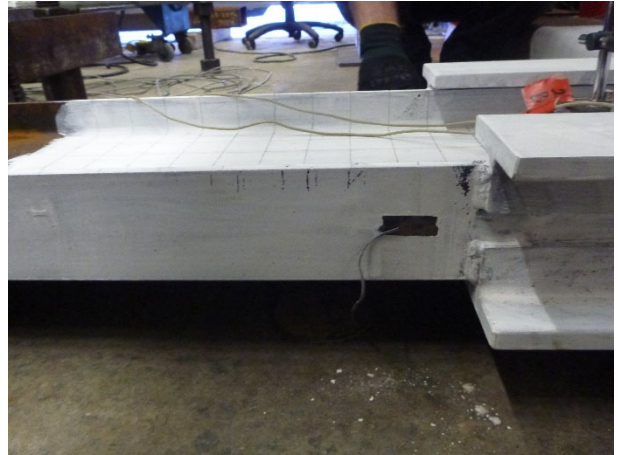
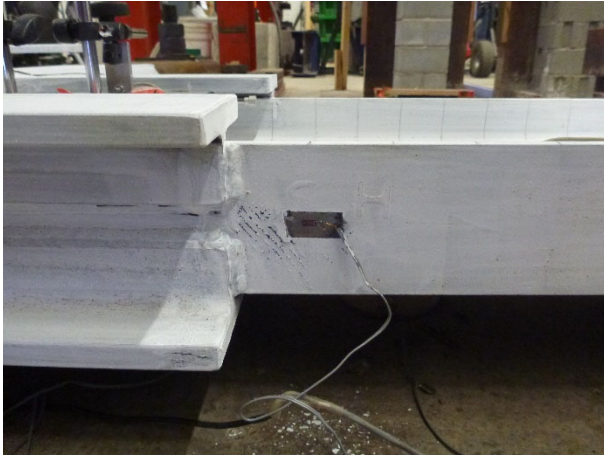
(i) 0.05 rad



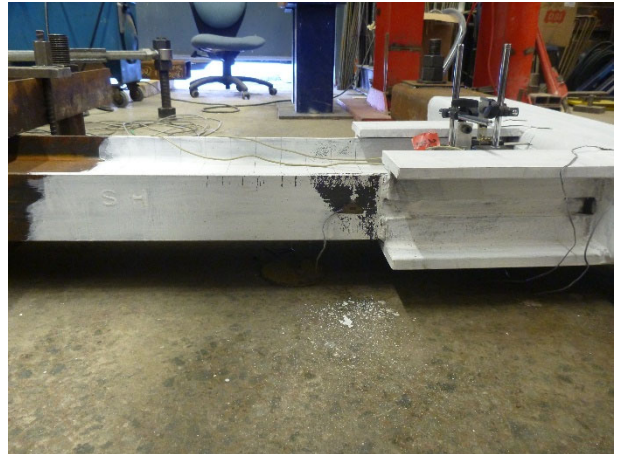
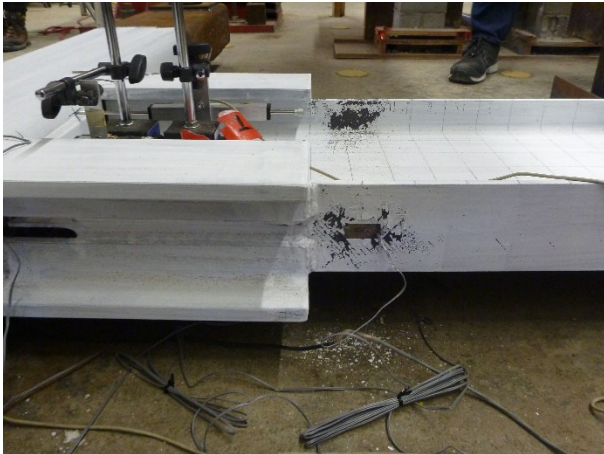
(j) 0.00375-0.05 rad

**Fig. H.9.** T2 hysteretic curves

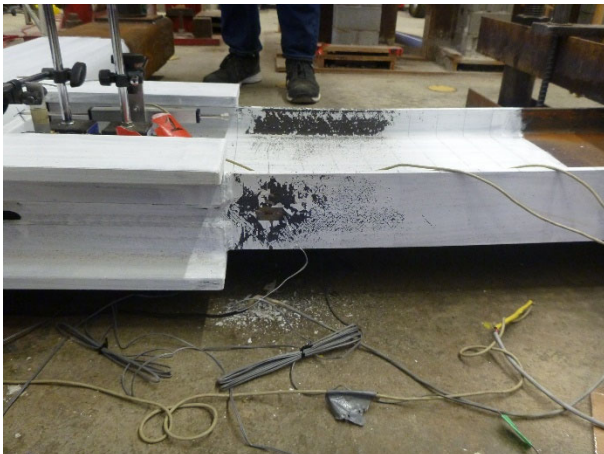
### H.3.2. TESTING PHOTOS



Cycle 20 (0.01 rad)

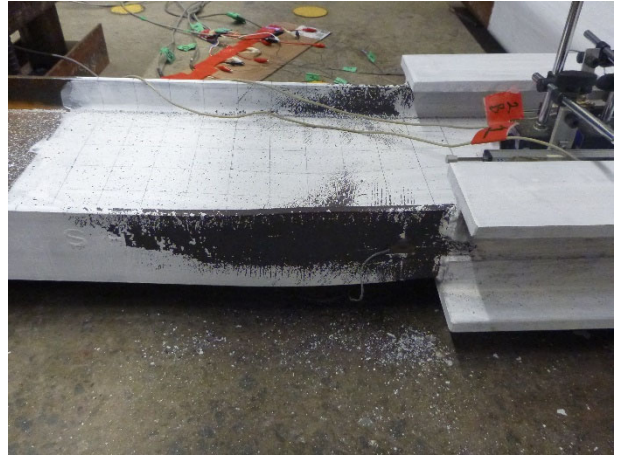
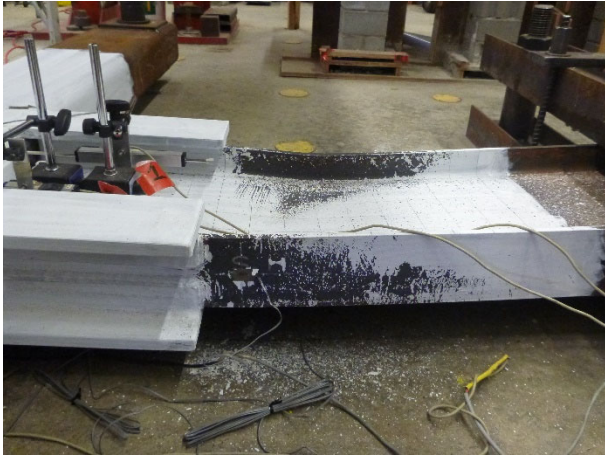


Cycle 22 (0.01 rad)



Cycle 26 (0.02 rad)





Cycle 29 (0.03 rad)



Cycle 31 (0.05 rad)



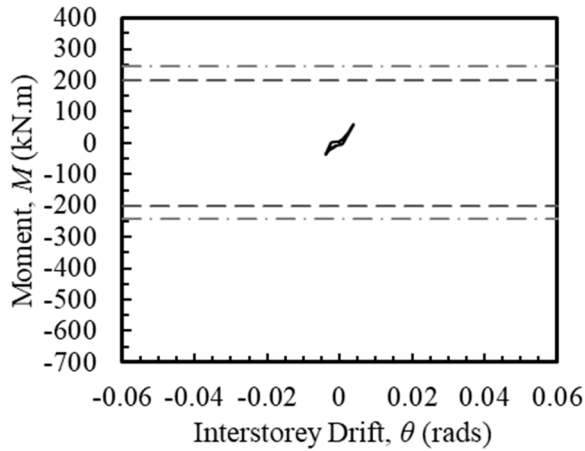
Cycle 32 (0.05 rad)

**Fig. H.10.** T2 testing photos

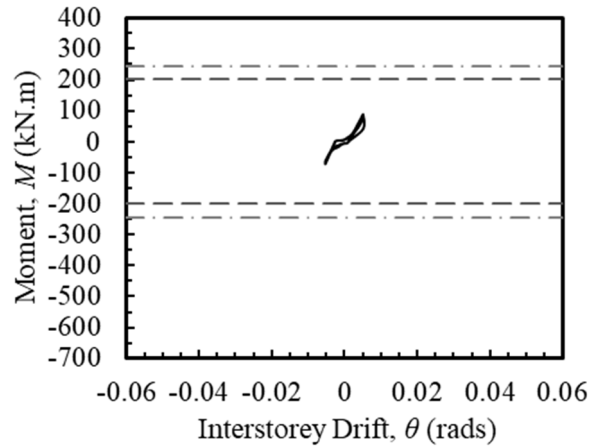
## H.4. CYCLIC RESULTS FOR CONNECTION ASSEMBLY T3

Test conducted on March 21st, 2023, from 8:30 am to 11:35 am. Yielding and limewash chipping started at cycle 23. After cycle 24 loud snapping sounds occurred periodically from the system slipping threads on the columns anchor bolts. Deformations in the web began at cycle 27. The test was concluded after cycle 29 (0.04 rads) to not overwork testing setup more than required to prove limited ductility moment connection performance.

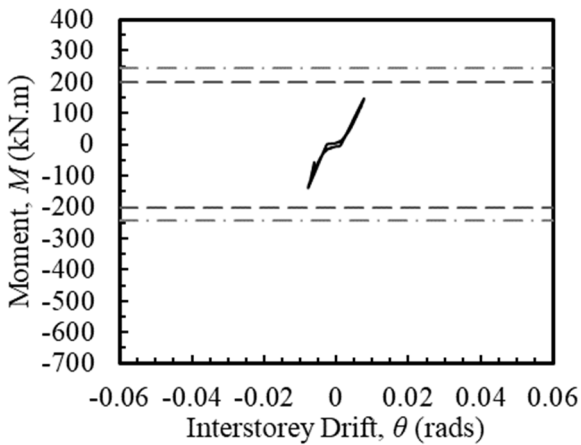
### H.4.1. HYSTERETIC CURVES



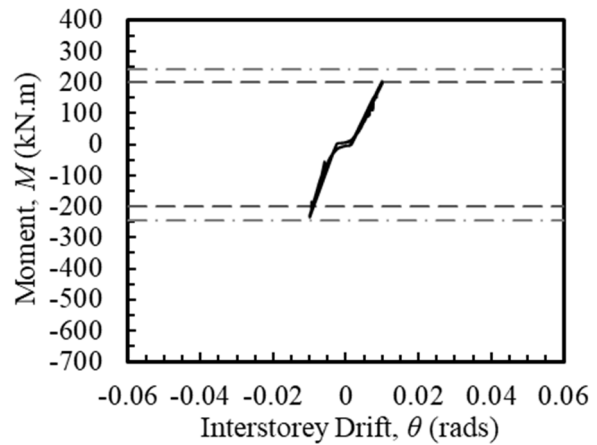
(a) 0.00375 rad



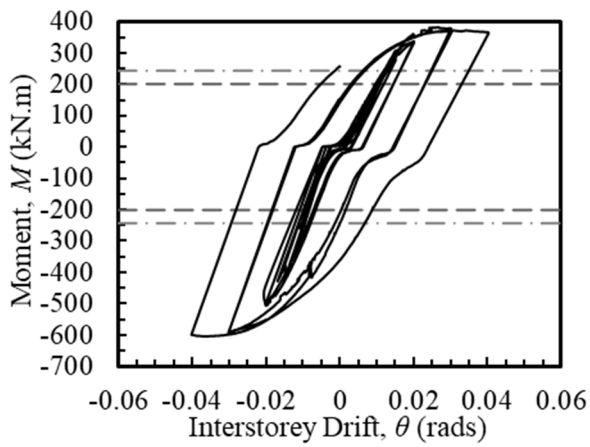
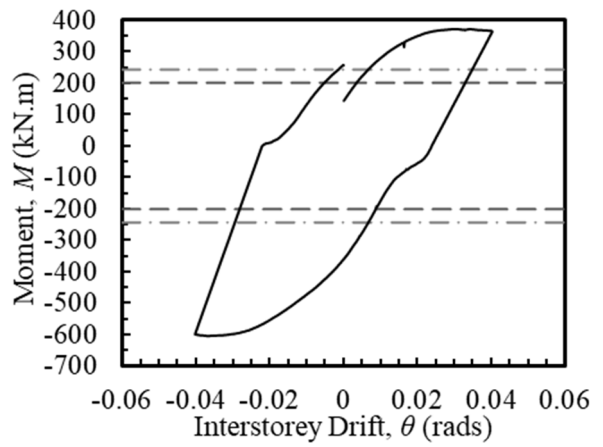
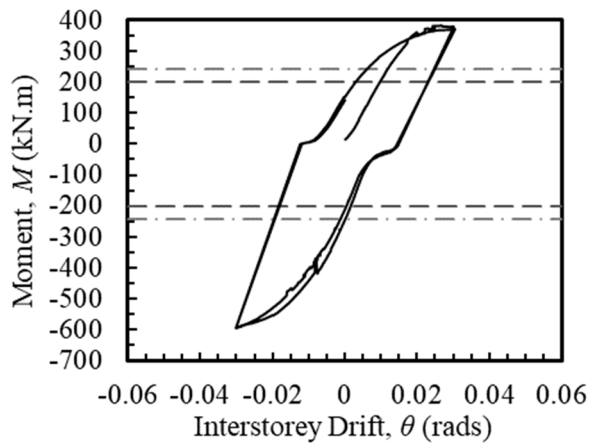
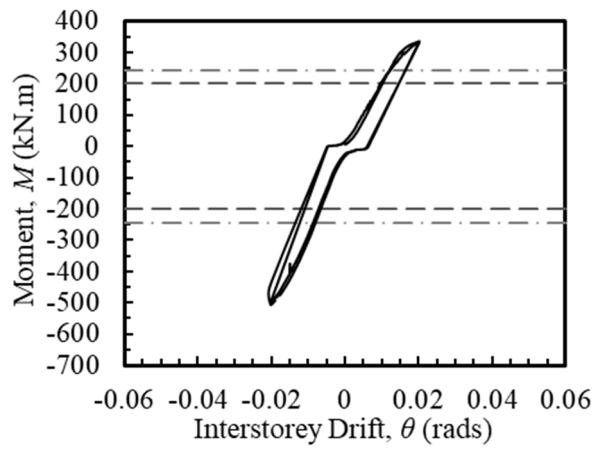
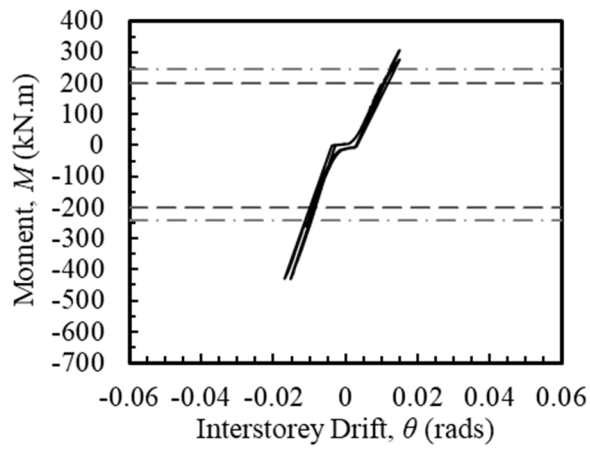
(b) 0.005 rad



(c) 0.0075 rad



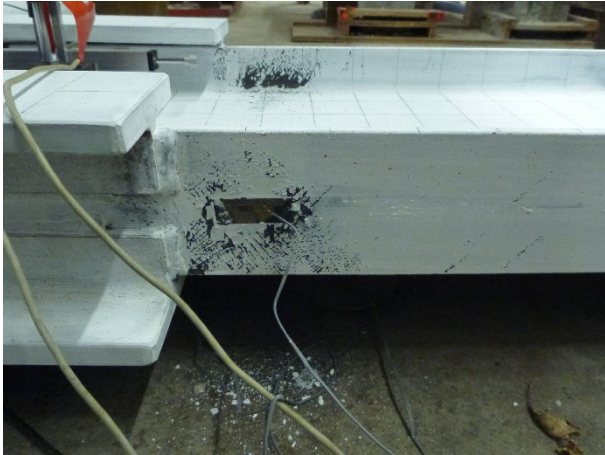
(d) 0.01 rad



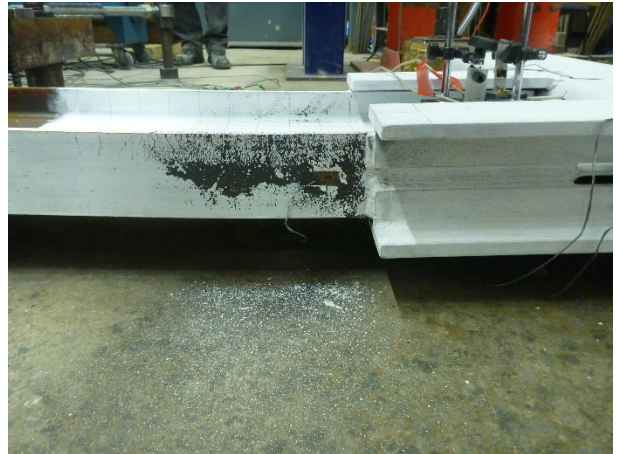
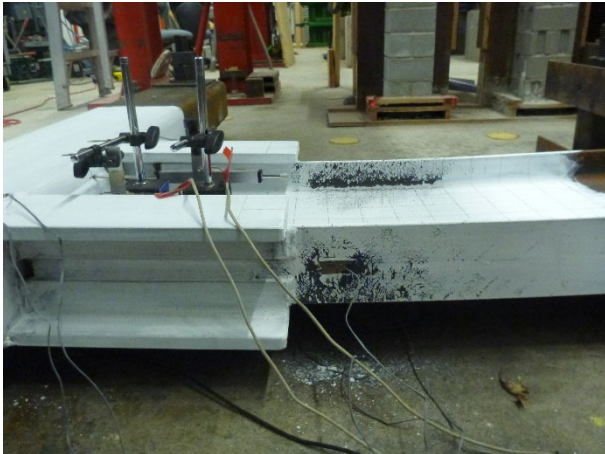
**Fig. H.11.** T3 hysteretic curves



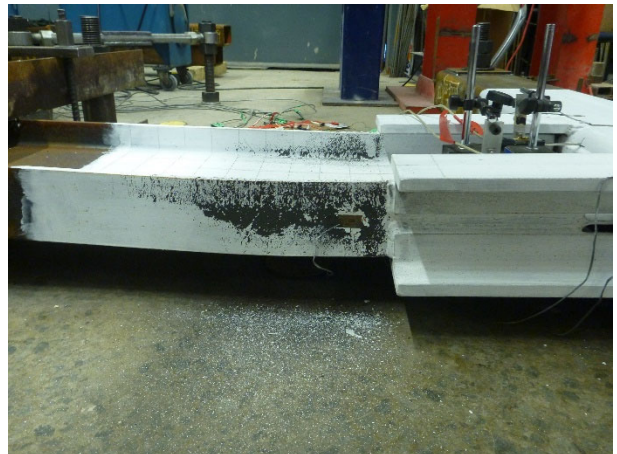
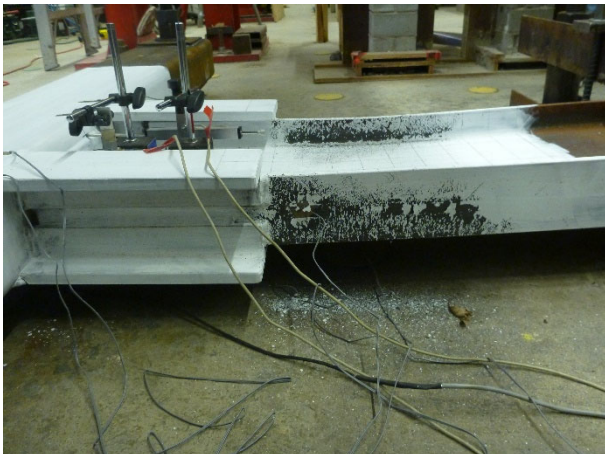
#### H.4.2. TESTING PHOTOS



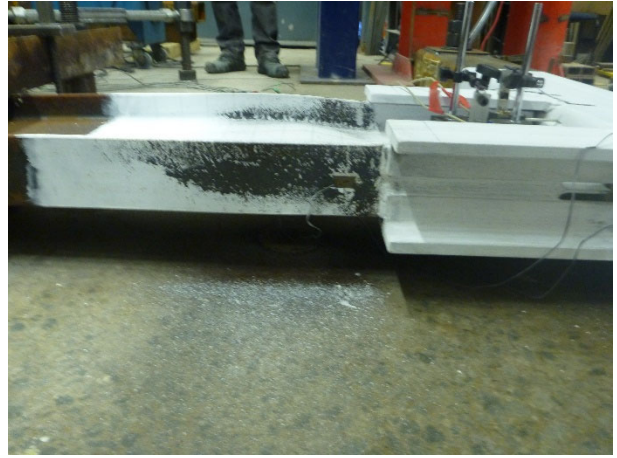
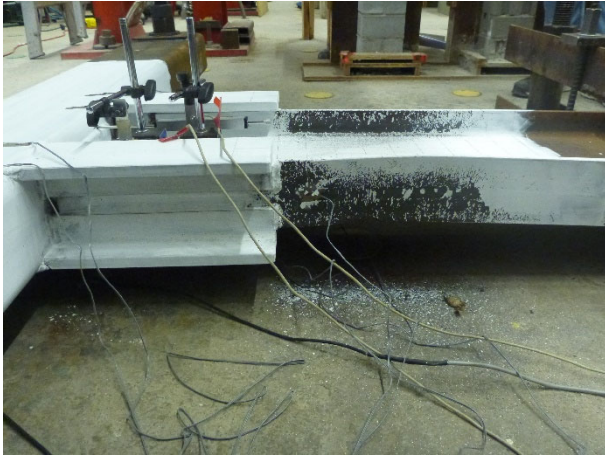
Cycle 24 (0.015 rad)



Cycle 26 (0.02 rad)



Cycle 28 (0.03 rad)



Cycle 29 (0.04 rad)

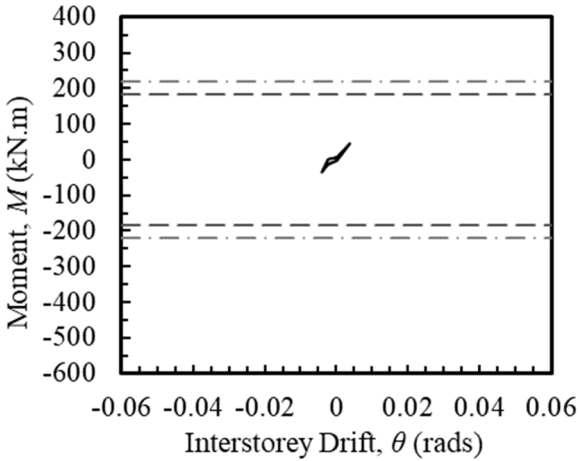
**Fig. H.12.** T3 testing photos



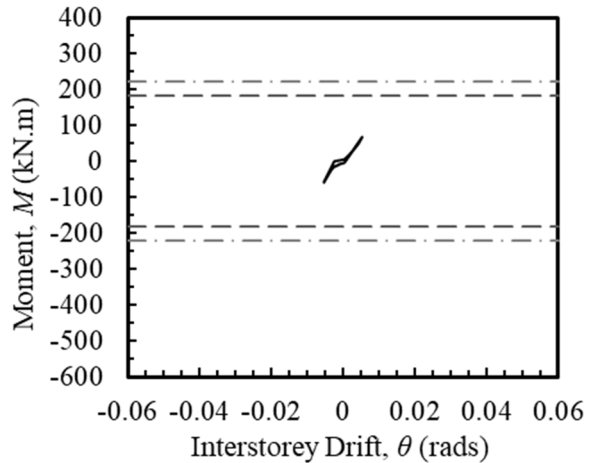
## H.5. CYCLIC RESULTS FOR CONNECTION ASSEMBLY DP1

Test conducted on May 2nd, 2023, from 8:30 am to 12:30 pm. Yielding and limewash chipping started at cycle 23. A loud bang occurred at cycle 23 but no visible reason was found. The beam was creaking after cycle 29.

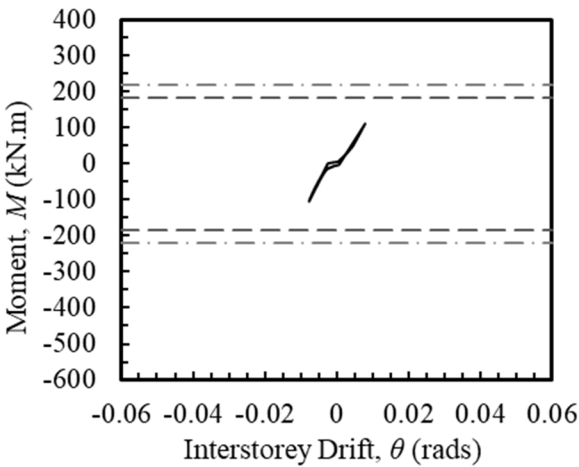
### H.5.1. HYSTERETIC CURVES



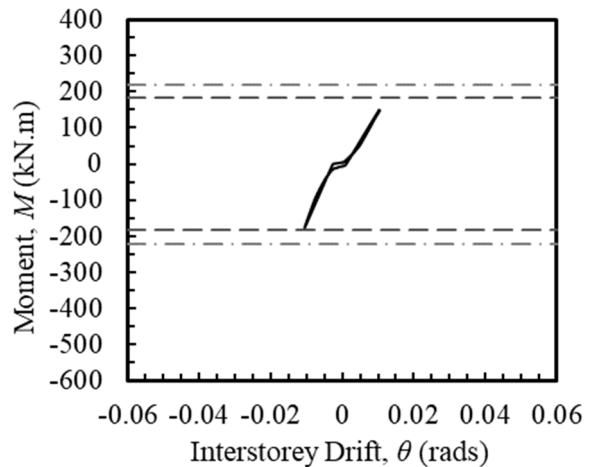
(a) 0.00375 rad



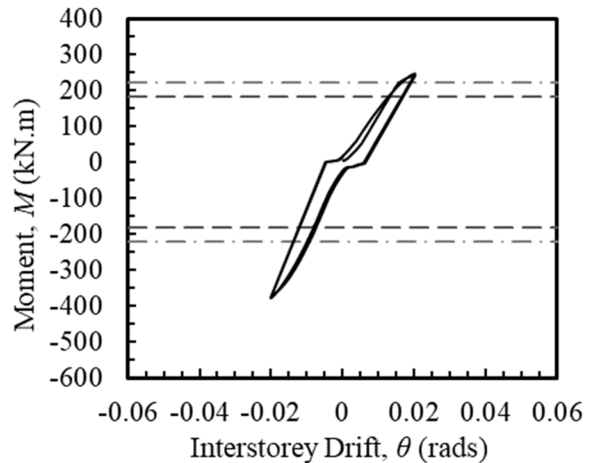
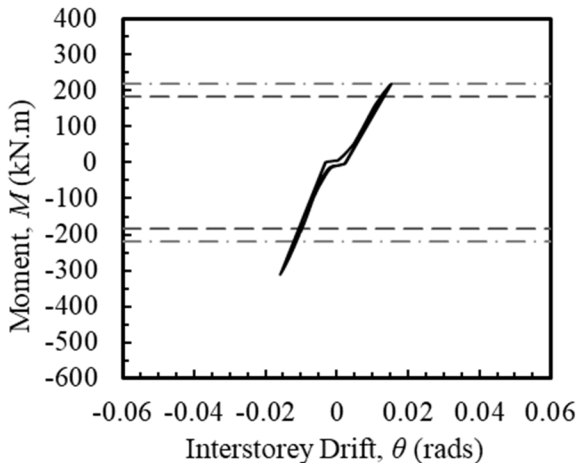
(b) 0.005 rad

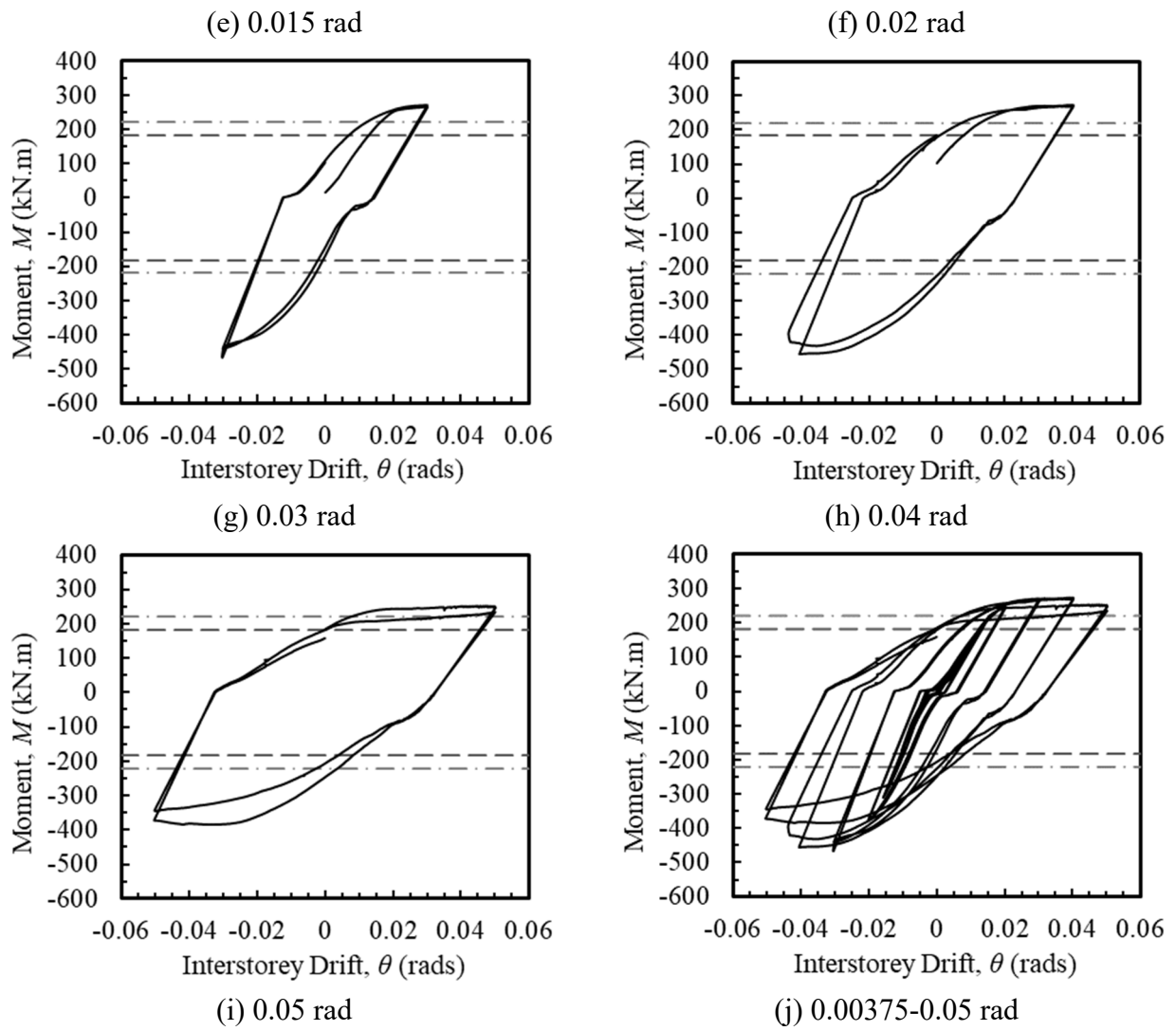


(c) 0.0075 rad



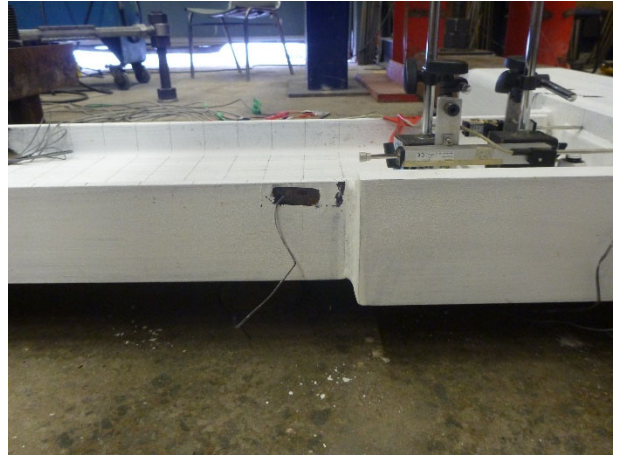
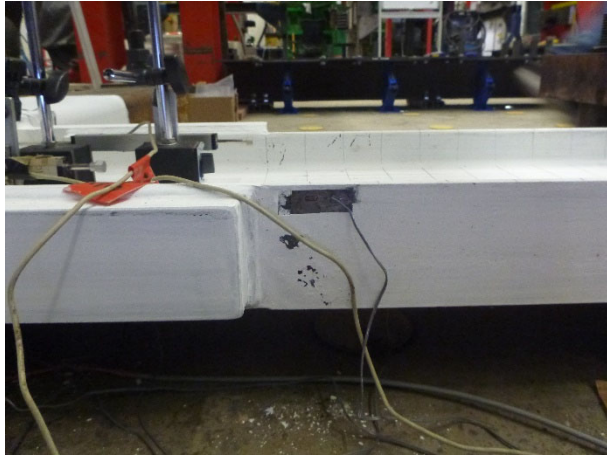
(d) 0.01 rad



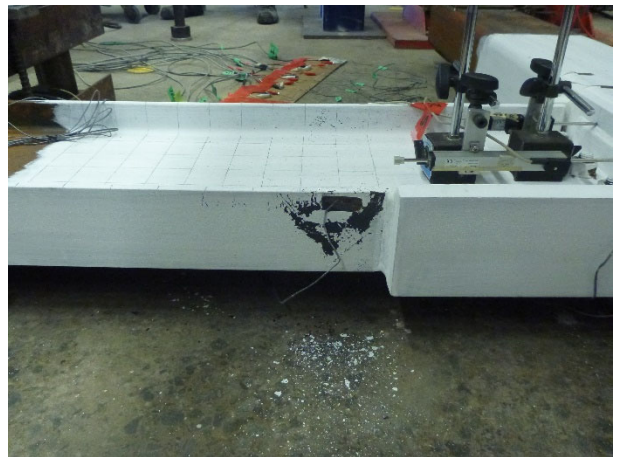
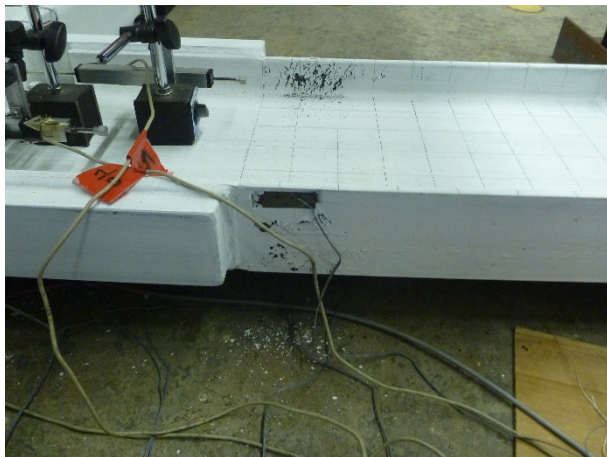


**Fig. H.13.** DP1 hysteretic curves

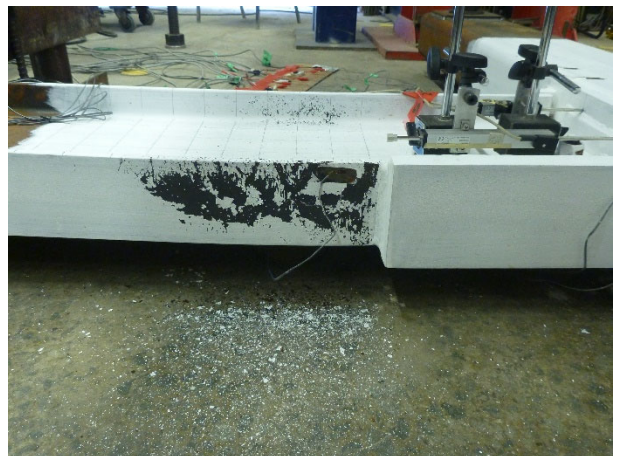
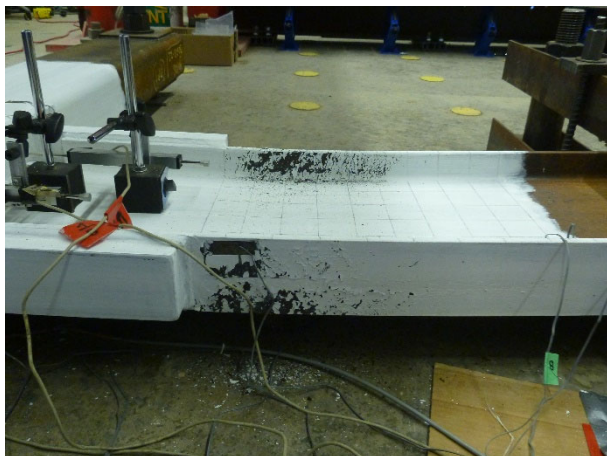
## H.5.2. TESTING PHOTOS



Cycle 23 (0.015 rad)

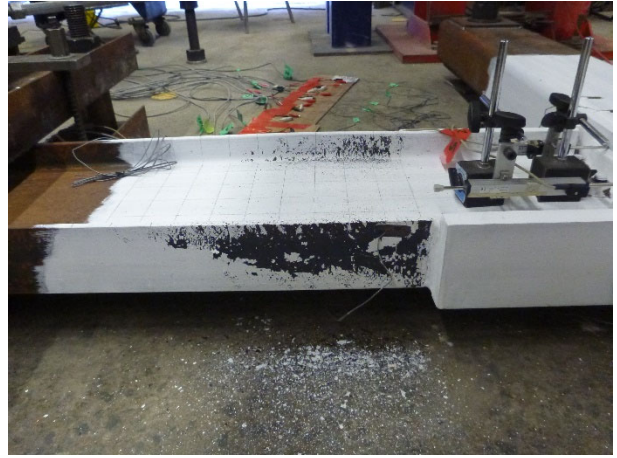
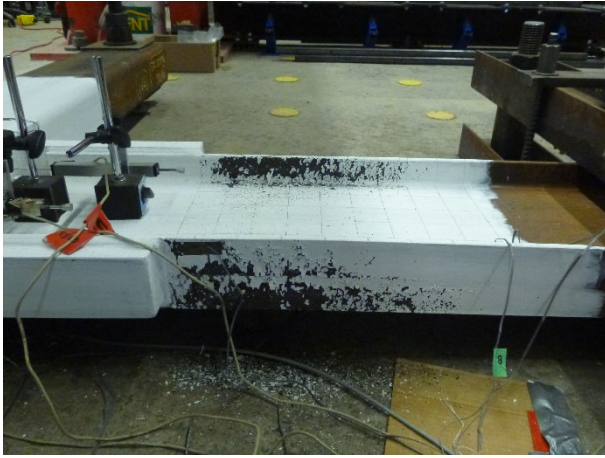


Cycle 25 (0.02 rad)

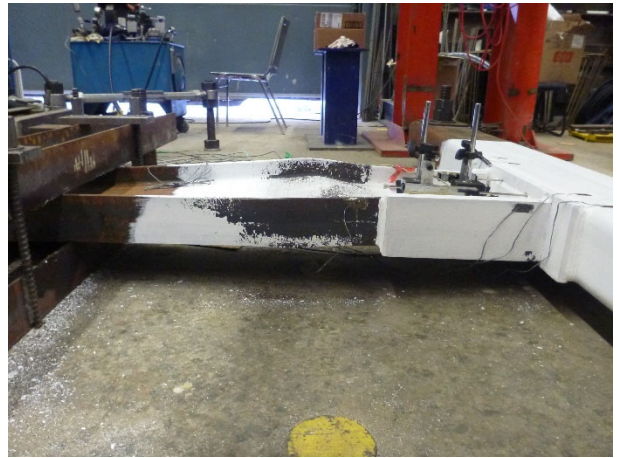
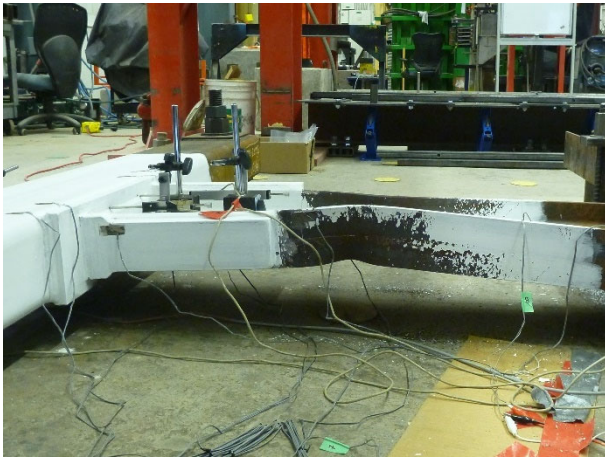


Cycle 27 (0.03 rad)





Cycle 29 (0.04 rad)



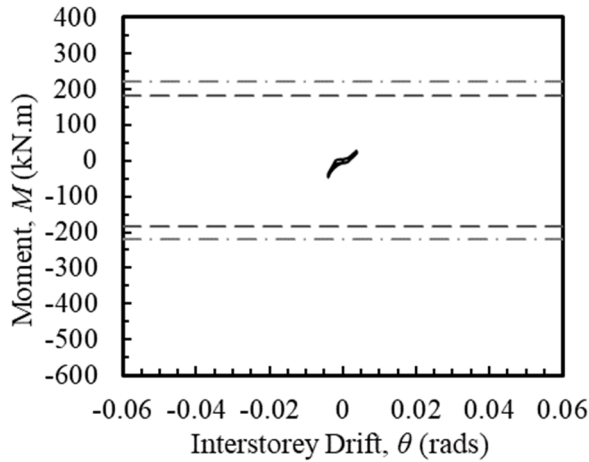
Cycle 32 (0.05 rad)

**Fig. H.14.** DP1 testing photos

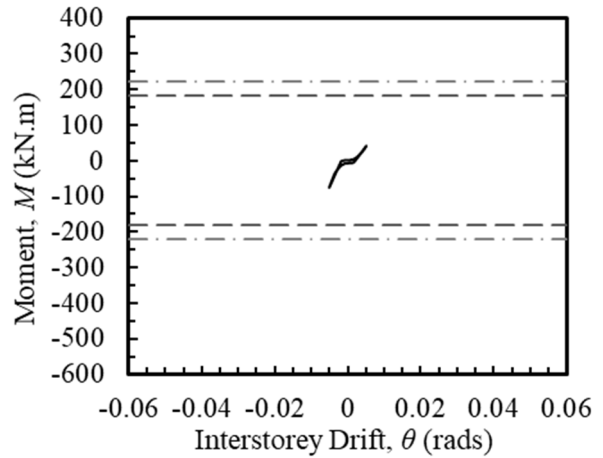
## H.6. CYCLIC RESULTS FOR CONNECTION ASSEMBLY DP2

Test conducted on March 7th, 2023, from 9:00 am to 2:20 pm. This was the first cyclic test conducted as part of this thesis project. Testing rate started at 2 mm/min and ended with a speed of 6 mm/min. Due to technical issues that occurred at cycle 20 and no photos or videos were collected for the remaining portion of the testing. Yielding and limewash chipping started at cycle 22. After cycle 27 the test needed to be paused for lunch (1 hour). During cycle 29 the steel beam made popping sound when deformations changed directions.

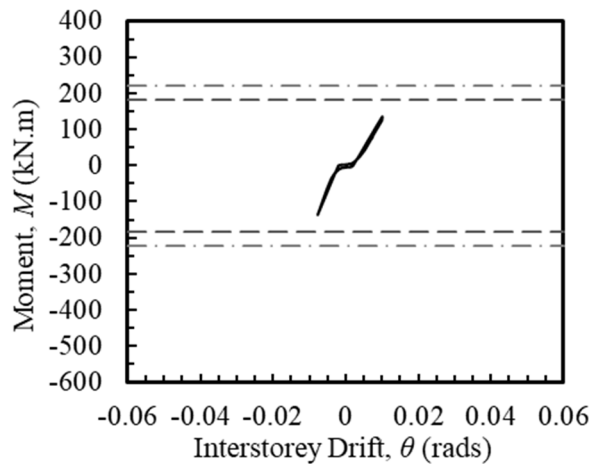
### H.6.1. HYSTERETIC CURVES



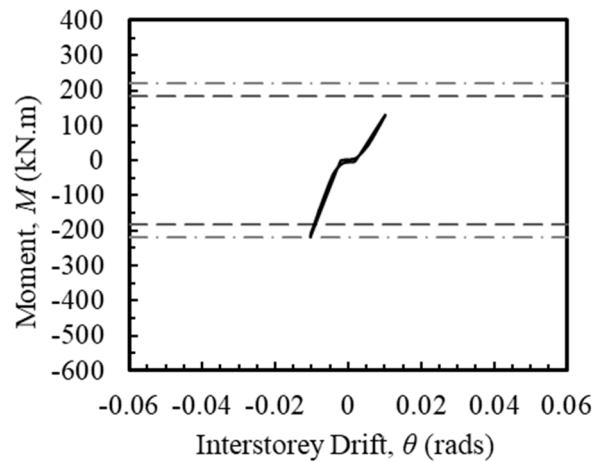
(a) 0.00375 rad



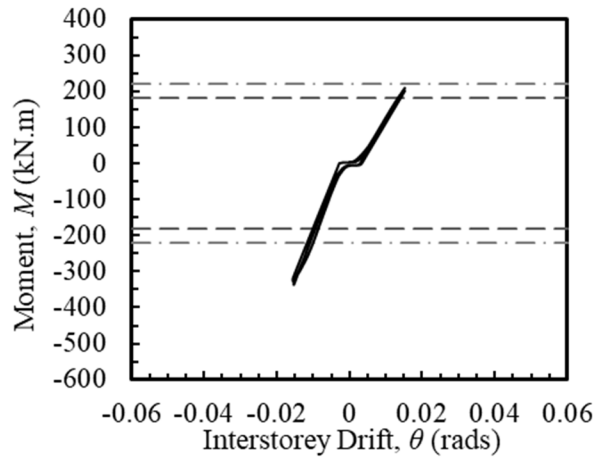
(b) 0.005 rad



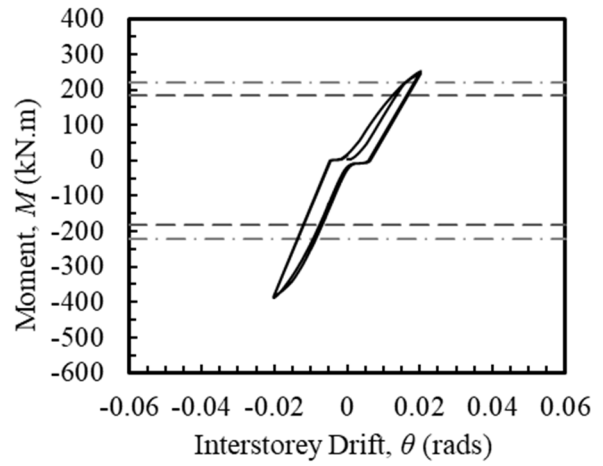
(c) 0.0075 rad



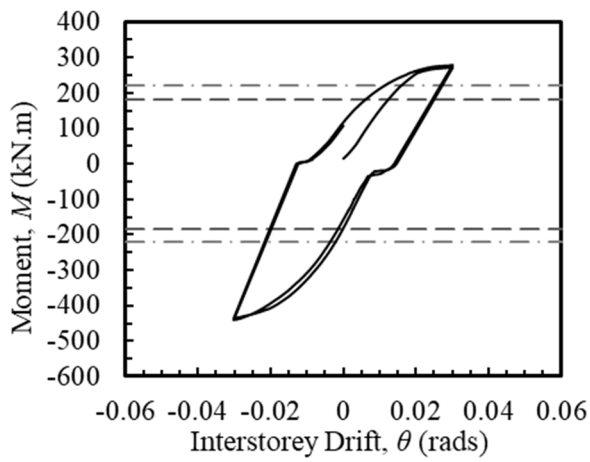
(d) 0.01 rad



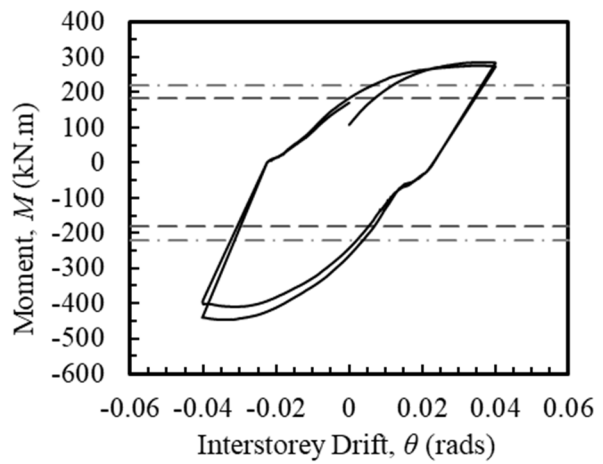
(e) 0.015 rad



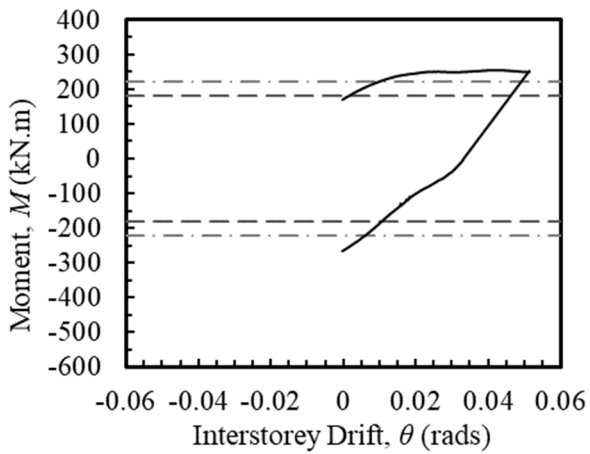
(f) 0.02 rad



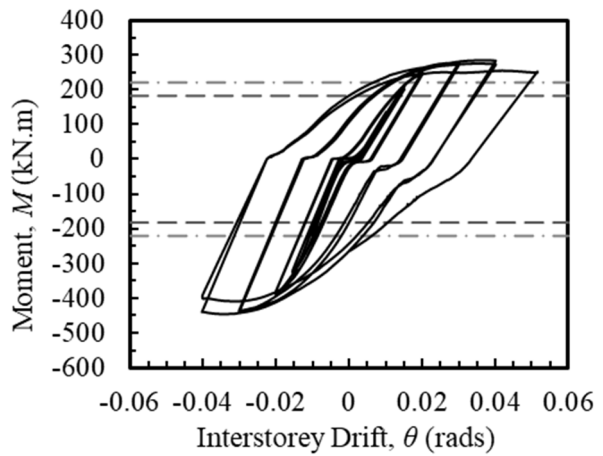
(g) 0.03 rad



(h) 0.04 rad



(i) 0.05 rad



(j) 0.00375-0.05 rad

Fig. H.15. DP2 hysteretic curves

## H.6.2. TESTING PHOTOS



**Fig. H.16.** DP2 post-testing photos

# Appendix I: DOCUMENTATION FROM MARID INDUSTRIES LIMITED

Site measurement sheets and checklists used during the on-site visits to Marid Industries while the fabrication process was ongoing located in this appendix. Additionally, there are mill test reports included for the base metals and weld metal used in the projects.



# I.1. SITE MEASUREMENTS AND CHECKLISTS

## Marid Visit Measurements and Checklist

Date: October 13th - 17th, 2022

HSS & W-Shape Members							
Prototype	$b_o$ (mm)	$h_o$ (mm)	$t_o$ (mm)	$b_B$ (mm)	$w_B$ (mm)	$d_B$ (mm)	$t_B$ (mm)
Nominal	152.4	254.0	8.58	102.0	6.60	313.0	10.80
T1	155.5	254.5	9.50	103.0	6.67	313.0	10.22
T2	155.0	255.0	9.57	103.0	6.96	314.0	10.10
T3	154.5	254.0	9.39	102.0	6.70	313.5	9.95
DP1	155.5	253.0	9.53	105.0	6.74	312.0	10.24
DP2	154.0	253.5	9.50	102.5	6.88	312.0	10.26
DP3	154.0	253.5	9.24	104.0	6.69	312.0	10.32

Doubler & Flange Plates							
Prototype	$b_D$ (mm)	$d_D$ (mm)	$t_D$ (mm)	$b_F$ (mm)	$b'_F$ (mm)	$d_F$ (mm)	$t_F$ (mm)
Nominal	152	530	22	125	85	325	32.00
DP1	153.0	530.5	22.47	125.0	85.0	325.0	32.00
DP2	153.0	531.0	22.23	126.0	85.0	323.0	32.00
DP3	152.0	531.0	22.37	126.0	85.5	324.5	32.00

T-Stiffeners				
Prototype	$b_T$ (mm)	$w_T$ (mm)	$d_T$ (mm)	$t_T$ (mm)
Nominal	105	10.2	60	17.4
T1	109.0	10.55	62.5	17.54
T2	108.5	10.41	62.1	17.29
T3	108.6	10.33	62.9	17.24

Clip Angles			
Prototype	$b_A$ (mm)	$d_A$ (mm)	$t_A$ (mm)
Nominal	50.8	76.2	6.4
T1	52.0	76.0	6.49
T2	51.0	76.0	6.48
T3	50.5	75.0	6.51
DP1	51.0	75.5	6.52
DP2	51.0	76.0	6.50
DP3	50.0	75.0	6.50

Marid Visit  
Measurements and Checklist

Date: October 13th - 17th, 2022

<input checked="" type="checkbox"/>	<b>Material Mill Sheets</b>				
<input checked="" type="checkbox"/>	HSS254x152x9.5	<u>1</u>	x Heats	QTY:	<u>1</u>
<input checked="" type="checkbox"/>	W310x33	<u>2</u>	x Heats	QTY:	<u>2</u>
<input checked="" type="checkbox"/>	W200x71	<u>1</u>	x Heats	QTY:	<u>1</u>
<input checked="" type="checkbox"/>	22mm PL	<u>1</u>	x Heats	QTY:	<u>1</u>
<input checked="" type="checkbox"/>	32mm PL	<u>1</u>	x Heats	QTY:	<u>1</u>
<input checked="" type="checkbox"/>	Weld Metal	<u>1</u>	x Heats	QTY:	<u>1</u>
<input checked="" type="checkbox"/>	<b>Steel Off-Cut or Sample Material</b>				
<input checked="" type="checkbox"/>	HSS254x152x9.5	(68 lbs)		QTY:	<u>1</u>
<input checked="" type="checkbox"/>	W310x33	(44 lbs)		QTY:	<u>1</u>
<input checked="" type="checkbox"/>	W200x71	(96 lbs)		QTY:	<u>1</u>
<input checked="" type="checkbox"/>	22mm PL	(35 lbs for 3)		QTY:	<u>3</u>
<input checked="" type="checkbox"/>	32mm PL	(51 lbs for 3)		QTY:	<u>3</u>
<input checked="" type="checkbox"/>	Weld Metal	(120 lbs)		QTY:	<u>1</u>
<input checked="" type="checkbox"/>	<b>Final Product Summary</b>				
<input checked="" type="checkbox"/>	T-Stiffeners Prototype Connections			QTY:	<u>3</u>
<input checked="" type="checkbox"/>	Doubler Plate Prototype Connections			QTY:	<u>3</u>
<input checked="" type="checkbox"/>	Beam Test Connection			QTY:	<u>1</u>
<input checked="" type="checkbox"/>	Anchor Plates			QTY:	<u>24</u>

Marid Visit  
Measurements and Checklist

Date: October 13th - 17th, 2022

**Welder Information**

Floor Manager Chris Clark

Welders Name Shelden Butler (started at Marid in 1999) - Day 1  
Gordon Densmore (started at Marid in 2000) - Day 2 & 3

Voltage set at 26.4 and varies +/- 0.2 while welding

Amperage ranges from 226-281 depending on weld being made

Welding Speed

$$\frac{\text{length (in)}}{\text{time (s)}} = \frac{9}{41.68} = \underline{13.0} \text{ ipm}$$

Welding Material Speed

$$\frac{\text{length (in)}}{\text{time (s)}} = \frac{34}{10} = \underline{204} \text{ ipm}$$

# I.2.MILL TEST REPORTS

**Customer Name** Mand Industries, Ltd.      **Customer PO#** PO-53524      **Shipper No** 533632      **Heat Number** 851368\_1

**REF/BOL:** 81082669

MATERIAL TEST REPORT BY DELIVERY : 81082669 - Apr 22, 2022 - Page 11

**Sold To:**  
 Triad Metals Inc.  
 953 Farewell Street  
 Oshawa ,ON,L1H 6N8  
 CA

**Ship To:**  
 Triad Metals Inc.  
 953 Farewell Street  
 Oshawa ,ON,L1H 6N8  
 CA

**Atlas Tube**  
 200 Clark Street  
 Harrow,ON,CA,NOR1G0  
 519.738.5000 / 519.738.3537

Heat #: 851368 I		Made In: CA										Melted and Poured In: CA			
C	Mn	P	S	SI	Al	CU	CB	MO	NI	CR	V	TI	B	N	
0.19	0.78	0.007	0.009	0.018	0.039	0.062	0.005	0.005	0.022	0.04	0.002	0.002	0.0002	0.003	

Material Group#: 100060375	Certification: CSA G40.21-13 50W CLASS C	Yield	Tensile	Eln,2In	CE
		063957 Psi	074454 Psi	33.3 %	0.34

Mill	Mill Location	Method	Recycled Content	Post Consumer	Pre-Consumer (Post Industrial)	% Harvested	Within Miles of Location
STELCO	Nanticoke,ON	BOF	36.90%	19.80%	14.40%	100.00%	1,000.00

Material	Customer Item	Customer Note
10.0x6.0x375x500(02x2)-CSA		

Bundle No	Pcs	Purchase Order	Sales Order	Sales Order Note
M201592745	4	507232	0001728317	

Authorized by Quality Assurance: **Jason Richard**  
 The results reported on this report represent the actual attributes of the material furnished and indicate full compliance with all applicable specification and contract requirements. CE calculated using the AWS D1.1 method. This document is in compliance with the requirements of EN 10204 type 3.1





**WELDED TUBE  
OF CANADA CORP.**  
111 Reynde Rd  
Concord, Ontario L4K 2E9  
Tel (805) 609-1111  
Fax (805) 730-4070  
Tel Free 1-800-565-TUBE (8873)

TEST REPORT  
PATRIKI S'ESSA:

NUMBER: NEMHO 1 209201  
DATE: 19/05/22  
PAGE: 1

1120 JACIER BOUCARDE INC.  
5-0 RUE SAVANE  
SAINT-HUBERT  
JIV 6C2 CDA

Customer P.O. WCC BOLS Ship Date WCC Items Description

5J09 66/804 1/05/22 S:0528 ASTM A500 GR. B & C; EPM, IC.020-6.030-.375-36.000

PO # 17228/28 QU # CAN - 0008/0/1  
HEAT # 319502  
MILL TAG: 209601



CHEMICAL COMPOSITION

HEAT	TYPE	C	Mn	P	S	Si	Cu	Ni	Cr	Mo	Sn	V	Co	Ti	N	B	Al	Zn	CE
319502	HEAT	.130	.830	.014	.008	.170	.060	.026	.040	.004	.003	.006	.002	.003	.030		.045		.343

TENSILE PROPERTIES

HEAT	TEST LOT	TYPE/SIZE	ORIENT	L/C COND	D.2 OFFSET	TENSILE		ELONG (2")
						YIELD	TS	
319502	S-1-50*	L	B	AM	58.8	12.7	41	

LEGEND S-STPIP L-L/VERTICUAL T-TRANSVERSE B-BODY W-WELD M-MAS WELDED N-NORMALIZED OT-OTEMPERED AND TEMPERED SN-STRESS RELIEVED

Company of Quality CANADA  
Does not contain mercury, cadmium or lead.  
Direct all inquiries to: [Welding@weldingtube.com](mailto:Welding@weldingtube.com)

We hereby certify that the product was manufactured, sampled, tested and inspected in accordance with the latest edition of the specification and any other requirements designated in the purchase order or contract. The tests were found to meet all such requirements.





Contract No.	
Customer	WIRTH STEEL
PO No.	462021078611
L/C No.	
Commodity	H-BEAM
Specification	ASTM A572 GR60/A572/CSA G4021-13 S550M305W40

## INSPECTION CERTIFICATE

### EN 10204(2004) TYPE 3.1



— PAGE: 13/51

Factory	63, Jungbong-Daero, Dong-gu, Incheon, S. Korea
Certificate No.	IH20210904618-3
Class certificate No.	
Issue date	2021-10-18

Dimensions	Length	Heat No.	Quantity (PCS)	Weight (kg)	Chemical Composition														Tensile Test			BEND TEST			Impact Test(U)			Remarks (Impact Specimen 12#)				
																			Yield Ratio	Yield Ratio			V-Notch	V-Notch								
					C	Si	Mn	P	S	Cu	Ni	Mo	Cr	Al	V	Nb	N	CEq		σ <sub>TS</sub>	σ <sub>YS</sub>	σ <sub>EL</sub>		σ <sub>TS</sub>	σ <sub>YS</sub>	σ <sub>EL</sub>	AVG		1	2	3	
x100														x100	x1000	%			%													
10K10X49	60.00 FT	E 227042	4	5,332	19	17	62	25	7	23	8	1	18	3	14	1	109	35	520	370	28.4	0.712										
12X4X14	60.00 FT	D 169319	6	3,049	16	15	60	22	5	24	10	2	19	2	2	15	99	33	555	428	23.5	0.772										
12X4X14	60.00 FT	D 169334	24	9,144	16	15	61	23	4	21	10	3	22	3	2	15	131	33	561	433	22.0	0.772										
12X4X22	60.00 FT	D 169312	8	4,792	15	13	61	17	5	22	9	2	14	2	1	14	124	30	563	432	23.0	0.768										
12X6-1/2X30	60.00 FT	D 169332	6	4,896	16	15	62	22	9	22	9	2	17	3	2	16	123	32	553	427	22.5	0.773										
12X6-1/2X35	50.00 FT	D 169335	6	4,764	17	14	61	20	4	23	11	2	18	3	2	15	115	33	539	399	23.4	0.741										
12X6-1/2X35	60.00 FT	D 169325	6	5,718	16	16	61	27	5	30	9	2	22	3	3	16	133	34	537	397	26.3	0.740										
12X6X40	50.00 FT	D 169547	2	1,814	16	14	67	21	9	26	16	6	19	2	2	17	90	35	548	408	26.5	0.745										
12X6X40	50.00 FT	D 169548	4	3,628	17	17	67	23	9	25	19	6	23	2	2	17	100	37	549	406	26.0	0.740										
12X6X40	60.00 FT	D 169544	2	2,178	18	14	66	27	12	26	15	5	28	2	3	18	106	38	540	400	26.5	0.741										
<b>SUB TOTAL</b>			<b>70</b>	<b>45,314</b>															<b>558</b>	<b>404</b>	<b>26.0</b>	<b>0.730</b>										

0201 20905

\*\*\*\*\* N E X T \*\*\*\*\*

Note: Melted and Poured in Republic of Korea

(1) Ceq: (C+Cr+V+Mo)/5 + (Cu+Ni)/15 + Mn/6  
 (2) Gauge length: 200 mm  
 (3) Y.R. = Y.S./T.S.

WE HEREBY CERTIFY THAT THE MATERIAL HAS BEEN MADE AND TESTED IN ACCORDANCE WITH THE ABOVE SPECIFICATION AND ALSO WITH THE REQUIREMENTS CALLED FOR THE ABOVE ORDER.

General Manager of Q.A. Team

2021-10-20 08:40:40

2021-10-21

HMS 10204-34 HK102037

Customer Name

Marid Industries, Ltd.

Customer PO#

PO-53319

Shipper No

533059

Heat Number

4120723

**JINDAL STEEL & POWER LIMITED**

Post Box No. 16, Kharis Road, Raigarh (Chhattisgarh)-PIN 495001 INDIA  
Registered Office: Post Box No. 6, O.P. Jindal Marg, Hisar (Haryana)  
Corporate Office: Jindal Centre, 12 Bhikaji Cama Place, New Delhi- 110066 INDIA  
Phone: (0762) 227001-227010; Fax: (0762) 227021-227022; Gram: PKG IRON  
Email: qcrainmill@jspi.com



Test Certificate No. : 0000495443

Customer: M/s MINMETALS, INC.

120 SCHOR AVE LEONIA, NJ 07605-2208, UNITED STATES LEONIA, PIN-00000

MILL TEST CERTIFICATE

Date : 26.10.2021; Time : 00:28:07

Page 1 of 1

**TEST RESULTS**

Test Method : Tensile ASTM A370, Impact and Hardness : ASTM A370 ; Chemical : ASTM E 415

Process of Manufacture : EAF/NOF-LRF-CCM-Hot Rolling

Supply Condition : As Rolled

Heat No.	Length in Mtr	Pes / in MT	Weight in MT	Chemical Analysis										Mechanical Properties																	
				LA/PAL	%C	%S	%P	%SI	%Mn	%Al	%CU	N2 (%)	%V	%Nb	%Ti	%CE	%MO	%Ni	%Cr	P	Bend Test Mand/Dia(ZT)	YS MPa	UTS MPa	%EL**	Impact(J) Temp °C (Orice)	I	II	III	Avg		
4120723	18.288	3	3.895	0.18	0.008	0.016	0.20	1.29	0.035	0.007	0.0073	0.032	0.001	0.003	0.40	0.002	0.008	0.01	P	Satisfactory(2.0T)	404	540	28								
4120723	18.288	3	3.895	0.17	0.006	0.018	0.21	1.30	0.034	0.006	0.0072	0.031	0.002	0.003	0.39	0.002	0.008	0.01	P	Satisfactory(2.0T)	401	537	27	0	L	88	92	100	93		
<b>Section Total :</b>	<b>3</b>	<b>3</b>	<b>3.895</b>																												
<b>Grand Total :</b>	<b>3</b>	<b>3</b>	<b>3.895</b>																												

Section & Grade: W 8 X 8 X 48 & ASTM A992/A572G-50/CSA350W

Dimension & Dimensional Tolerance as per ASTM A6, TC as per EN 10204 Inspection certificate "Type 3.1"

Certified that the materials(s) mentioned above against the respective heat numbers(s) has / have satisfied the requirements of chemical and mechanical properties of the grade  
\*\* Gauge Length = 50/200 mm, L.A.:Ladle Analysis, P.A.:Product Analysis, P.:Product

FORMAT No. F13 (8.6.0-05) /02.08.2017

Purchase Order No. & Date : PROV/EXP/STR/11024-B/06.09.2021  
Despatch Advice No : 27356256  
Truck/Wagon No. : CG13AL8309  
Created by : JAYANAND RUBM Changed by : JAYANAND RUBM Printing Date 01.12.2021 & Time 22:49:47

SC01A

Authorised Signatory ( Quality Control )  
For Jindal Steel & Power Limited





# Test Certificate

1770 Bill Sharp Boulevard, Muscatine, IA 52761-9412, US

**WARNING:** This product can expose you to chemicals including nickel and nickel compounds, which are known to the State of California to cause cancer. For more information go to [www.P65Warnings.ca.gov](http://www.P65Warnings.ca.gov).

Form TC1: Revision 4: Date 8 Feb 2019

**Customer:**  
SAMUEL SON & CO. LTD  
1260 APPLEBY LINE  
BURLINGTON  
ON L7L5G6

**Customer P.O.No.:** 1PP255481 & 41-68829  
**Mill Order No.:** 41-68829  
**Product Description:** CSA G40.21(1318) 50MT/350WT - CAT  
4150W/ASTM A572-50(21)/A708-50(21)  
LCVN 20FT-LBS @ -50F (27J @ -45C)

**Shipping Manifest:** MR458048  
**Ship Date:** 22 Mar 22  
**Cert No:** 081157368  
**Cert Date:** 22 Mar 22 (Page 1 of 1)

Size: 0.500 X 96.00 X 480.0 (IN)

### Charpy Impact Tests

Heat Id	Piece Id	Tested Thickness	YS (KSI)	UTS (KSI)	%RA	T <sub>2in</sub>	T <sub>8in</sub>	Hardness			Abs. Energy (FTLB)			% Shear			Test Dir	Test Temp	Test Temp	BOWTT
								1	2	3	1	2	3	Avg	1	2				
A2C239	C28	0.496 (DISCRT)	L 65	75	39	T		203	209	197	203	-50F	L	7.5						
A2C239	C28	0.496 (DISCRT)	L 61	71	39	T		191	202	198	197	-50F	L	7.5						

### Chemical Analysis

Heat Id	C	Min	P	S	Si	Total	Al	Cu	Ni	Cr	Mo	Cb	V	Ti	B	ORGN
A2C239	.05	1.44	.011	.003	.07	.031	.028	.29	.08	.15	.02	.047	.005	.014	.0001	USA

KILLED STEEL  
MERCURY IS NOT A METALLURGICAL COMPONENT OF THE STEEL AND NO MERCURY WAS INTENTIONALLY ADDED DURING THE MANUFACTURE OF THIS PRODUCT.

KILLED STEEL, PRODUCED TO A FINE GRAIN PRACTICE  
MTR EN 10204-2004 INSPECTION CERTIFICATE 3.1 COMPLIANT  
100% MELTED, POURED, AND ROLLED IN THE USA  
CHARPY FULL SIZE EQUIVALENT = ABSORBED ENERGY AVG X 10 / TEST SIZE IN MM

PRODUCTS SHIPPED:  
A2C239 C28 PCES: 1, LBS: 6534  
A2C239 C29 PCES: 1, LBS: 6534

PO # 199255481 00 # CUM - 00276501  
HEAT # A2C239  
MILL TAG: C28



WE HEREBY CERTIFY THAT THIS MATERIAL WAS TESTED IN ACCORDANCE WITH, AND MEETS THE REQUIREMENTS OF, THE APPROPRIATE SPECIFICATION  
Burlington, IA 52761-9412  
PRINCIPAL METALLURGIST

Customer Part #



1051 Tapscott Road, Toronto, ON M1X 1A1, CA

# Test Certificate

**WARNING:** This product can expose you to chemicals including nickel and nickel compounds, which are known to the State of California to cause cancer. For more information go to [www.P65Warnings.ca.gov](http://www.P65Warnings.ca.gov)

Form TC1: Revision 4: Date 5 Feb 2019

<b>Customer:</b> RUSSEL METALS INC. 28 LAKESIDE PARK DRIVE LAKESIDE NS B3T1A3		<b>Customer P.O. No.:</b> M02138823		<b>Mill Order No.:</b> 41-635046-20		<b>Shipping Manifest:</b> TT092747																		
<b>Product Description:</b> CSA G40.21(13/1) D44W/200W / A3TM A30(19) A709(19)36/ASME SA36(19)		<b>Ship Date:</b> 11 Mar 21		<b>Cert No:</b> 021103081		<b>Cert Date:</b> 11 Mar 21 (Page 1 of 1)																		
<b>Size:</b> 0.875 X 96.00 X 240.0 (IN)																								
<b>Tested Pieces:</b>		<b>Charpy Impact Tests</b>																						
Heat Id	Place Id	Tested Thickness	Ys (KSI)	UTS (KSI)	%RA	Elong %	Zin	Dir	Hardness			Abs. Energy (FTLB)			% Shear			Tst Dir	Tst Temp	Tst Dir	Tst Temp	BDWT Tmp %Shr		
									1	2	3	1	2	3	1	2	3						1	2
E1B052	F65	0.249 (DISCRT)	L 63	79	31	1																		
E1B052	F66	0.875 (DISCRT)	L 56	75	44	1																		
E1B052	F69	1.254 (DISCRT)	L 58	76	39	1																		
<b>Heat</b>																								
<b>E1B052</b>																								
KILLED STEEL MERCURY IS NOT A METALLURGICAL COMPONENT OF THE STEEL AND NO MERCURY HAS INTENTIONALLY ADDED DURING THE MANUFACTURE OF THIS PRODUCT. KILLED STEEL, PRODUCED TO A FINE GRAIN PRACTICE MTR EN 10204:2004 INSPECTION CERTIFICATE 3.1 COMPLIANT 100% MELTED, POURED, AND ROLLED IN THE USA PRODUCTS SHIPPED: E67 PCS: 1, LBS: 5717 E1B052																								
<b>Chemical Analysis</b>																								
C: .18   Mn: 1.01   P: .011   S: .002   Si: .04   Test At: .034   Cu: .26   Ni: .14   Cr: .09   Mo: .04   Co: .003   V: .001   Ti: .0001   B: .0100   N: .0100   ORGN: USA																								

0201 16565

WE HEREBY CERTIFY THAT THIS MATERIAL WAS TESTED IN ACCORDANCE WITH AND MEETS THE REQUIREMENTS OF THE APPROPRIATE SPECIFICATION  
Checked by: Daryl Banman  
Checked by:

voestalpine Bohler Welding Canada Ltd.

Meyerside Dr. 1745, Units 1-3  
L5T 1C8 Mississauga  
Canada

## Certificate Schedule F

as per: ASME/AWS A5.01

No. : 2022-2025328406-40-31400331-004

Rev. 0 Page 1 of 1

PO no.	4280006884	of	22.06.2022
Order no.	1025221857		
Delivery note/pos./split	2025328406/000000/000040	of	24.06.2022
Product	Tubular cored electrode		
Trade name	<b>diamondspark 52 RC</b>		
Standard designation	EN ISO 17632-A: T46 4 P M21 1 H5/T46 2 P C 1 1 HS AWS AS.20: E71T1M/T-9M/T-12M-JDH4/E71T1C/T-9C/T-12C DH4 AWS AS.20: E71T1M/T-9M/T-12M-JDH4 / E71T1C/T-9C/T-12C DH-		
Dimension	0.052 in / 1.40 mm		300003
Serial no.	31400331		0364111F 0252
Quantity	2005,8 KG		

## Chemical composition in % of the weld metal

C	Si	Mn	P	S	Cr	Mo	Ni	V	Cu					
0.0546	0.41	1.10	0.0136	0.0081	0.0351	0.0025	0.015	0.0118	0.136					

## Mechanical properties

AWS B4.0

Tensile test							
T	Rel/ Rp 0,2 MPa	Rp 1,0 MPa	Rm MPa	A (Lo= 4d) %	Z %	WBH PWHT	Remarks
20°C	≥ 460		490-660	≥ 22			
Impact test							
T	Impact energy KV/J	Average KV/J	Lateral expansion mm	Shear fracture %	WBH PWHT	Remarks	
-50°F	≥ 27						

Town  
Sugar LandDate  
24.06.2022

This certificate was issued by DP-equipment and does not require signature.

Authorized representative  
Russel Fuchs

# Appendix J: PROCEDURE FOR SOLDERING STRAIN GAUGE WIRE ENDS

Soldering the ends of the strain gauges can be helpful when using the alligator clips for the DAC. For materials, the flux and solder wire will either be in the teams' supply or must be requested from a lab technician. The soldering machine is either available in the lab space or much be requested when needed from a lab technician.

### PPE

Protective Eyeglasses

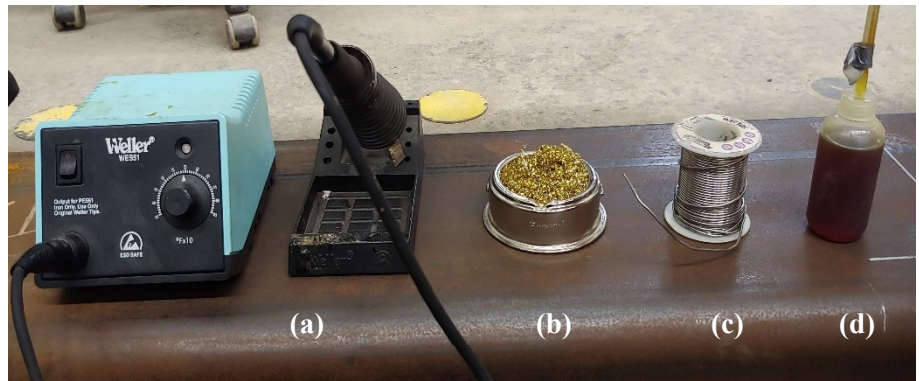
### Materials

Soldering Machine (a)

Dry Tip Cleaner (b)

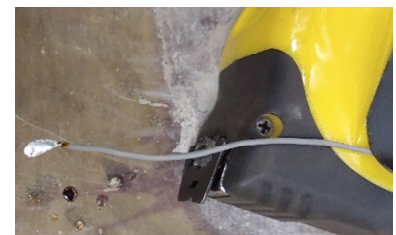
Solder Wire (c)

Flux (d)



### Procedure

- Make a loop in the strain gauge wire.
- Place wire into holder. I used the clip of a measuring tape as seen in photos.
- Cover loop in a liberal amount of flux.
- Apply small amount of solder to the end of the iron.
- Steam off the flux and apply a base coat of solder.
- Add a bubble of solder to the loop.
- Let cool before moving.





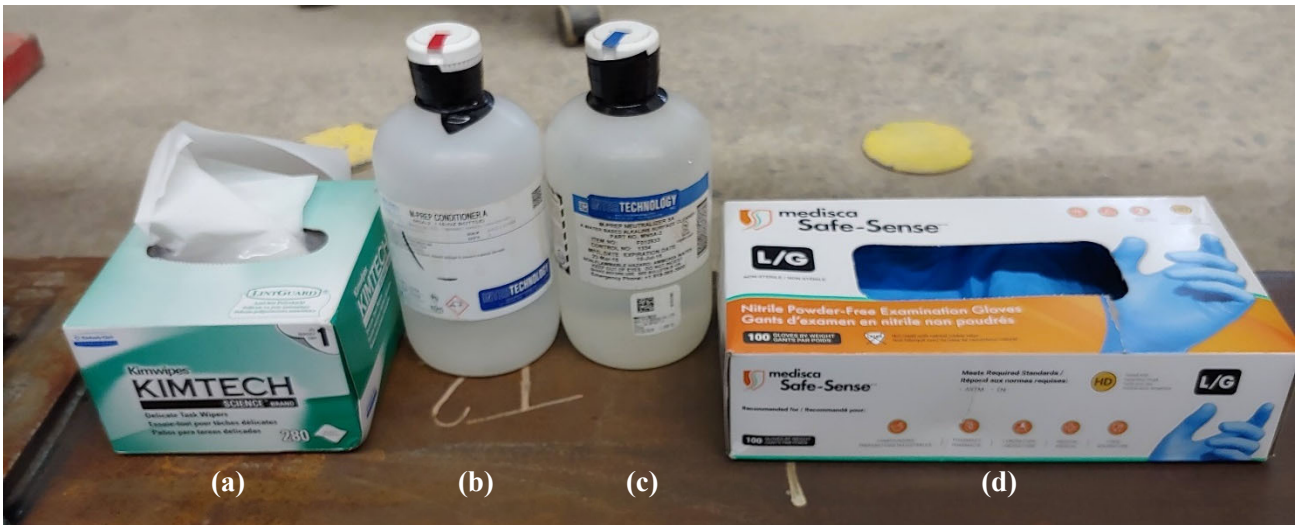
# Appendix K: PROCEDURE FOR INSTALLING STRAIN GAUGES TO STEEL

## Materials

- Lint Free Tissues, Kimwipe (a)
- Acid, M-Prep Conditioner A (b)
- Base, M-Prep Neutralizer (c)
- Gloves (d)
- Strain Gauge Glue (e)
- Tape, Dollar store is ideal (f)
- M-Coat A (g)
- Pencil (h)
- Marker/Scriber (i)
- Painter Tape (j)
- Scissors (k)

## PPE

- Gloves
- Protective Eyeglasses
- Mask

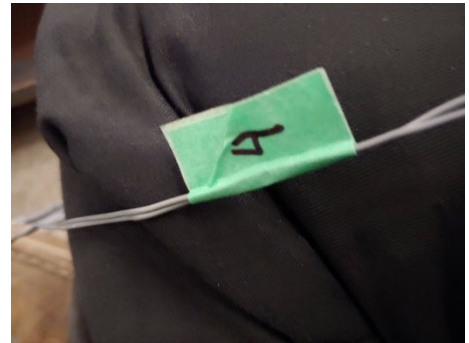


## Procedure

- Outline the approximate location for the strain gauge.
- Check strain gauge Ohm readings using the multimeter. Readings should be  $350 \pm 5$  ohms.
- Sand the surface of the steel using a spade sander until rust free, smooth, and shiny.
- Remark location lines for the strain gauges using scriber.
- Clean the area for the strain gauge using the acid (red cap) on a kimwipe. Continue wiping until the wipe comes away clean.
- Wipe cleaned area using the base on a kimwipe
- Cover cleaned and neutralized area with a piece of tape with both ends folded over for ease of lifting both sides. Dollar store tape is preferred.
- Partially lift the tape up to align the strain gauge into position with the grey side facing upwards and the all red side against the steel. Place the tape back down over the gauge to keep it in place.
- Peel the tape back from the opposite side than you used for placement just enough to place one drop of strain gauge glue to the back of the gauge. Replace the gauge and tape into place and hold down 60 seconds to ensure full contact.
- Once the glue is set, gently remove while pulling the tape horizontally. Do not rip off tape as it may remove the gauge with it.
- Gently release the copper wires if they get glued down, using the tip of a mechanical pencils works best.



- Optionally: cover the gauge with M-Coat A, only one to two swipes are required. M-Coat A is used to prevent environmental contaminants from getting on the gauge.
- Label gauges at the “plug-in” location using painting tape and marker. These labels are extremely helpful for ensuring strain gauge label number matches the channel it is plugged into in the DAC. Knowing the proper channel numbers makes understanding the data excel file extremely important.
- Additionally, if applying a limewash (see Appendix J), cover the gauges carefully using the same clear tape with one end folded over to remove easily one coating is completed. Remove tape in the same manner as when removing after gluing.



# Appendix L: LIMEWASH FORMULA

Text Limewash (Limewash) was used to visually see areas of yielding and high stress during testing. Instructions for the white was found on wikiHow (<https://www.wikihow.com/Make-Whitewash>) and modified to suit the project. Amounts of ingredients presented makes approximately 1L or 4 cups of limewash, if keep in a closed container this should provide 22.5m<sup>2</sup> of coverage (based on 1.5 m<sup>2</sup>/specimen x 3 specimens x 5 coats).

## Ingredients

1 ½ Cups Hydrated/Masonry Lime  
½ Cup Fine Grade Salt (Table Salt)  
4 Cups Water (warm)

## PPE

Rubber Gloves  
Protective Eyeglasses  
Dust Mask  
Lab Coat or Coveralls (Optional)

## Materials

Wire Brushes  
Sandpaper/Sanding Block  
Mild Dishwashing Detergent (Dawn)  
Lint-Free or Scrap Cloths  
Bucket/Container for Washing  
Pail/Bucket (10.5L) with Lid  
Paint brush  
Stir Stick

## Making the Limewash

- Mix salt and warm water in pail until salt is fully dissolved (The salt keeps the mix from drying in the pail)
- Add the lime to the salt water (Important to wear a mask at this step as hydrated lime is harmful if inhaled)
- Mix well until the lime is fully dissolved. The mixture should be tinner than traditional paint.

## Preparing Steel Surface

- Clean rust and debris from the areas intended to be limewashed using first wire brushes and then sandpaper. In areas where rust will not remove easily adding a small amount of water with a cloth will add in cleaning and avoid rust and debris from becoming airborne.
- Wash the areas with dish detergent and water solution. Then wipe down areas again with a damp clean cloth.

## Applying the Limewash

- Ensure surface is clean and completely dry.
- Using a paint brush apply the wash to the metal with smooth, even strokes in one direction.
- Allow limewash to dry completely before applying more coats. To remove/ minimise appearance of brush strokes on steel and to get a fully opaque looking for testing 4-6 coats may be required.